

Studies of Lattice Models of Branched Polymers

A Thesis
Submitted to the
Tata Institute of Fundamental Research, Mumbai
For the degree of Doctor of Philosophy
in Physics

by

Sumedha

Dept. of Theoretical Physics
School of Natural Sciences
Tata Institute of Fundamental Research
Mumbai

April, 2005

Acknowledgements

I feel great respect and admiration for my adviser Prof. Deepak Dhar. Besides his brilliance, his honesty and uncompromising approach towards science are exemplary. His ideas and intuition have contributed a lot to this thesis. I hope I have learnt some of his ways of doing physics.

Besides my adviser two people from whom I benefited greatly during my PhD are Prof. Mustansir Barma and Prof. Satya Majumdar. Mustansir gave a wonderful course on phase transitions which built a base for many things I learnt in later years. Satya was always very encouraging and willing to discuss during his visits to TIFR. I have also learnt a lot from interactions with my seniors Rajesh, Sanjib and Kavita.

I would also like to thank DST and organisers of two SERC schools which I attended during my PhD. Both schools helped me get a wider perspective and were refreshing and fruitful. In recent years we had regular journal club in our group and I thank all my juniors for making it worthwhile and keeping it alive.

The office staff of theory group at TIFR is just amazing. Pawar, Bathija, Shinde and Ogale were always ready to help with almost anything. Also Anindya, Ashiq and Ajay Salve have been very helpful with computers.

Besides all this, TIFR has been a great experience. Everybody from canteen staff to security guards was very friendly and helpful. I had a very good time with my officemates Dariush and Subhendu. Especially, Dariush's logical approach to everything in life was many a times helpful. I have cherished friendship of many people in TIFR. Some of my most relaxing times were spent with Nabanita. I also had great fun playing badminton with Benny, Rahul, Ajay and others and organising hostel events with Benny. Besides that there were hikes in Sahyadris, long gossip sessions in canteen and hostel day events. I enjoyed the friendship of many other people in TIFR like Ramanan, Amit, Ajay, Rabeya, Meera, Yeshpal, Krishnan, Amitava, Saurav, Vijay, Malickarjun, IG and Vishal.

Throughout my PhD my parents were very encouraging. Also my brother, sister-in-law and Keshu have been very supporting. A special thanks to Chethan for all his encouragement and support for last eight years.

Declaration

This thesis is a presentation of my original research work. Wherever contributions of others are involved, every effort is made to indicate this clearly, with due reference to the literature, and acknowledgement of collaborative research and discussions.

The work was done under the guidance of Professor Deepak Dhar, at the Tata Institute of Fundamental Research.

Sumedha

In my capacity as supervisor of the candidate's thesis, I certify that the above statements are true to the best of my knowledge.

Deepak Dhar

Contents

Synopsis	vii
1 Introduction	1
1.1 Preliminaries	1
1.2 Definition and Notation of Self-avoiding walk and Lattice animals	3
1.2.1 Self-Avoiding Walk	4
1.2.2 Lattice Animals	5
1.2.3 Dimensional Reduction	7
1.3 Directed Lattice Animals	8
1.3.1 Definition	8
1.3.2 Directed animal and Hard core lattice gas problem	9
1.4 Polymers with interaction	10
1.4.1 Adsorption-Desorption transition in polymers	11
1.5 Spiral Trees	12
1.6 Monte Carlo simulations of polymers	15
1.6.1 Dynamic MC methods	16
1.6.2 Importance Sampling	17
1.6.3 Incomplete Enumeration	18
2 Distribution of transverse distances in directed animals	22
2.1 Relation between transverse size distribution generating function and hard core lattice gas density-density correlation function	22
2.2 Directed Animals on a square lattice	25
2.3 Scaling Function in Large Dimensions	29
2.4 Generalized directed animals	32

3	Adsorption-Desorption transition for Directed Branched Polymers	35
3.1	The Model	35
3.2	General Results	38
3.3	Two dimensional Directed Branched Polymer in presence of 1-d penetrable surface	40
3.4	Two dimensional Directed Branched Polymer in presence of 1-d impenetrable surface	42
3.5	Three dimensional Directed Branched Polymer in presence of an attractive line	47
4	Incomplete Enumeration Monte-Carlo Method	50
4.1	Efficiency	51
4.2	Optimising the Incomplete enumeration algorithm	53
4.2.1	Systems with Uniform genealogical tree	53
4.2.2	Systems with recursively defined genealogical tree	55
4.2.3	Self avoiding Walks	57
4.3	Improved Incomplete Enumeration (IIE)	58
4.3.1	Systems with recursively defined genealogical tree	59
4.3.2	IIE for Self avoiding walks	60
4.4	Lattice Animals and Branched Polymers	61
4.4.1	Lattice animals on a Binary tree	62
4.4.2	Heuristic argument for the stretched exponential behaviour of $P(n)$ at $p = 1/4$	69
4.4.3	Lattice Animals on a 2 dimensional square lattice	72
5	Rooted Spiral trees	74
5.1	Lower Bound on Growth Constant on a Square lattice	74
5.2	Spiral trees on a square lattice	81
5.2.1	Exact enumeration	81
5.2.2	Monte-Carlo analysis	85
5.3	Spiral trees on a cubic lattice	88
5.4	Spiral trees in four dimensions	89
6	Summary and Discussion	95
6.1	Directed animals (Directed branched polymers)	95

6.2	Incomplete enumeration algorithm	96
6.3	The Spiral trees problem	98
	Bibliography	99

List of Figures

0.1	A Directed animal (directed branched polymer) of size 50, rooted on the surface, on a square lattice drawn tiled at 45°	ix
0.2	An example of a genealogical tree. The numbers labelling the sites indicate the order in which they are added (1 represents the root site). The tree shown is for directed lattice animals on a square lattice.	xv
0.3	$1/P(n)$ of IE as a function of size n for SAW on a 2, 3 and 4 dimensional hyper-cubic lattice.	xvi
0.4	A node at level $r - 2$ on the genealogical tree of lattice animal enumeration on a binary tree with k descendants. Here $k \leq (r - 1)$	xviii
0.5	Randomly generated spiral tree of 1000 sites in 2-dimensions using incomplete-enumeration MC program	xix
0.6	Schematic picture of a rooted spiral tree defined in the first quadrant with a backbone with long offshoots	xx
1.1	Polyethylene in linear and branched polymer forms	2
1.2	A self avoiding walk with 9 steps on a square lattice	4
1.3	A lattice animals of 15 sites on a square lattice	5
1.4	Schematic figure of a directed animal of size 20 on a square lattice.	8
1.5	Schematic of a rooted spiral tree on square lattice	13
1.6	An example of a genealogical tree.	19
2.1	A part of Cayley tree with coordination number 3.	31
3.1	A directed branched polymer of size 50.	36
3.2	Directed branched polymer on a square lattice in presence of a 1-d impenetrable line	43
3.3	Sticking Fraction in presence of a line for a directed branched polymer in 1+1 and 2+1 dimensions.	45
3.4	Density profile of a 2-dimensional DBP in presence of a 1-dimensional surface	47

4.1	Plot of optimum values of p_i on a $(23, 233)$ tree of depth 30.	56
4.2	T_n/n^2 of IE as a function of size n for SAW on a 2, 3 and 4 dimensional hyper cubic lattice.	57
4.3	Probability of getting a walk of size n for IE and IIE as a function of n . . .	60
4.4	T_n/n^2 of IIE vs size n for SAW on a 2, 3, 4, 5, 6, 7, 8 and 10 dimensional hyper cubic lattice.	61
4.5	A node on the genealogical tree of lattice animals enumeration on a binary tree with k descendants	63
4.6	First few levels of the genealogical tree for lattice animals on a binary tree. .	64
4.7	Plot of $P(k, r)$ versus scaled $k - k^*(r)$	65
4.8	Plot of $P(k+1)$ as a function of $P(k)$ at $p = 1/4$ for $r = 25000, 26000, 28000$ and 30000	66
4.9	The width $k^*(r)$ of the travelling front as a function of $r^{1/3}$ for different values of p	69
4.10	Plot of $-\log(P(2, r))$ as a function of $r^{1/3}$	70
4.11	Plot of $\log T_n$ for $m = 2/3, 5/6$ and 1 as a function of x	71
4.12	Plot of $-\log(P(2, r))$ versus $r^{0.4}$ for lattice animals	72
4.13	Plot of $-\log(P(r))$ versus $r^{0.32}$ for directed animals	73
5.1	Randomly generated spiral trees of 1000 sites on square lattice.	75
5.2	A simple counting problem of backbone with arbitrary long straight offshoots. .	77
5.3	An example of an irreducible spiral graph with no articulation point.	78
5.4	Schematic figure of spiral trees contributing to $B_i(x)$	79
5.5	Some examples of graphs contributing to $V_i(x)$ and $W_i(x)$ respectively. . .	79
5.6	Convergence of λ_n for spiral trees on a square lattice.	83
5.7	Convergence of θ_n for spiral trees on a square lattice.	85
5.8	Plot of $\frac{I_{pl,n}}{n^{2.312}}$ as a function of n for Monte-Carlo generated spiral trees . . .	87
5.9	Plot of $I_{pl,n}$ versus n for Monte-Carlo generated spiral trees on a square lattice. .	88
5.10	Monte-Carlo estimates of ratios of the number of configurations on a square lattice.	89
5.11	A spiral tree of six sites on a cubic lattice with a back-turn (drawn by a thicker line)	94

List of Tables

5.1	Series for the number of quadrant spiral trees on a square lattice	80
5.2	The number of spiral trees on a square lattice and their average moment of inertia.	82
5.3	Values of λ_n , θ_n and ν_n from sequential fit to data for spiral trees of size n to $n + 3$ on a square lattice. See Fig. 5.6 and Fig. 5.7	84
5.4	Estimates of critical exponents and growth constant from differential approximants. We looked at approximants for $l \geq 9$ and $l - 3 \leq m \leq l + 3$. We have tabulated here 20 values which showed the best convergence.	86
5.5	Exact enumeration values of the number of spiral trees ST_1 on a cubical lattice and their average moments of inertia.	90
5.6	Exact enumeration values for number of spiral trees ST_2 on a cubical lattice and their average moments of inertia.	91
5.7	Values of λ_n , θ_n and ν_n from sequential fit to data for spiral trees ST_1 on a cubical lattice.	91
5.8	Values of λ_n , θ_n and ν_n from sequential fit to data for spiral trees ST_2 on a cubical lattice.	92
5.9	Estimates of critical exponents and growth constant from series analysis in three and four dimensions.	92
5.10	Exact enumeration data for the number of spiral trees ST_1 on four dimensional hyper-cubic lattice and their average moments of inertia.	93
5.11	Exact enumeration data for the number of spiral trees ST_2 on four dimensional hyper-cubic lattice and their moments of inertia.	93
5.12	Estimates of critical exponents and growth constants from Monte-Carlo simulations in four dimensions.	94

Synopsis

Polymers are long chain molecules consisting of a large number of units(monomers), which are held together by chemical bonds. When the constituting monomers can attach themselves to at most two other monomers, we get linear polymers(LP). Whereas when some of the constituting monomers have a functionality of ≥ 3 , one gets branched polymers(BP) [1]. Many naturally occurring and artificially synthesized materials contain randomly branched polymers.

Linear and branched polymer molecules in solution are highly flexible and change their conformation (often). Prediction of their average conformations can be done using equilibrium statistical mechanics. The large-scale properties can be captured in simpler lattice models. They are more amenable to rigorous analysis, and are easier to investigate numerically using both Monte-Carlo methods and series analysis approach.

The lattice models of self-avoiding walk(SAW) and lattice animals(LA) respectively model linear and branched polymers in dilute solutions. SAW are random walks which never visit the same site again, while LAs are the connected cluster of sites on a lattice. LA are also considered as percolation clusters [2]. Lattice animals are related to many other models in statistical physics, like the Ising model (Fortuin-Kastelyn clusters) [3].

In this thesis, we studied Monte-Carlo methods for linear and branched polymers. We also studied two variants of lattice animals known as directed lattice animals(DA) and spiral trees. DAs use the same geometry as lattice animals but the bonds are directed in this case. This additional direction leads to many interesting properties like anisotropic scaling and direction dependent critical properties besides making the system analytically more tractable. We also study a lattice model of rooted spiral trees. A rooted spiral tree is a acyclic connected subgraph of a lattice such that the projection of the path joining any site of the tree to the root on $x - y$ plane contains no left turn.

Directed animals have found correspondence with many other lattice models, which makes this problem a very interesting problem to study. The exponents of $(d + 2)$ lattice animals, $(d + 1)$ directed animals and d dimensional hard-core lattice gas at negative activity are related to each other [4]. Besides, the geometrical structure of directed animals describes qualitatively diverse situations such as trees, river networks and dilute polymers in a flowing

solvent etc. Directed animals problem is also related to $p \rightarrow 0$ limit of directed percolation problem. And hence a better understanding of it will also help to understand the directed percolation problem.

In this thesis, we studied the directed lattice animals and obtained relation between the average number of sites at a given transverse distance \mathbf{x} from the origin for $(d + 1)$ -dimensional directed animals from the density-density correlation function of the lattice gas in d dimensions [5].

Study of directed animals close to impenetrable and penetrable walls/ lines provides models for study of phase transition in presence of surface. We study the adsorption-desorption phase transition of directed branched polymer in $(d + 1)$ dimensions in contact with a line [6]. We solved the model exactly in $(1 + 1)$ and $(2 + 1)$ dimensions.

For rooted spiral trees, we obtained an exact lower bound on the growth constant on a square lattice. We study the problem on hyper-cubical lattice in 2, 3 and 4 dimensions using exact enumeration and Monte-Carlo techniques [7]. This model was earlier conjectured to show a dimensional reduction by four. We find that our numerical studies do not support this conjecture.

Monte-Carlo(MC) simulations are a very important tool for studying polymers, as exact results are hard to come by and are available only for the simplest models. While there are many good algorithms known for linear polymers [9], Monte-Carlo simulations of branched polymers have been less successful [10]. Algorithms used for simulating linear polymers can often be adapted for branched polymers, but they are usually found to be less efficient. A better understanding of the efficiency of Monte Carlo algorithms for generating branched polymers seems desirable. We study a particular genetic type Monte-Carlo algorithm called incomplete enumeration(IE) for linear and branched polymers in this thesis [8]. We found a qualitative difference in the efficiency of the algorithm for LPs and BPs. The average time to generate an independent sample of n sites for large n varies as n^2 for linear polymers, but as $\exp(cn^\alpha)$ for branched (undirected and directed) polymers, where $0 < \alpha < 1$.

We will now describe the models and results in more detail.

Directed lattice animals

A directed animal or a directed branched polymer on a lattice, rooted at the origin is a connected cluster such that any site of the animal can be reached from the root by a walk which

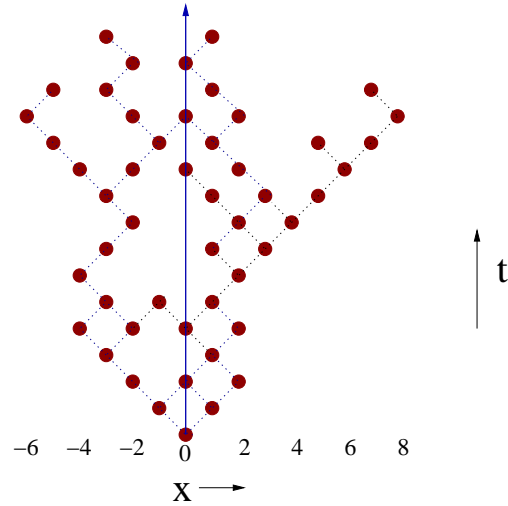


Fig 0.1: A Directed animal (directed branched polymer) of size 50, rooted on the surface, on a square lattice drawn tiled at 45° .

never goes opposite to the preferred direction. For example, on a square lattice drawn tilted at 45° in Fig. 1, a directed site animal or a directed branched polymer \mathcal{A} rooted at the origin is a set of occupied sites including origin, such that for each occupied site (x, t) other than the origin, at least one of the two sites $(x - 1, t - 1)$ and $(x + 1, t - 1)$ is also occupied. The number of sites in \mathcal{A} will be denoted by $s = |\mathcal{A}|$. We define $n(x|\mathcal{A})$ as the number of sites of \mathcal{A} having the transverse coordinate x , and $\phi(\mathbf{x}, s)$ as average of $n(x|\mathcal{A})$. We define A_s as the number of distinct animals having s sites, with the generating function $A(y) = \sum_{s=1}^{\infty} A_s y^s$. We also define a generating function $\Psi(\mathbf{x}, y)$ as

$$\Psi(\mathbf{x}; y) = \sum_s \phi(\mathbf{x}, s) A_s y^s \quad (0.1)$$

For large s , A_s varies as $\lambda^s s^{-\theta}$, where θ is a critical exponent. The radius of gyration R_s is expected to vary as s^{ν_\perp} , where the exponent ν_\perp is related to the animals number exponent θ by the hyper-scaling relation $\theta = d\nu_\perp$.

The directed site animal enumeration (DSAE) problem in $(d + 1)$ dimensions is related to time development of thermal relaxation of a hard core lattice gas (HCLG) with nearest neighbor exclusion on d dimensional lattice, with the rates which satisfy detailed balance condition with fugacity $z = p/(1 - p)$ (here p is the probability with which a sites gets occupied in the HCLG model). Then if $\rho(p)$ is the average density of particles in the steady state of this system, in [11], it was shown that $A(y) = -\rho(p = -y)$.

We have generalized the derivation of this result to the case where the value of p at site i is p_i and all p_i need not be equal. Then the rates of this process still satisfy detailed balance condition corresponding to the Hamiltonian

$$H = +\infty \sum_{\langle ij \rangle} n_i n_j - \sum_i (\ln z_i) n_i \quad (0.2)$$

where $z_i = p_i / (1 - p_i)$. The probability that site i is occupied in the steady state depends on the p_j 's for all sites j , and will be denoted by $\rho_i(\{p_j\})$. In the corresponding DA problem, we have to define the weight of an animal \mathcal{A} as product of weights of all occupied sites, the weight corresponding to a site with \mathbf{x} -coordinate j being y_j . If $A_i(\{y_j\})$ is the sum of weights of all animals rooted at i , then taking derivative of $A(\{y_j\})$ with respect to y_i , we find the generating function $\Psi(\mathbf{x}; y)$ and the density- density correlation function of gas($G(\mathbf{i}, \mathbf{k})$) to be related as

$$\Psi(\mathbf{x}; y) = -\frac{1}{1+y} G\left(\mathbf{x}; z = -\frac{y}{1+y}\right) \quad (0.3)$$

This relation holds in all dimensions. For the special case $d = 1$, it is a simple exercise to calculate $G(x; z)$ explicitly and we hence get the explicit expression for $\Psi(x; y)$ on square lattice to be

$$\Psi(x; y) = \frac{y}{(1+y)(1-3y)} \left[1 - \sqrt{\frac{1-3y}{1+y}}\right]^{|x|} \left[1 + \sqrt{\frac{1-3y}{1+y}}\right]^{-|x|} \quad (0.4)$$

This gives $\phi(x, s)$ for large s to be

$$\phi(x, s) \sim \frac{\sqrt{3\pi s}}{4} \operatorname{erfc}\left(\frac{\sqrt{3}x}{2\sqrt{s}}\right) \quad (0.5)$$

Hence we find the scaling function of distribution of transverse distances for a $(1 + 1)$ dimensional directed animal to be an error function.

The case $x = 0$ is special, in that the density-density correlation function $G(0, z)$ is always equal to $\rho(1 - \rho)$ for hard-core lattice gas for any d dimensional lattice. Hence, if one knows ρ as a function of the activity z (equivalently, in the DA problem, one knows the animal numbers generating function $A(y)$), then one can determine $\Psi(0; y)$ in terms of $A(y)$ alone.

Directed branched polymer(DBP) near an attractive line

We study the DBP in presence of $1d$ line parallel to the preferred direction. This is positioned along the main diagonal of the lattice (Fig. 1). We considered only the case when the polymer is rooted at the surface.

We assign a fugacity y to all allowed sites of the cluster. Further, if we associate an additional energy $-E$ with each site on the surface, each site on the surface will have an additional weight and the fugacity of sites about the diagonal, denoted by y_0 is equal to wy where $w = \exp(E/kT)$. Hence $w > 1$ would correspond to an attractive surface.

We define $A(w, y)$, the grand partition function of the polymer as

$$A(w, y) = \sum_{\mathcal{A}} y^{|\mathcal{A}|} w^{n_0} \quad (0.6)$$

where $n_0 = n(0|\mathcal{A})$. If we define, $A_s(w)$ as the partition function of the polymer made of exactly s monomers, then $A(w, y) = \sum_{s=1}^{\infty} A_s(w) y^s$.

There is a critical value w_c of wall activity such that for $w > w_c$ the polymer tend to stick to the surface. For $w < w_c$, only a finite number of monomers stick to the surface, and at $w = w_c$, the critical point of the surface transition, the number of adsorbed monomers as a function of polymer size in large s limit have a behavior given by $\phi_c(0, s) \sim s^\alpha$, where α is known as the crossover exponent of the surface transition.

The fraction of polymer segments at the surface, represented by $C_{st}(w, y)$, is the order parameter of the surface phase transition and is zero for $w \leq w_c$. In general, in the large polymer limit, near critical value of w , as $w \rightarrow w_c^+$, $C_{st}(w, y)$ is expected to have scaling form

$$C_{st}(w, y) = \epsilon^{1-\alpha} h(\Delta w \epsilon^{-\alpha}) \quad (0.7)$$

where $\epsilon = 1 - y/y_\infty(w)$ and $\Delta w = w - w_c$. $y_\infty(w)$ is the value of the fugacity y at which the polymer size diverges for a given w . The scaling function $h(u)$ where $u = \Delta w \epsilon^{-\alpha}$, is a function of w and y which are both intensive thermodynamic variables. As $u \rightarrow \infty$, $h(u) \sim u^{(1-\alpha)/\alpha}$.

We find that $A(w, y)$ can be expressed in terms of $A(1, y)$ and this is given by

$$A(w, y) = \frac{w(1+y)A(1, y)}{(1+wy) + A(1, y)(1-w)} \quad (0.8)$$

For $\mathbf{x} = 0$, the density density correlation of HCLG is always equal to $\rho(\rho - 1)$ for any d dimensional case and hence $\Psi(0; 1, y)$ can be completely expressed in terms of $A(1, y)$. These results hold for all dimensions. Hence, in the presence of $1d$ surface, a DBP in $d + 1$ dimensions rooted on the surface can be studied using the mapping to HCLG. The generating functions $A(w, y)$ and $\Psi(0; w, y)$ can be completely expressed in terms of animal number generating function when wall is neutral i.e, in terms of $A(1, y)$. We used these results to study the surface effects for DBP in 2 and 3 dimensions.

Directed Branched Polymer in presence of 1-d penetrable surface

For a penetrable surface, since the configurations spanning through the surface are allowed, there is no loss of entropy per monomer to take into account (Fig 1). Hence, $w = 1$ corresponds to a zero gain in free energy per monomer of the surface. This implies that $w_c = 1$ for a DBP in any dimension in presence of a $1d$ line as long as $A(1, y)$ is divergent at a finite value of y .

But as we go to higher dimensions even though entropy loss and energy gain balances each other at $w = 1$, the polymer might start binding to a line only at wall activity greater than 1. For directed branched polymers, when $A(1, y)$ has no divergence, $w = 1$ is not the critical point of the surface transition. Instead it is given by

$$w_c = \frac{1 + 1/A(1, y_c)}{1 - y_c/A(1, y_c)} \quad (0.9)$$

where y_c is the large polymer limit fugacity value of the polymer with neutral wall i.e, when $w = 1$. As an example, on a Bethe lattice with co-ordination number 3, $A_B(1, y) = \frac{1 - \sqrt{1-4y}}{2y}$ and $y_c = 1/4$. At $y = 1/4$ the function $A_B(1, y) = 2$, and substituting in Eq.3.23 we get $w_c = 12/7$, which is greater than 1.

In $(1 + 1)$ -dimensions we have obtained the expressions for $A(w, y)$ and $\Psi(x; w, y)$. The generating functions $A(w, y)$ and $\Psi(x; w, y)$ have branch cut at $y = 1/3$. For $w = 1$, they also have a pole singularity at $y = 1/3$. Hence, clearly the phase transition from desorbed to adsorbed phase occurs at $w = 1$, i.e $w_c = 1$. The sticking fraction $C_{st}(w, y)$ can also be exactly calculated and we get it to be

$$C_{st}(w, y) = \left[\frac{y(1-w)}{1+y} + \frac{1+wy}{\sqrt{(1+y)(1-3y)}} \right]^{-1} \quad (0.10)$$

From this, near the critical point, we get the scaling form of $C_{st}(w, y)$ to be $C_{st}(w, y) = A\sqrt{\epsilon} h(u)$ where $\epsilon = 1 - y/y_\infty(w)$ and $u = c\epsilon^{-1/2}\Delta w$ and we get

$$h(u) = \left[1 + u^2 \right]^{\frac{1}{2}} \quad (0.11)$$

with constant $A = \sqrt{3}/2$ and $c = \sqrt{3}/4$. This gives the order parameter $C_{st}(w)$ near the critical point to be proportional to Δw .

In $(2 + 1)$ dimensions, a DBP on a simple cubic lattice with nearest and next nearest neighbor connections gets mapped to the hard hexagon gas model in 2 dimensions at negative activity in the disordered regime, which was solved by Baxter. He obtained the equation for the average density of the gas. It was shown by Joyce that there is an algebraic equation in z (activity of the gas) and ρ (density of the gas). Using his solution we obtained a twelfth-order polynomial equation in $A(w, y)$, where the coefficients are functions of w and y . In presence of 1-dimensional line the polymer undergoes a desorption-adsorption transition at $w = 1$. For $w \leq 1$ the dominant singularity is $y_c = 2/(9 + 5\sqrt{5})$ and $y_\infty(w) = y_c$. For $w > 1$, $y_\infty(w)$ can be obtained by from the fact that the $A(w, y)$ tends to infinity at this point and the coefficient of highest order term of the polynomial equation must be zero. With, $y = y_\infty(w)(1 - \epsilon)$ and $w = 1 + \Delta w$ we obtained the scaling function of $C_{st}(w, y) = \epsilon^{5/6}h(u)$ to be

$$h(u) = \frac{6a_0}{1 + y_c} (1 + cu^6)^{\frac{5}{6}} - 6cu^5 \quad (0.12)$$

where $u = \Delta w\epsilon^{-1/6}$. The scaling function $h(u)$ for both $(1 + 1)$ and $(2 + 1)$ is a function of two thermodynamic variables w and y .

Two dimensional Directed Branched Polymer in presence of 1-d impenetrable surface

In the presence of an impenetrable surface, because of loss in entropy per monomer on the wall, the transition from desorbed to adsorbed phase takes place at a non trivial value of adsorption activity. We study a DBP in $(1 + 1)$ dimension on a square lattice, in presence of an impenetrable surface, about the diagonal, by mapping the problem to the HCLG in 1-d with fugacity 0 for all sites along the negative axis. Using the mapping we obtained the expressions for $A(w, y)$ and $\Psi(x; w, y)$. In this case we find $w_c = 3$. This value is

greater than the value for $(1 + 1)$ d DBP with a penetrable surface. For $w > 3$, the closest singularity to the origin occurs at $y_s = \frac{\sqrt{4w-3}-1}{2w}$. Near the critical point for $w = 3 + \Delta w$ and $y = y_s(1 - \epsilon)$, we get the same scaling form for $C_{st}(w, y) = A\sqrt{\epsilon}h(u)$, with the same scaling function $h(u)$ (Eq. 0.11). The constant $A = 2/\sqrt{3}$ and $c = 1/3\sqrt{3}$ in this case.

We also obtained the function $\phi(x, s)$ in three regions giving the spread of sites as a function of distance from the wall. Here we give these results for the impenetrable case only because the qualitative behavior in both impenetrable and penetrable case is exactly same for $(1 + 1)$ dimensional system. These are as follows

$$\phi_{de}(x, s) = \frac{3}{2}x \exp\left(-\frac{3x^2}{4s}\right) \quad (0.13)$$

$$\phi_c(x, s) = \frac{\sqrt{3\pi s}}{2} \operatorname{erfc}\left(\frac{\sqrt{3}x}{2\sqrt{s}}\right) \quad (0.14)$$

$$\phi_{ad}(x, s) = s \exp(-x) \quad (0.15)$$

$$(0.16)$$

where de, c and ad represents desorbed, critical and adsorbed phases respectively.

Hence we found that at $w = 3$ not just the crossover exponent α is equal to $1/2$, but even the scaling form of $\phi(x, s)$ is same as that of a $(1 + 1)$ dimensional DA in bulk [5] and hence same as that of the penetrable wall at the critical point. This unusual result can be understood as coming from exact cancellation of decrease in entropy and increase in internal energy at the critical point. Also note that the value of exponent $\alpha = 1/2$ for DBP is equal to the estimates of α for branched polymers and linear polymers in 2 dimensions. In fact for adsorption of an undirected d dimensional branched polymer to a $d - 1$ dimensional surface, the crossover exponent α is conjectured to be $1/2$ in all spatial dimensions.

Incomplete enumeration Monte-Carlo algorithm for linear and branched polymers

In order to study the thermodynamic properties of the polymers, one has to average over all allowed configurations of the polymer of a given number of monomers, with excluded volume interactions. The averages are defined with all configurations considered to be equally likely. Monte-Carlo methods allows us to study much larger sizes, than possible by exact enumeration techniques [12].

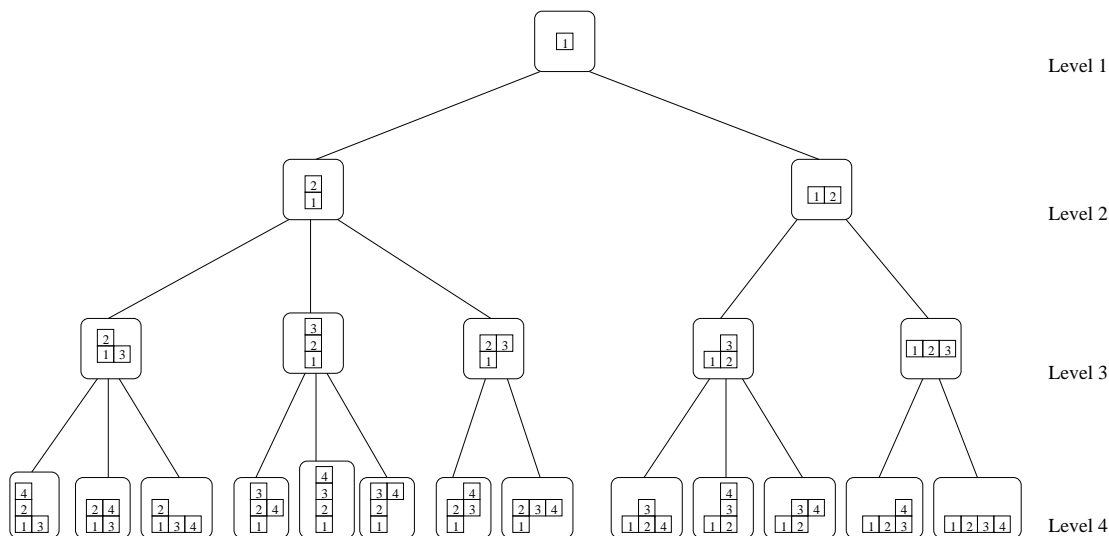


Fig 0.2: An example of a genealogical tree. The numbers labelling the sites indicate the order in which they are added (1 represents the root site). The tree shown is for directed lattice animals on a square lattice.

The IE algorithm is a simple modification of exact enumeration algorithm for generating polymers. We arrange all configurations in a genealogical tree, whose nodes are the different configurations of the polymer, such that all polymer configurations of n sites are at level n and are connected to a unique parent at level $(n - 1)$. Clearly, the tree depends on the rule used to define parenthood. For example, Fig. 0.2 shows a genealogical tree for directed lattice animals on a square lattice for $n \leq 4$, using one such choice.

The time required to construct the genealogical tree up-to level n in the exact enumeration algorithm increases exponentially with n . The basic idea of the IE algorithm is to decrease this time by randomly pruning the genealogical tree.

In IE, any bond in the genealogical tree connecting level r to level $(r + 1)$ is removed with probability $(1 - p_r)$ independent of the other bonds. If a configuration gets disconnected from the root node, automatically all its descendants are also removed. We make a depth first search of the pruned genealogical tree up-to depth n to determine the different configurations that remain at level n . We run the algorithm several times to generate a large sample. The probability of enumeration of a particular r site configuration in a given run $\Xi_r = \prod_{i=1}^{i=r-1} p_i$, is same for all configurations of size r . This ensures that the sample of configurations obtained is unbiased.

We take unit of CPU time as the time required to add or delete a configuration on the

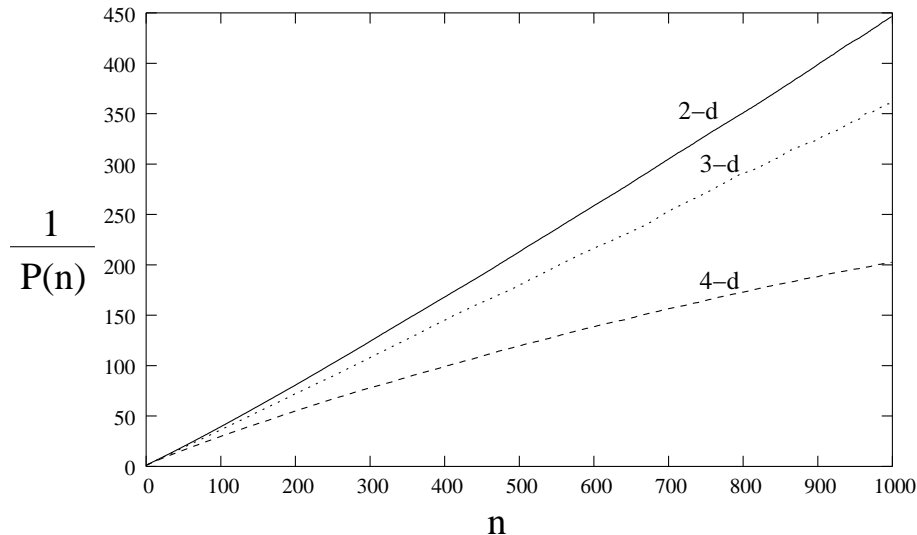


Fig 0.3: $1/P(n)$ of IE as a function of size n for SAW on a 2, 3 and 4 dimensional hypercubic lattice.

genealogical tree. Since time to scan is proportional to the number of nodes on the tree, the average CPU time per run is given by $\tau_n = \sum_{j=1}^n A_j \Xi_j$, where A_j is the total number of configurations of size j .

Let T_n be the average CPU time required to obtain one run which generates at least one configuration of size n . If τ_n is the average CPU time for one Monte-Carlo run, then we have

$$T_n = \frac{\tau_n}{P(n)} \quad (0.17)$$

where $P(n)$ is the probability that a single run produces at least one sample of n monomers.

Consider the case in which $p_i = p$ for all i . So long as $p\lambda > 1$, the average number of configurations of size n will grow exponentially with n . This implies that T_n increases exponentially with n . Also, if $p\lambda < 1$, then $P(n)$ decreases exponentially and again T_n increases exponentially with n . Thus a good choice of p is near $1/\lambda$. However, finding the optimal choice of $\{p_i\}$ for a given problem is non trivial.

The simplest of enumeration problems is the enumeration on a uniform genealogical tree. On a binary tree ($\lambda = 2$), we show that for $p_i = \frac{1}{2}$, we get $T_n = n^2/4$ for large n . From systematic optimisation we saw that there exist a nontrivial optimal value for each p_i which depends on the depth of the genealogical tree to be reached. However even with this choice for large n we get $T_n \approx n^2/4$. For a k -node uniform tree, with $p_i = 1/k \forall i$, we get $T_n = \frac{(k-1)n^2}{2k}$.

We consider IE for SAW. The genealogical tree for SAW is not uniform. In this case it is difficult to determine the probabilities of connection up-to level n analytically but we have estimated $P(n)$ numerically by simulations. We choose p_i , so that on the average we get order one configurations of size n per run for large n . With this choice of p_i our numerical simulations show that the probability of reaching level n goes down as $1/n$ in 2,3 and 4 dimensions (Fig. 0.3). This also implies that p_c is indeed $1/\lambda$ on the SAW genealogical tree. Hence we conclude that $T_n \sim n^2$ for SAWs independent of dimension.

Genealogical tree of branched polymers differs in two important ways from genealogical tree of linear polymers. There are several choices of rules to define parentage, but for simple rules, the degree of a node is not bounded. The number of possible descendants of a node is of the order of its perimeter sites and hence the maximum of the degree of nodes at level n increases with n . We study the IE algorithm, for BPs on a binary tree.

For BPs on binary tree, the genealogical tree is as shown in Fig.0.4. The growth constant of the tree is 4. If $P(k, r)$ is the probability of a node with k offsprings to be connected to at-least one node r levels below it, then $P(k, r)$ has a recursion

$$P(k, r + 1) = 1 - \prod_{s=2}^{k+1} (1 - pP(s, r)), \quad k = 2 \text{ to } \infty \quad (0.18)$$

with initial conditions $P(k, 1) = 1 \forall k \geq 2$ and p is the probability with which we choose any edge of the tree. $P(2, r)$ will give the probability of connection of root to level r on the genealogical tree. Eq. (4.18) is a nonlinear equation. At $p = 1/4$, from numerical iteration of Eq.4.18 till $O(10^4)$, we find $P(n) \sim \exp(-cn^{1/3})$, with $c = 2.47 \pm 0.01$ and hence, $T_n \sim \exp(cn^{1/3})$ to leading order.

We also prove a rigorous lower bound on $P(n)$. We find, $P(n) \geq \exp(-cn^{1/3})$, where c is a constant and is equal to 5.04.

Thus our numerical simulations and qualitative arguments show that probability of connection goes down as an stretched exponential at $p = 1/4$. Similar behaviour for BPs and DBPs on square lattice was observed in numerical simulations. Hence, for branched polymers, $T_n \sim \exp(cn^\alpha)$ for IE algorithm.

This suggest that IE is a rather inefficient algorithm for BPs. However, the causes that make IE inefficient are also operative in the much larger class of genetic type algorithms. The high degree of correlations between different samples generated is a common feature of many of these algorithms which employ pruning and enrichment. Whether our results can

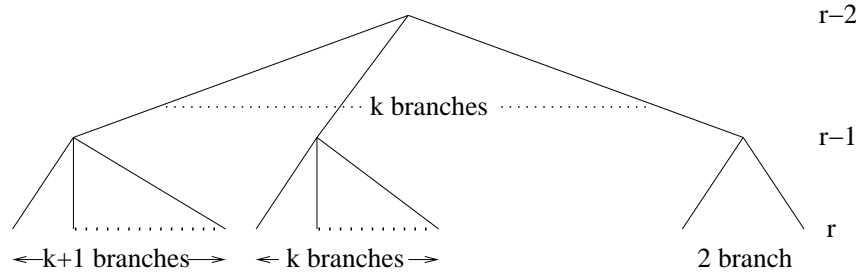


Fig 0.4: A node at level $r - 2$ on the genealogical tree of lattice animal enumeration on a binary tree with k descendants. Here $k \leq (r - 1)$

be generalised to a larger class of PERM type algorithms seems to be an interesting question for further study.

Rooted spiral trees on hyper-cubical lattices

Spiral structures are very common in nature. Some examples of the beautiful spiral structures in galaxies, shoot arrangement in plants, polymers with spiral structure etc may be found in the book by Hargittai [13]. In statistical mechanics, lattice models of spiral self avoiding walks have been studied and can be solved exactly in two dimension [14], though no solution is known for the self avoiding walks without the spiral constraint. For a model of spiral trees on the basis of numerical evidence, and guided by the fact that magnetic field acting perpendicular to motion of a charged particle produces spiralling motion and reduction by two in effective dimensionality, Bose et. al [15] conjectured that the spiral tree problem would show a dimensional reduction by four. They conjectured the exponents of the spiral tree problem follow the relations $\theta = (d - 4)\nu_{pl}$ for $d = 2$ and $\theta = (d - 4)\nu_{\perp}$ for $d > 2$, where θ is the entropic exponent and ν_{pl} and ν_{\perp} are the exponents related to the radius of gyration in the plane in which the tree has a rotational constraint and perpendicular to that plane respectively.

Since then this problem has not been studied further. We revisited the problem and obtained a significantly longer series for rooted spiral trees. Specifically in two dimensions we have added twelve terms to the earlier series of 25 terms. In three and four dimensions we generated a seventeen and a thirteen term series respectively. We also perform MC simulations using the improved incomplete enumeration MC algorithm [8] and generated spiral trees up to sizes of 1000 in two dimensions.

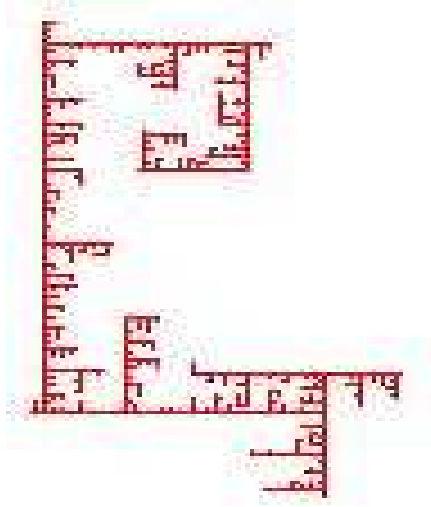


Fig 0.5: Randomly generated spiral tree of 1000 sites in 2-dimensions using incomplete-enumeration MC program

Series expansions give $\lambda = 2.11433 \pm 0.0001$, $\theta = -1.3667 \pm 0.001$ and $2\nu = 1.3148 \pm 0.001$ on a square lattice. With Monte-Carlo simulations we get the estimates as $\lambda = 2.1145 \pm 0.0010$, $\theta = -1.364 \pm 0.01$, and $2\nu = 1.312 \pm 0.02$. Our analysis of exact series and MC samples do not support the conjectured dimensional reduction by four in this problem.

Fig. 0.5 shows picture of a typical spiral trees of one thousand sites. Clearly, their structure is very different from lattice trees without spiral constraint. Because of the constraint they tend to branch much less. One notes very long one dimensional structures with infrequent turns. Hence, simple counting of structures of kind shown in Fig.0.6 should give a good estimate. We determined the generating function of such graphs and found the growth constant λ' of these trees to be 1.93565. This is a rigorous lower bound on λ_{spiral} for spiral trees on a square lattice. Note that our numerical estimate of λ_{spiral} on the square lattice is $\lambda_{spiral} \approx 2.114$.

Bibliography

- [1] P. G. de Gennes, Scaling Concepts in Polymer Physics (Cornell University Press, 1979); P. G. de Gennes 1972, Phys. Lett. A, **38**, 339
- [2] Stauffer and Aharony, Introduction to Percolation Theory 2nd ed. (Taylor and Francis, London 1992)
- [3] C.M. Fortuin and P.W. Kastelyn 1972, Physica, **57**, 536
- [4] G. Parisi and N. Surlas 1981, Phys. Rev. Lett., **46**, 871; D. C. Brydges and J. Z. Imbrie, math-ph/0107005; D. Dhar 1986, Physica A **140**, 210
- [5] Sumedha and Deepak Dhar 2003, J. Phys. A: Math and General, **36**, 3701.
- [6] Sumedha, Directed Branched Polymer near an Attractive Line 2004, J. Phys. A: Math. Gen., Vol. **37**, 3673.
- [7] Sumedha, Rooted Spiral Trees on hypercubical lattices (in preparation)
- [8] Sumedha and Deepak Dhar, Efficiency of Incomplete enumeration for Monte-Carlo simulation of linear and branched polymers, cond-mat/0408640, (submitted to J. Stat. Phys.).
- [9] N. Madras and A. D. Sokal 1988, J. Stat. Phys. **50** 109; E. J. Janse van Rensburg, S. G. Whittington, and N. Madras 1990, J. Phys. A, **23** 1589; P. Grassberger and W. Nadler 2000, cond-mat/0010265, Proceedings der Heraeus-Ferrienschule "Vom Billardtisch bis Monte Carlo: Spielfelder der statistischen Physik", Chemnitz, October 2000; T. Kennedy 2002, J. Stat. Phys. **106** 407-429.
- [10] E. J. Janse van Rensburg and N. Madras, J. Phys. A: Math. Gen. **25** 303-333 (1992); J. Phys. A: Math. Gen. **30** 8035-8066 (1997); E. J. Janse van Rensburg and A. Rechnitzer 2003, Phys. Rev E **67** 0361161-0361169; H. P. Hsu, W. Nadler and P. Grassberger 2004, cond-mat/0408061

-
- [11] D. Dhar 1983, Physical Review Letters **51**, 853
- [12] C Vanderzande 1998, Lattice Models of Polymers, Cambridge Lecture Notes in Physics, Cambridge University Press
- [13] I Hargittai and C A Pickover eds. 1992, Spiral Symmetry, World Scientific, Singapore.
- [14] V Privman, 1983, J. Phys. A:Math. Gen **16** L571; A J Guttmann and N C Wormald , 1984, J. Phys. A:Math. Gen. **17** 271
- [15] I Bose, P Ray and D Dhar 1988, J. Phys. A:Math. Gen **21** L219

Introduction

1.1 Preliminaries

A linear polymer is a large molecule, consisting of a backbone of atoms or group of atoms (called monomers) which are joined in a sequence by covalent bonds. If there are side-groups or side-chains attached to the monomers and if these side chain are also large molecules, then the molecule is a branched polymer [1]. For example, the most important and versatile among the hundreds of commercial plastics is polyethylene. Polyethylene is used in a wide variety of applications because its structure allows it to be produced in many different forms. The low density polyethylene (LDPE) is a branched polymer (Fig. 1.1). It is characterized by a large degree of branching, forcing the molecules to be packed rather loosely forming low density material. LDPE is soft and pliable and has applications ranging from plastic bags, containers, textiles, and electrical insulation, to coatings for packaging materials. Whereas the high density polyethylene (HDPE) (see Fig. 1.1) demonstrates little or no branching, enabling the molecules to be tightly packed. HDPE is much more rigid than LDPE and is used in applications where rigidity is important like plastic tubing, bottles and bottle caps.

An important feature of polymers is the large number of rotational degrees of freedom about the covalent bonds between the monomers. These conformational degrees of freedom make an important entropic contribution to the free energy of the polymer, and have many effects on the chemical and physical properties of the polymer [2, 3]. Even though real polymer molecules live in continuous space and have complicated monomer-monomer interaction, they can be modeled by lattice models like random walk, self avoiding walks and lattice animals. The explanation for these simple models being so successful in describing many of the large scale properties of polymers, lies in the idea of universality [4, 5] which plays a central role in the modern theory of critical phenomena. Critical statistical mechanical systems are divided into a small number of universality classes, which are typically characterized by spatial dimensionality, symmetries and other general properties. In the vicinity

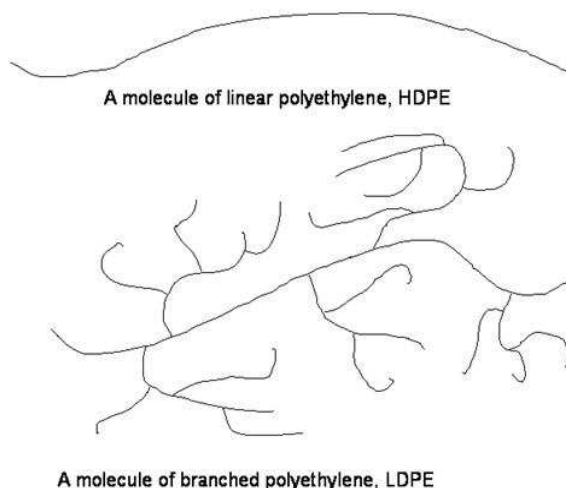


Fig 1.1: Structure of low density and high density polyethylene

of a critical point, the leading asymptotic behaviour is exactly the same for all systems of a given universality class. The details of chemical structure, interaction energies and so forth are completely irrelevant (except for setting the non universal scale factors). Moreover, this universal behaviour is given by simple scaling laws, in which the dependent variables are generalised homogeneous functions of parameters which measure the deviation from criticality. Hence, if we consider a polymer on length scales above the persistence length (the length above which one can ignore correlations present on the monomer level), the large scale properties are independent of molecular details and this universality leads to the hope that they can be captured in lattice models. These models are attempts at representing, in a simple manner, the entropic contribution to the free energy made by the conformational degrees of freedom in these molecules. For example, a lattice random walk has been used as a model of a linear polymer [2]. This model takes into account the contributions of the conformational degrees of freedom to entropy, but fails to explain asymptotic properties of a linear polymer in a good solvent because it ignores the effects of excluded volume, which controls the asymptotic properties of the polymer. Introducing self avoidance, we get a model of self avoiding walks (SAW) and this model is very successful in predicting the large scale structure of linear polymers, it has been studied extensively in the mathematics and physics literature [6]. Similarly, the model of lattice animals (LA), which consists of clusters of connected sites on a lattice, is a natural model for randomly branched polymers [1, 7].

Besides being models of linear and branched polymers respectively, the models of SAW and LA are linked to many other statistical mechanical models as well. The model of SAW

can also be seen as the $n \rightarrow 0$ limit of the n -vector model [8]. Similarly, model of branched polymer has connections with models like percolation [9], Lee-Yang edge singularity [10] and hard core lattice gas [11]. Lattice animals are the $p \rightarrow 0$ limit of the percolation models. Percolation itself is a model of disorder and has very wide applications. It is a special case ($q \rightarrow 1$) of a wider class of models known as q -state Potts models [12].

The models of SAW and LA have been studied vastly in the last many years. Like many other combinatorial problems, these models are easy to state, but remarkably difficult to solve. Some universal properties like critical exponents are known for the SAW problem through conformal invariance in two dimensions [13] and for LA through super-symmetry arguments [10] in two, three and four dimensions. Still, a complete solution has not been possible for SAW and LA on any regular lattice for $d \geq 2$. In this thesis, we study a variant of LA known as directed lattice animals (DA) which is analytically more tractable and capture the essential features of the LA problem. We also study a spiral variant of LA known as spiral trees. Approximate methods, such as perturbation theory and self consistent field theory, typically break down in the long polymer limit. Hence, considerable work has been devoted to developing numerical methods for the study of polymers [14, 15]. We study the efficiency of a particular Monte-Carlo simulation method for linear and branched polymers.

In this chapter we will review the earlier known results and summarize our own results for these problems. The plan of this chapter is as follows: In Section 1.2 we will define the models of SAW and LA. In Section 1.3 we define the model of directed lattice animals and discuss the known results for them. We solved a model of DA in presence of an attractive surface and studied the adsorption-desorption transition. Adsorption-desorption transition of polymers is discussed in Section 1.4. In Section 1.5 we define and discuss the spiral tree problem. In Section 1.6 we give a short outline of popular Monte-Carlo methods used for polymer simulation and describe a particular algorithm, incomplete enumeration (IE), which we have studied, in detail.

1.2 Definition and Notation of Self-avoiding walk and Lattice animals

In this section we will describe the models of self avoiding walk and lattice animals in brief.

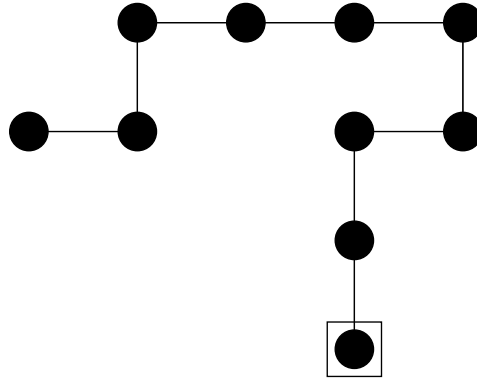


Fig 1.2: Schematic of a SAW with 9 steps on a square lattice. The squared vertex represents the origin.

1.2.1 Self-Avoiding Walk

An N -step self-avoiding walk (SAW) [6] ω on a d -dimensional lattice is defined as a sequence of distinct points $\omega_0, \omega_1, \dots, \omega_N$ such that each point is a nearest neighbour of its predecessor. The number of steps in the walk will be denoted by $|\omega| \equiv N$ (Fig. 1.2). There is nothing special about ω_0 and any of the sites of the lattice can be chosen as the origin. If the walk has to visit a particular point ω_i , then we get rooted SAW's. The walks in which no site is assigned the special status of root are unrooted walks. Hence, the total number of rooted walks of size N are exactly N times the total number of unrooted SAW's. The number (A_N) of possible configurations for N -step unrooted SAW's on a d -dimensional lattice, is exponential in N and is believed to have the asymptotic behavior

$$A_N \sim C\mu^N N^{\gamma-1} \quad (1.1)$$

Here μ is the connective constant of the lattice, C is a constant and γ is a critical exponent. The connective constant is lattice dependent while critical exponents are believed to be universal and hence depend only on the dimension and not on the lattice. On the d -dimensional hyper-cubic lattice for any d , it is easy to derive simple bounds on μ , which are, $d \leq \mu \leq 2d - 1$.

In order to study the thermodynamic properties of the polymers, one has to average over all allowed configurations of the polymer with a given number of monomers. The averages are defined with all configurations considered to be equally likely. For example, one of the important quantities is the average moment of inertia of a polymer of size N . This is the

average squared distance from the origin, averaged over all configurations of N -steps walks. We denote it by R_N^2 . If ω_i represents the site coordinates of the i^{th} point of the walk, then $R_N^2 = \frac{1}{N} \sum_i \langle |\omega_i - \omega_0|^2 \rangle$, where $\langle \rangle$ denotes average over all configurations of SAW.

$$R_N^2 \sim N^{2\nu} \quad (1.2)$$

where ν is a critical exponent.

The upper critical dimension of SAW is four. In dimensions above four, SAW lie in the same universality class as random walks and $\gamma = 1$ and $\nu = 1/2$ for SAW's in $d \geq 4$. The exact value of μ is not known for hyper-cubic lattices in any dimension $d \geq 2$, although for honeycomb lattice in two dimensions it is known to be $\sqrt{2 + \sqrt{2}}$ [16]. Also there is a conjecture for its value on square lattice based on long series expansions [17]. Using sub-multiplicity arguments one can easily show that $A_N \geq \mu^N$ and hence $\gamma \geq 1$ in all dimensions. Also in two dimensions value of critical exponents is known from conformal field theory. In particular, γ and ν are respectively $43/32$ and $3/4$. But still the full expression for the quantities like A_n and R_N^2 for all N , is not known on any regular lattice in $d \geq 2$.

1.2.2 Lattice Animals

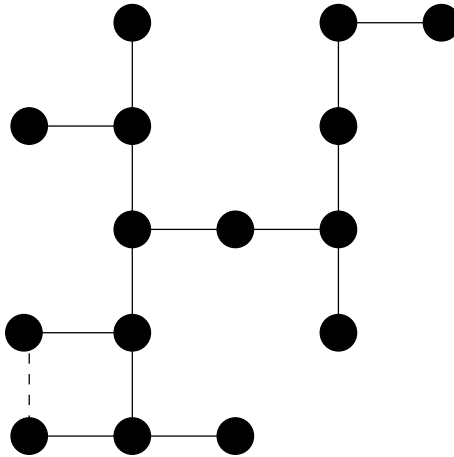


Fig 1.3: The figure shows a lattice site animal of size 15 and lattice bond animal of size 14 on a square lattice. The dashed edge, is present for the site animal but need not be present for the bond animal.

Lattice animals are the connected subgraph of a lattice. If they are specified by the number of sites, they are called site animals and if they are specified by the number of

bonds, they are called bond animals [3]. For a site animal, all edges in between sites of a cluster is always present (Fig 1.3). Hence number of site animals with N sites are always less than the number of bond animals with N bonds on any d -dimensional lattice for $d > 1$. Just like SAW, the number of rooted lattice animals are N times the number of unrooted LAs. Unrooted LAs are expected to have a asymptotic behaviour of the form

$$A_N \sim C\lambda^N N^{-\theta} \quad (1.3)$$

Here again λ is lattice-dependent growth constant and θ is a critical exponent which depends only on the dimension. One can also define the moment of inertia of a LA of size N . The ν for animals is defined by Eq. 1.2. Bond and site animals are believed to lie in the same universality class and hence are believed to have same θ and ν . The growth constant λ is not universal and is different for bond and site animals. A subset of lattice animals with no cycles, are known as bond or site trees. They are also believed to lie in the same universality class, though again λ is different for trees and animals. The existence of growth constant λ for unrooted lattice trees and animals has been proved rigorously using concatenation and super multiplicity arguments [18]. Also a rigorous lower bound for θ for unrooted lattice trees and animals has been proved [19] using the pattern theorem. Specifically, it is $\theta \geq (d-1)/d$, for any dimension $d \geq 2$.

The upper critical dimensions of these models is eight and the mean field exponents are $\theta = 5/2$ and $\nu = 1/4$ [20]. The lattice animals problem has been shown to be related to the Yang-Lee edge problem in two less dimensions. Actually, the exponents θ and ν are not independent here and are related to each other by the hyper-scaling relation

$$\theta = (d-2)\nu + 1, \quad \text{for } d < 8 \quad (1.4)$$

for unrooted lattice animals [21]. Hence $\theta = 1$ in $d = 2$. This model is not conformally invariant [22] and hence the exponent ν is not known in two dimensions. In three dimensions both θ and ν are known through the correspondence with Yang-Lee edge problem in one dimension. In three dimensions $\theta = 3/2$ and $\nu = 1/2$. But again the model of LA has not been solved exactly and the growth constant λ is not known for any regular lattice for $d \geq 2$.

1.2.3 Dimensional Reduction

Lattice animals (or branched polymers) and directed animals (or directed branched polymers) are two important examples of systems showing dimensional reduction (directed animals will be discussed in Sec1.3). Dimensional reduction is an important concept. For the problem of branched polymers, the field theory was formulated by Lubensky and Isaacson [7]. They had also noticed that the first terms in the ϵ -expansion of the critical exponents for dimension d below the upper critical dimension eight, were same as those of the Yang-Lee edge singularity in $d - 2$ dimensions. The Yang-Lee edge problem is the problem of an Ising model in a purely imaginary magnetic field and is described by a scalar field theory with cubic interaction and purely imaginary coupling. Parisi and Sourlas [10] used super-symmetry arguments to support this dimensional reduction by two in lattice animals and conjectured that the branched polymer problem in d dimensions lies in the same universality class as the Yang-Lee edge problem in $d - 2$ dimensions.

Besides this the Yang-Lee edge problem is believed to lie in the same universality as the classical gas with short-range repulsive interaction in the grand canonical ensemble [23]. Hence this relates the branched polymer problem to the universal repulsive gas singularity in $d - 2$ dimensions. This has very recently been proved to be true by Brydges and Imbrie [11].

The directed animal problem similarly shows a dimensional reduction by one and it was shown that the DA problem in $d + 1$ dimension is related to the time development of thermal relaxation of a hard core lattice gas (HCLG) with nearest neighbour exclusion (nne) in d dimension by Dhar [24]. Besides, Cardy [25] had given a relation between DA problem in $d + 1$ dimension and the Yang-Lee edge singularity problem in d dimensions. Hence we have four different problems, closely linked with each other. While correspondence between LA and HCLG with nearest neighbour exclusion and DA and HCLG are known rigorously, correspondence between LA, DA and Yang-Lee edge and hence between Yang-Lee and HCLG is strongly believed to hold but has not been shown rigorously and proving these correspondences is an important open problem.

1.3 Directed Lattice Animals

1.3.1 Definition

Directed animals, just like the lattice animals are connected subgraphs of a lattice, but the bonds are directed in this case. This additional direction leads to many interesting properties like anisotropic scaling and direction dependent critical properties besides making the model lie in a different universality class than LA's. A DA rooted at the origin, is a cluster of connected sites such that any site of the animal can be reached from the root by a walk which never goes opposite to the preferred direction. Fig. 1.4 shows a directed animal on a square lattice in two dimensions. Each site (x, t) has two bonds directed outwards towards the sites $(x + 1, t + 1)$ and $(x - 1, t + 1)$. A directed site animal \mathcal{A} rooted at the origin is a set of occupied sites including origin, such that for each occupied site (x, t) other than the origin, at least one of the two sites $(x - 1, t - 1)$ and $(x + 1, t - 1)$ is also occupied. The origin is the source of the DA shown in Fig. 1.4. One can also define DA's with a source having more than one site along the $t = 0$ line.

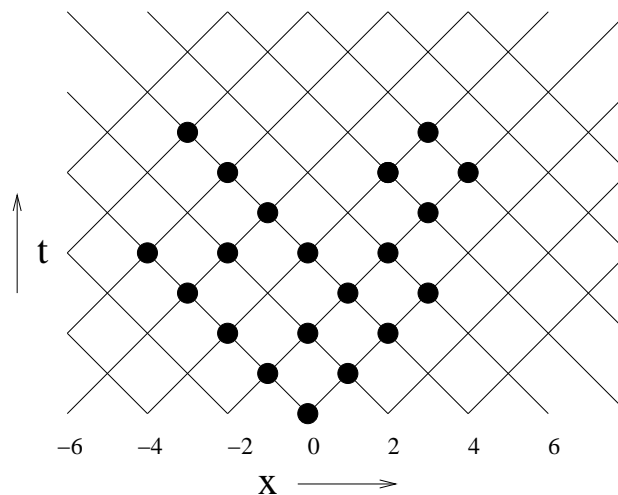


Fig 1.4: Schematic figure of a directed animal of size 20 on a square lattice.

Just like LA, the bond and site directed animals and trees are also believed to lie in the same universality class. The total number of DA, A_N is believed to have the same asymptotic behaviour as Eq. 1.3. But the average mean square displacement of a directed animal scales differently in transverse and longitudinal directions. Hence, instead of a single exponent ν which characterises the shape of LA, there are two critical exponents in DA, ν_{\perp} and ν_{\parallel} . If

R_{\perp} and R_{\parallel} denote the mean square displacement in the transverse and longitudinal planes respectively, then they are expected to scale as

$$R_{\perp} \sim N^{2\nu_{\perp}} \quad (1.5)$$

and

$$R_{\parallel} \sim N^{2\nu_{\parallel}} \quad (1.6)$$

Directed animals have found correspondence with many other lattice models, which makes this problem very interesting to study [26, 27, 28, 29, 30, 31]. The exponents of $(d+2)$ dimensional lattice animals, $(d+1)$ dimensional directed animals and d dimensional hard-core lattice gas at negative activity are related to each other [24, 25]. Besides, the geometrical structure of directed animals describe qualitatively diverse situations such as trees, river networks and dilute polymers in a flowing solvent etc. Directed animals problem is also related to $p \rightarrow 0$ limit of the directed percolation problem [32]. And hence a better understanding of it will also help to understand the directed percolation problem. The DA problem is also related to a recently studied model of quantum gravity [33], and there is an unexpected relation between the number of distinct eigenvalues for the Potts model partition function on strips of width w and the number of directed animals with w sites in two dimensions [34].

1.3.2 Directed animal and Hard core lattice gas problem

From Fig. 1.4 one can easily see that the configurations of occupied sites on the line with fixed t depends only on the configuration on the line $t-1$ for directed animals. Hence, if we take t as the time coordinate of a site, directed animals can be said to have a Markovian property in terms of this variable [35]. Let C be the configuration of occupied sites on the line with a given t and $A_C(z)$ be the sum of weights of all distinct configurations of animals with the given source C . If the weight of an animal of size n is z^n , then we can write

$$A_C(z) = z^{|C|} \left[1 + \sum_{C'} A_{C'}(z) \right] \quad (1.7)$$

where $|C|$ is the number of sites in C and the sum over C' is over all possible configurations of occupied sites at time $t+1$, consistent with C .

Now, consider a discrete time Markov process on a linear chain with stochastic evolution given by the rule: At time $\tau = 0$ all sites below the line $x + y = 0$ on a square lattice are

unoccupied (here x, y are the usual Cartesian co-ordinates on a square lattice). At time τ , sites on the line $x + y = \tau$ are examined for occupancy. If both $(x, y + 1)$ and $(x + 1, y)$ are unoccupied, the site (x, y) is occupied with probability p , otherwise left unoccupied. Then the probability that a site $A \equiv (x, y)$ is eventually occupied is p times the probability that both $A' \equiv (x + 1, y)$ and $A'' \equiv (x, y + 1)$ are empty. That is

$$P_A = p [1 - P_{A'} - P_{A''} + P_{A'A''}] \quad (1.8)$$

which has same form as earlier equation when C consists of a single occupied site. In general, similar equations hold for other sites also and hence we can write

$$A_C(z = -p) = (-1)^{|C|} P_C \quad (1.9)$$

The above lattice gas model is the hard core lattice gas with repulsive interaction. This establishes an equivalence between the DA problem and HCLG with negative fugacity. The above mentioned dynamic rules satisfy detailed balance and the generating function of DA's with a single point source is equivalent to the average density of HCLG with negative fugacity. All the three equations are valid in all dimensions and this correspondence holds in all dimensions.

In this thesis, we study the directed lattice animals problem, extend the correspondence with HCLG and obtained relation between the average number of sites at a given transverse distance \mathbf{x} from the origin for $(d + 1)$ -dimensional directed animals from the density-density correlation function of the lattice gas in d dimensions. Specifically, we relate $\phi(\mathbf{x}, s)$, the average number of sites at a transverse distance \mathbf{x} in the directed animals with s sites in d transverse dimensions, to the two-point correlation function of a lattice gas with nearest neighbor exclusion in d dimensions. For large s , $\phi(\mathbf{x}, s)$ has the scaling form $\frac{s}{R_s^d} f(|\mathbf{x}|/R_s)$, where R_s is the root mean square radius of gyration of animals of s sites. We determine the exact scaling function for $d = 1$ to be $f(r) = \frac{\sqrt{\pi}}{2\sqrt{3}} \text{erfc}(r/\sqrt{3})$. We also show that $\phi(\mathbf{x} = 0, s)$ can be determined in terms of the animals' number generating function of the directed animals. We will discuss these results in Chapter 2.

1.4 Polymers with interaction

Lattice animals and self-avoiding walks as defined in Sec.1.2 define athermal polymers which have no attractive forces acting between monomers. They are models of polymers

in dilute solution in a good solvent. At high temperatures, in the dilute limit, good solvent is a good approximation. But when the temperature is lowered, the effective monomer-monomer interactions become stronger [2]. This self interaction, which is attractive, leads at low enough temperatures to a strong size reduction. This is called the collapsed phase of the polymer. In this phase the polymer collapses to a compact globular shape with its fractal dimension equal to the dimension of the system, i.e. the radius of gyration scales with N as $R_G \sim N^\nu$ with $\nu = 1/d$. The temperature where collapse occurs is known as the θ point (this θ has no connection with the critical exponent θ defined in Eq. 1.3). At this point the polymer actually undergoes a second order transition from a swollen phase whose large scale properties can be characterized by non-interacting lattice models of polymers to the compact phase. In the collapsed phase of the polymer the density of monomers makes a jump as a function of chemical potential i.e. the polymer undergoes a first-order transition. There is actually a line of second order phase transitions and the θ point separates this line of second order transitions from a line of first order ones in the temperature and chemical potential plane. The θ point is hence a tricritical point. In the case of branched polymers, the collapsed phase may be modelled by compact lattice animals, which are animals with no holes. Recently, Wu et. al. have shown that the generating function of compact lattice animals is precisely the reduced partition function of the infinite-states Potts model [36]. Hence depending on the property of interest it is easy to modify the models of SAW and LA. For example, when a polymer is close or even attached to a surface its critical properties may change. When there is an attractive interaction between the monomers and the surface, it can get adsorbed to the surface. Hence the polymer can undergo adsorption-desorption transition as a function of surface-monomer interaction.

1.4.1 Adsorption-Desorption transition in polymers

Adsorption-desorption transition, has important applications in areas ranging from technology such as in lubrication, adhesion, surface protection to biology [2, 37]. For example, adsorbed polymers are used for surface-modification of medical implants [38]. There have been several theoretical studies of the behavior of a polymer near a surface [2, 39, 40, 41, 42, 43]. Especially, the effect of surface for an idealized polymer (with no self-exclusion), modeled by random walks has been studied extensively. There are many exact results known for Gaussian random walks in presence of a surface [44, 45]. In comparison, linear polymers with self exclusion and branched polymers are less well studied. For a self-avoiding walk in the vicinity of a surface the exact critical exponents are known from conformal field theory [13].

Directed polymer chain adsorption, modeled by a directed SAW, is one of the few solvable models of surface effects in 2 and 3 dimensions [41]. For directed walks, self exclusion is automatic, and nontrivial effects of excluded volume interaction are not seen. For branched polymers (modeled by lattice animals), a relation between the exponent characterizing the number of animals, in the presence of surface, and in the bulk is known from conformal invariance and by a simple argument given by De’Bell et. al [13, 46].

The enumeration of directed site animals in $d + 1$ dimensions is related to hard-core lattice gas (HCLG) at negative activity with repulsive interactions in d dimensions and to the Yang-Lee edge problem in d dimensions [11, 24, 23, 47]. In Chapter3 of this thesis we study the adsorption-desorption phase transition of the directed branched polymer in $d + 1$ dimensions in contact with a line by mapping it to a d dimensional hard core lattice gas at negative activity. We solve the model exactly in $1 + 1$ dimensions, and calculate the crossover exponent related to fraction of monomers adsorbed at the critical point of surface transition, and we also determine the density profile of the polymer in different phases. We also obtain the value of crossover exponent in $2 + 1$ dimensions and give the scaling function of the sticking fraction for $1 + 1$ and $2 + 1$ dimensional directed branched polymer.

1.5 Spiral Trees

Spiral structures are very common in nature. Some examples of the beautiful spiral structures in galaxies, shoot arrangements in plants, polymers with spiral structure etc may be found in the book by Hargittai [48]. In an attempt to understand the spiral structures, spiral models of SAW and LA have been defined and studied. In the presence of spiral constraint, a SAW or a LA can grow either in the same direction as it has been growing in or inturn or branch out in a specific rotational direction.

Lattice models of spiral self avoiding walk (SSAW) have been studied and solved exactly in two dimensions for square and triangular lattices by mapping them to the combinatorial problem of the number of partitions of an integer N [49, 50]. In the asymptotic limit, the number of partitions is known from the work by Hardy and Ramanujam [51, 52]. For a square lattice the number of SSAW of size $N(A_N)$ in the asymptotic regime is given by

$$A_N = CN^{\frac{-7}{4}} \exp \left[2\pi \left(\frac{N}{3} \right)^{\frac{1}{2}} \right] \quad (1.10)$$

where $C = \frac{\pi}{4 \times 3^{5/4}}$. Hence we see that the rotational constraint has a non trivial effect on the

scaling form of SAW and in fact the general form conjectured for SAW in Eq. 1.1 does not hold for SSAW. Instead of exponential growth with the size of the walk, one sees a stretched exponential growth. In contrast to SSAW, no exact solution is known for the problem of SAW's on any regular lattice with $d \geq 2$.

In this thesis we study a lattice model of spiral trees using numerical techniques in 2, 3 and 4 dimensions. Spiral trees are a subclass of lattice trees. In a tree every cluster site is attached to the origin through a unique path. In a spiral tree, this path has a specific rotational constraint. A model of spiral trees and animals was proposed by Li and Zhou [53], which, based on numerical studies, was suggested to be in a new universality class.

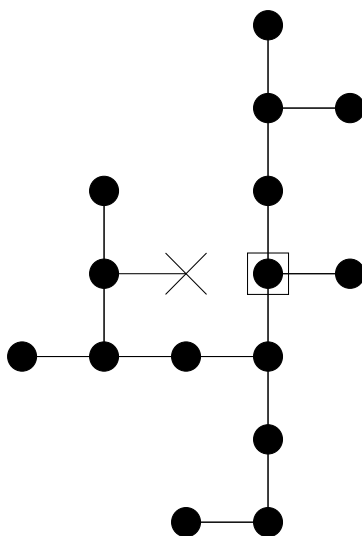


Fig 1.5: A rooted spiral tree of 15 sites on a square lattice. The root is the site enclosed in the square. At the root site the tree is free to choose any of the four neighbouring sites. We count the spiral tree by number of sites and hence all bonds between two occupied sites is always assumed to be present. The site marked by X , if present will result in a loop for spiral site trees and hence will not be allowed. But it can be present in a spiral bond tree.

We define a rooted spiral tree as an acyclic connected subgraph of a lattice such that the projection to the $x - y$ plane of the path joining any site of the tree to the root contains no left turn (Fig. 1.5). We will measure the size of a spiral tree by the number of sites present in the tree. These are called spiral site trees. The number of possibilities for spiral bond trees are more than that for spiral site trees but both are supposed to lie in the same universality class. The total number of distinct rooted spiral trees, A_N is expected to have a asymptotic behaviour of the form given in Eq. 1.3. Spiral trees are a subset of lattice trees, and clearly, $\lambda_{spiral} \leq \lambda_{all}$, where λ_{all} is the growth constant for all trees, $\lambda_{all} \approx 3.795$ on a square lattice [55].

For the conventional lattice animals, one can prove $\theta \geq 0$ through concatenation and super-multiplicity arguments [18, 19]. Concatenation does not work for spiral trees. Interestingly, our numerical studies give a negative value of θ in two and three dimensions.

The spiral trees are anisotropic. We measure the average extent of a N -site spiral tree in the $x - y$ plane and perpendicular to the $x - y$ plane through the moment of inertia tensors, $I_{pl,N}$ and $I_{\perp,N}$ respectively. In the asymptotic limit, they are expected to vary as

$$I_{pl,N} \sim AN^{2\nu_{pl}+1} \quad (1.11)$$

and

$$I_{\perp,N} \sim AN^{2\nu_{\perp}+1} \quad (1.12)$$

where ν_{pl} and ν_{\perp} define the length scale of the spiral tree in the planar and perpendicular direction respectively.

Based on numerical evidence, and guided by the fact that a magnetic field acting perpendicular to the motion of a charged particle produces spiralling motion and reduction by two in effective dimensionality, Bose et. al [54] conjectured that the spiral tree problem would show a dimensional reduction by four, and the exponents of the spiral tree problem would follow the following relations:

$$\theta = (d - 4)\nu_{pl} \text{ for } d = 2 \quad (1.13)$$

$$\theta = (d - 4)\nu_{\perp} \text{ for } d > 2 \quad (1.14)$$

where θ is the entropic exponent and ν_{pl} and ν_{\perp} are the exponents related to the radius of gyration in the plane in which the tree has a rotational constraint and perpendicular to that plane respectively.

Since then this problem has not been studied further. Dimensional reduction is an intriguing possibility. The lattice tree model without spiral constraint is known to show a dimensional reduction by two (Sec. 1.2.3). The directed version, show a dimensional reduction by one. For both models, the tree and animals are believed to lie in the same universality class. In this thesis, we revisit the problem and obtain a significantly longer series for rooted spiral trees. Specifically in two dimensions we have added twelve terms to the earlier series of 25 terms. In three and four dimensions, we generated a seventeen and a thirteen term series respectively. The earlier known series in three and four dimensions had thirteen and nine terms respectively. In the process, we also correct some mistakes in the earlier reported

series. We also perform Monte-Carlo (MC) simulations using the improved incomplete enumeration algorithm (Sec 1.6) and generate spiral trees up to sizes of 1000 in two dimensions. Our analysis of the exact series and the MC samples does not support the conjectured dimensional reduction by four in this problem. We also derived in two dimensions, the generating function for enumeration of a subset of all possible spiral trees and give a non trivial lower bound on the growth constant of rooted spiral trees on a square lattice. Our results for the spiral tree problem are discussed in Chapter 5.

1.6 Monte Carlo simulations of polymers

Numerical methods are important for studying polymers, as exact results are hard to come by and are available only for the simplest models. The numerical methods used for polymer problems essentially lie in two classes: exact enumeration and Monte Carlo (MC) simulation.

An exact enumeration algorithm generates all the possible configurations of the polymer up to certain length. But since the number of configurations grow exponentially with polymer size, the computational complexity of the algorithm for enumeration of all configurations increases exponentially with the size of the polymer. Hence, usually the largest polymer studied using this has size between 10 to 100. One then performs an extrapolation to the limit $N \rightarrow \infty$, using techniques such as the ratio method, Pade approximants etc. Sometimes one can exploit the symmetry of the problem and in that case one need to count only a subset of all configurations. This subset still grows exponentially in most of the problems. For example, for self avoiding polygons, Enting [56] developed a method based on transfer matrices known as finite lattice method. This has been improved a lot by many modifications over the years and very recently SAW's up to size 71 on the square lattice, have been enumerated [57].

In contrast, using Monte-Carlo methods we can probe much larger polymer sizes ($N \approx 10^3 - 10^5$). A Monte-Carlo simulation is actually a computer experiment which generates a random sample. Repeating many times one obtains many random samples and then one uses statistical techniques to obtain an estimate of the desired quantity. Hence MC simulations are just like laboratory experiments and contain statistical errors. By now there are many excellent books dealing with the subject. For example, for application of MC techniques to polymers see [14, 15].

Broadly speaking, MC algorithms fall in two classes [15]: the Metropolis type and the genetic type. The Metropolis type algorithms generate a time sequence of configurations of

the polymer using a Markovian evolution. The transition probabilities from one configuration to the next are so chosen that the time average of properties of the system are equal to that from the desired distribution. These may use local moves as in Rouse dynamics [58], bi-local moves as in the reptation algorithm [59] or nonlocal moves as in the pivot [60] and cut-and-paste [61] algorithms. There is inevitably some correlation between different configurations generated in an evolution. These algorithms become inefficient if the correlation time becomes very large, eg. simulating polymers in a random medium.

In the genetic algorithms, one randomly generates a small random number of configurations in each run. The probability that a given configuration is obtained in a run is proportional to the desired distribution. One repeats the process for many runs to get a large sample. Examples of this type are, the enrichment [62] and the pruned-enriched Rosenbluth method (PERM)-like [63] algorithms. We studied a algorithm called Incomplete enumeration (IE) in this thesis which falls in this class.

While there have been many studies of linear polymers using various Monte-Carlo techniques like pivot [60, 64, 65], PERM [63], Berreti-Sokal algorithm [66], branched polymers have been less studied. Algorithms used for simulating linear polymers can often be adapted for branched polymers, but they are usually found to be less efficient. For example, in the pivot algorithm, the acceptance probability of the transformed configuration is found to be much less for branched polymers than for linear polymers [67]. The algorithm does not perform well for branched polymers adsorbed on a surface[68]. The PERM algorithm also seems to work less well for branched polymers than for linear polymers [69].

A better understanding of the efficiency of Monte Carlo algorithms for generating branched polymers is desirable. We have studied IE for linear and branched polymers in Chapter 4 of this thesis. In the next few sections we will describe some of these algorithms.

1.6.1 Dynamic MC methods

A critical step in developing an efficient MC algorithm is the simulation (sampling) from an appropriate probability distribution $\pi(x)$. Dynamic algorithms produce statistically correlated samples based on the idea of Markov chain Monte-Carlo sampling. For a simulation to converge on the correct probability density, the move should be ergodic which means that any configuration should be reached by any other configuration by a finite number of elementary moves of the algorithm. Also, the transition rates should satisfy detailed balance. The moves chosen can be bilocal or non local. In the last few years, there has been lots of

emphasis on non local move Markov chain based algorithms like the pivot. But it should be realised that it is often difficult to find valid nonlocal moves which are useful. There are two main reasons for this. Firstly, since a nonlocal move is very radical, the proposed configurations usually violate the constraints of the problem (like self avoiding constraint of SAW). It is therefore a nontrivial problem to invent a non local move whose acceptance probability does not go to zero too rapidly as $N \rightarrow \infty$. Secondly, a non local move usually costs a CPU time which depends on N . The two broad types of useful non local moves known at present are the pivot moves [60] and the cut and paste moves [61]. The algorithms employing non local moves might turn out to be good to study properties like radius of gyration of polymers in dilute systems, but it is less easy to estimate entropies with pivot like algorithm, and it becomes inefficient in dense or constrained systems where most of the global moves are forbidden. We will not discuss these algorithms any further and just mention that the pivot algorithm is considered the most successful algorithm for SAW till now [65]. For lattice animals also non-local move dynamical algorithms have been devised, but whereas one can generate SAW's of lengths up to lakhs with present algorithms, one can study lattice animals of sizes of order thousands only.

1.6.2 Importance Sampling

In most statistical mechanics problems simple sampling (generating independent samples directly from a desired distribution) is highly inefficient. Hence one has to either use the Markov chain MC (see Sec. 1.6.1) or importance sampling. We describe the latter in this section. In importance sampling strategy, random samples are generated from a trial distribution different from (but close to) the target one and then weighted according to the importance ratio. Still it is non-trivial to design a good trial distribution for doing importance sampling. One of the most useful strategies in these problems is to build up the trial distribution sequentially. This is known as sequential importance sampling (SIS) and the importance weights are computed recursively [70]. This strategy was first applied by Rosenbluth and Rosenbluth [71] for SAW's. It was basically an 'inverted restricted sampling' or 'biased sampling' algorithm. Its a stochastic growth algorithm in which the next step of the SAW is chosen randomly from all those possible next steps which do not lead to self-intersection. This generates different N step SAW's with different probabilities and a weight which is inverse of probability of generation of a given SAW is assigned to each SAW. This algorithm has two limitations

1. The weights vary widely in magnitude and hence the mean becomes dominated by very few samples with very large weights.
2. Regularly occurring trapping events, i.e. generation of configurations with no allowed neighbours for the next step, lead to exponential attrition.

This algorithm has been modified in recent times and used to great effect by Grassberger et al [63]. Their algorithm is known as the pruned-enriched Rosenbluth method (PERM) whose basic idea is to suppress large fluctuations in the weights of the configurations generated. The algorithm demands choosing pruning and enriching criterion. Basically one chooses two cutoffs for the weights, W_n^+ and W_n^- . Whenever the weight W_n is larger than W_n^+ , double the configuration and assign a weight which is half of the original weight to each copy. This is the enrichment step. Similarly, prune the sample by retaining every configuration with weight less than W_n^- with probability half after doubling its weight.

Actually PERM can be seen as a random walk in chain length with reflecting boundaries at $n = 0$ and $n = N$. While normal evolution steps correspond to forward steps in n , pruning events correspond to backward jumps at the last cloning time. The thresholds of pruning and cloning should be such that the number of configurations generated at step n should be independent of n as if it increase with n , that would imply that all configurations are descendants of only few ancestors and hence are strongly correlated. PERM has been successfully used to generate SAW's of $O(10^5)$ [72] and for the problem of collapse of linear polymers [73]. But PERM as described above fails badly for lattice animals or trees [69]. Recently, a new implementation of PERM has been developed for the problem of LA, which works better, but still one could generate samples of sizes of $O(10^3)$ only, using this algorithm.

1.6.3 Incomplete Enumeration

Incomplete Enumeration (IE) [74, 75, 76] is an important sampling algorithm which has naturally built in cut-off for pruning and enrichment, and is very simple to implement.

The IE algorithm is a simple modification of an exact enumeration algorithm for generating polymers. A good exact enumeration algorithm generates all possible configurations exactly once [77]. This is ensured by defining a rule which, given an n -site configuration of a polymer, identifies uniquely one of these sites as the 'last added site'. Removing this site must result in an allowed polymer configuration of $(n - 1)$ sites. The $(n - 1)$ site polymer

is called the parent of the n -site configuration. We start by arranging all configurations in a genealogical tree, whose nodes are the different configurations of the polymer, such that all polymer configurations of n sites are at level n and are connected to their parent at level $(n - 1)$. Clearly, the tree depends on the rule used to define parenthood. For example, Fig. 1.6 shows a genealogical tree for directed lattice animals on a square lattice for $n \leq 4$, using one such choice.

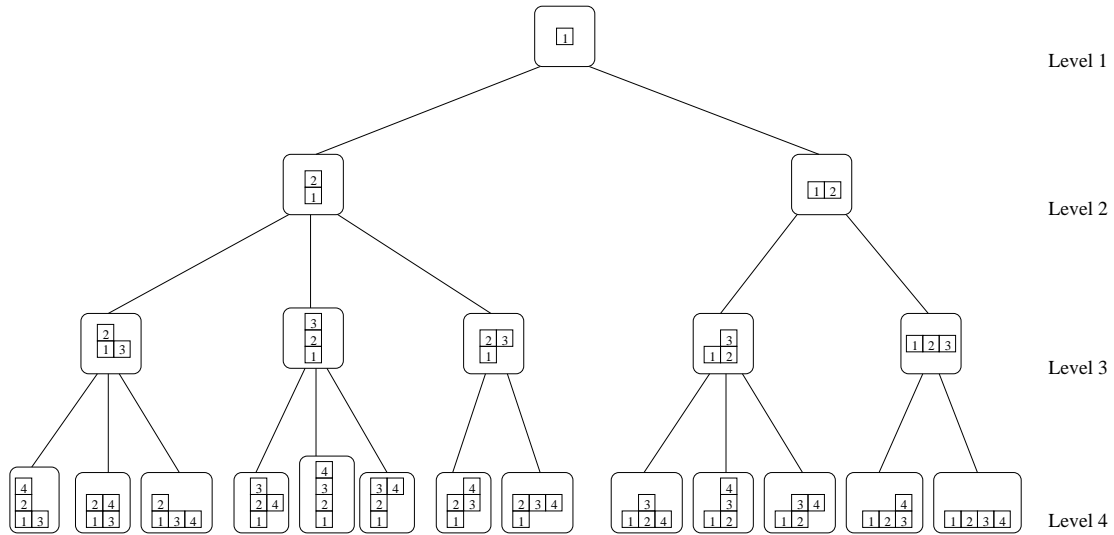


Fig 1.6: An example of a genealogical tree. The numbers labelling the sites indicate the order in which they are added (1 represents the root site). The tree shown is for directed lattice animals on a square lattice.

Since the number of configurations of polymer of size n increases exponentially with n , the time required to construct the genealogical tree up-to level n in the exact enumeration algorithm increases exponentially with n . The basic idea of the IE algorithm is to decrease this time by randomly pruning the genealogical tree.

In IE we choose a set of $(n - 1)$ real numbers p_i ($0 < p_i \leq 1$), for $i = 1$ to $(n - 1)$. Any bond in the genealogical tree connecting level r to level $(r + 1)$ is removed with a probability $(1 - p_r)$ independent of the other bonds. If a configuration gets disconnected from the root node, automatically all its descendants are also removed. We make a depth first search of the pruned genealogical tree up-to depth n to determine the different configurations that remain at level n . Pruning is decided as we go along in the depth-first search and hence memory requirement of this algorithm is just of $O(n)$. We run the algorithm several times to generate a large sample. The probability of enumeration of a particular r site configuration in a given

run is

$$\Xi_r = \prod_{i=1}^{i=r-1} p_i \quad (1.15)$$

This is same for all configurations of size r . This ensures that the sample of configurations obtained is unbiased. As a configuration can occur at most once in a single MC run, IE samples the population without replacement.

The different runs are mutually uncorrelated. However, the number of configurations produced within one run varies from run to run, and different configurations produced in the same run are correlated. Also, the fraction of runs generating configurations of size n goes down with increasing n .

In case of SAW's which model linear polymers, there is a natural labelling scheme in which one just labels the first point of the walk by 1, the second by 2 and so on. In case of branched polymers there are several different choices of labelling possible because one can generate a $(n - 1)$ site configuration by deleting any of the perimeter sites of the n -site configuration. We have used Martin's labelling scheme [77] for our cluster counting algorithms. Here we describe his algorithm for labelling a n -cluster briefly.

- Choose a rule for ordering the neighbours of any given site. For example, for DA on a square lattice (Fig. 1.6), we chose the rule that the upward neighbour is labelled before the right neighbour.
- We label the root as 1 and its neighbours are labelled 2, 3, 4.... in the order according to the priority rule.
- When all points adjacent to point 1 have been labelled, label any yet unlabelled points adjacent to point 2 according to the priority rule and then of point 3 and so on. This labeling hence induces a tree structure on the cluster which is the genealogical tree.

The labelling described above is just one way of labelling the configurations. One can invent many other labelling schemes, which would give rise to different genealogical trees. But we find that the nature of genealogical tree is qualitatively similar for different labelling schemes.

In this thesis, we have studied this algorithm for linear and branched polymers. We find the time to generate effectively one configuration of size n goes as $O(n^2)$ for SAW independent of dimensions. The performance of the algorithm is comparable to other successful

algorithms for generating SAW's. For branched polymers we find that this time instead shows a super-polynomial behaviour and goes as $\exp(n^\alpha)$, $0 < \alpha < 1$. We have made an improvement on this algorithm which we call Improved Incomplete enumeration (IIE). All this is dealt with, in Chapter 4 of this thesis.

Distribution of transverse distances in directed animals

In this chapter, we extend the known relation between the directed site animals enumeration (DSAE) problem and the hard-core lattice gases at negative activity, to obtain the average number of sites at a given transverse distance \mathbf{x} from the origin for $d + 1$ -dimensional directed animals from the density-density correlation function of the lattice gas in d dimensions [78]. This is discussed in Section 2.1. In Section 2.2, for $d = 1$, using the known simple exponential form of the lattice gas correlation function, we determine the scaling form for the average number of sites at a given transverse distance in a $1 + 1$ -dimensional directed animal having s sites, for large s . The average transverse size of the animal scales as $s^{\nu_{\perp}}$, where ν_{\perp} is known to be $\frac{1}{2}$ for $d = 1$. For large s , the average value of q -th transverse moment $\langle |x|^q \rangle$ varies as $R_s^q C_q$, where R_s is the root mean square radius of gyration of animals of s sites. Using the exact scaling function we are able to determine the universal constants C_q for all q . In Section 2.3 we derive the scaling function for DA on the Bethe lattice and in Section 2.4 we describe and solve a model of generalised DAs.

2.1 Relation between transverse size distribution generating function and hard core lattice gas density-density correlation function

We will denote the number of sites in a DA \mathcal{A} by $|\mathcal{A}|$ or s . Also, we define $n(x|\mathcal{A})$ as the number of sites of \mathcal{A} having the transverse coordinate x . For example, for the DA of 20 sites shown in Fig. 1.3, $n(x|\mathcal{A})$ takes the values 1, 3 and 0 for x equal to $-4, 2, 5$ respectively, with $|\mathcal{A}| = 20$. We shall define the radius of gyration¹ of \mathcal{A} as $\sqrt{\frac{1}{s} \sum x^2}$, where the sum is

¹In general the radius of gyration of a polymer is defined about a point (root), but here for the DA problem we define it about the preferred axis.

over all sites of the animal. For example, the animal shown in Fig. 1.3, has a squared radius of gyration $21/4$.

We define the generating function $A(y)$ by

$$A(y) = \sum_{\mathcal{A}} y^{|\mathcal{A}|} = \sum_{s=1}^{\infty} A_s y^s \quad (2.1)$$

For large s , A_s varies as $\lambda^s s^{-\theta}$, where θ is a critical exponent. The radius of gyration R_s is expected to vary as $s^{\nu_{\perp}}$, where the exponent ν_{\perp} is related to the animals number exponent θ by the hyper-scaling relation $\theta = d\nu_{\perp}$ [21].

For a directed animal of size s we define the generating function $\Psi(\mathbf{x}; y)$ as

$$\Psi(\mathbf{x}; y) = \sum_{\mathcal{A}} n(\mathbf{x}|\mathcal{A}) y^{|\mathcal{A}|} \quad (2.2)$$

where the summation over \mathcal{A} is the summation over all animal configurations. This can be written as

$$\Psi(\mathbf{x}; y) = \sum_s \phi(\mathbf{x}, s) A_s y^s \quad (2.3)$$

where $\phi(\mathbf{x}, s)$ is the value of $n(\mathbf{x}, \mathcal{A})$ averaged over all animals \mathcal{A} of size s .

The DSAE problem in $d + 1$ -dimensions is related to the time development of thermal relaxation of a hard core lattice gas (HCLG) with nearest neighbor exclusion on d dimensional lattice [24]. On a d dimensional body-centered hyper-cubical lattice, the dynamics of the lattice gas is defined as follows: The evolution is a stochastic discrete-time Markovian. At odd(even) times, all the odd(even) sites are examined in parallel, and if a site has all neighbors empty, it's occupation number is set to 1 with probability p , and to 0 with probability $(1 - p)$. The rates of transition satisfy the detailed balance condition corresponding to the Hamiltonian

$$H = +\infty \sum_{\langle ij \rangle} n_i n_j - (\ln z) \sum_i n_i \quad (2.4)$$

with $z = p/(1 - p)$.

Let $\rho(p)$ be the average density of particles in the steady state of this system. In [24], it was shown that we have

$$A(y) = -\rho(p = -y) \quad (2.5)$$

For the $d = 1$ nearest-neighbor-exclusion lattice gas, it is straight forward to determine the average density. It comes out to be

$$\rho(z) = \frac{1}{2} \left(1 - \sqrt{\frac{1}{1-4z}} \right) \quad (2.6)$$

Substituting $z = p/(1-p)$, and then $p = -y$ we get the animal number generating function on the square lattice to be

$$A(y) = -\frac{1}{2} \left[1 - \sqrt{\left(\frac{1+y}{1-3y} \right)} \right] \quad (2.7)$$

The animal numbers A_s , which are the coefficients in the Taylor expansion of $A(y)$ for square lattice can be written as [26]

$$A_s = \int_0^{2\pi} \frac{d\theta}{2\pi} (1 + \cos\theta)(1 + 2\cos\theta)^{s-1}. \quad (2.8)$$

For large s , $A_s \sim \frac{1}{\sqrt{3\pi}} 3^s s^{-\frac{1}{2}}$, which shows that in this case $\lambda = 3$, and $\theta = 1/2$.

The derivation of Eq.(2.5) is easily generalized to the case where the values of p at different sites are different. Let the probability that site i gets occupied at time $t + 1$ given that all its neighbors are unoccupied at time t be p_i . Then the rates of this process still satisfy the detailed balance condition corresponding to the Hamiltonian

$$H = +\infty \sum_{\langle ij \rangle} n_i n_j - \sum_i (\ln z_i) n_i \quad (2.9)$$

where $z_i = p_i/(1-p_i)$. The probability that site i is occupied in the steady state depends on the p_j 's for all sites j , and will be denoted by $\rho_i(\{p_j\})$. In the corresponding DA problem, we have to define the weight of an animal \mathcal{A} as the product of the weights of all occupied sites, the weight corresponding to a site with \mathbf{x} -coordinate j being y_j . Then define $A_i(\{y_j\})$ to be the sum of weights of all animals rooted at i . Then clearly $A_i(\{y_j\})$ is a formal power series in the variables $\{y_j\}$. If all $y_j = y$, this becomes independent of i , and reduces to the function $A(y)$. For unequal y_j 's, Eq.(2.5) becomes

$$A_i(\{y_j\}) = -\rho_i(\{p_j = -y_j\}) \quad (2.10)$$

Applying the operator $y_{\mathbf{x}} \frac{\partial}{\partial y_{\mathbf{x}}}$ on the weight of any particular animal, we get the weight

multiplied by the number of occupied sites with transverse coordinate \mathbf{x} in the animal. Thus,

$$y_{\mathbf{x}} \frac{\partial}{\partial y_{\mathbf{x}}} A_0(\{y_j\})|_{\{y_j=y\}} = \Psi(\mathbf{x}; y) \quad (2.11)$$

Let $\Omega(\{z_j\})$ be the grand partition function for the HCLG given by the Hamiltonian in Eq. (2.9) with $z_j = p_j/(1 - p_j)$. Then, $\Omega(\{z_j\})$ is a linear function of each of the variables z_j . Let η_j be the indicator variable taking value 1 if the site j is occupied, and 0 if not. The density-density correlation function of the gas $G(\mathbf{i}, \mathbf{k})$ is defined as

$$G(\mathbf{i}, \mathbf{k}; \{z_j\}) = \langle \eta_{\mathbf{k}} \eta_{\mathbf{i}} \rangle - \langle \eta_{\mathbf{k}} \rangle \langle \eta_{\mathbf{i}} \rangle = z_{\mathbf{k}} \frac{\partial}{\partial z_{\mathbf{k}}} \rho_{\mathbf{i}}(\{z_j\}). \quad (2.12)$$

When $z_j = z$ for all j , the correlation function depends only on $(\mathbf{i} - \mathbf{k})$ and hence can be written as $G(\mathbf{i} - \mathbf{k}; z)$.

Now, using Eq.(2.10), we get

$$\Psi(\mathbf{x}; y) = -\frac{1}{1+y} G\left(\mathbf{x}; z = -\frac{y}{1+y}\right) \quad (2.13)$$

This equation relates the pair correlation function $G(\mathbf{x}; z)$ of the HCLG with the function $\Psi(\mathbf{x}; y)$ which gives the density profile of the DA problem in all dimensions.

2.2 Directed Animals on a square lattice

For the special case $d = 1$, it is a simple exercise to calculate $G(x; z)$ explicitly, using transfer matrix methods [79]. This gives

$$G(x; z) = \frac{z}{1+4z} \left[\frac{1 - \sqrt{1-4z}}{1 + \sqrt{1+4z}} \right]^{|x|} \quad (2.14)$$

and we get the explicit expression for $\Psi(x; y)$ on square lattice to be

$$\Psi(x; y) = \frac{y}{(1+y)(1-3y)} \left[1 - \sqrt{\frac{1-3y}{1+y}} \right]^{|x|} \left[1 + \sqrt{\frac{1-3y}{1+y}} \right]^{-|x|} \quad (2.15)$$

This determines the density profile in the constant fugacity ensemble, where an animal having s sites has weight y^s . However, it is more instructive to look at the profile in the constant- s ensemble. This is obtained by looking at the Taylor coefficient of y^s in the above

equation. This can become rather messy. However, the behavior for large s can be determined easily.

In general, for any dimension d , for large s , $\phi(\mathbf{x}, s)$ has the scaling form

$$\phi(\mathbf{x}, s) \sim \frac{s}{R_s^d} f\left(\frac{|\mathbf{x}|}{R_s}\right) \quad (2.16)$$

Usually the argument of the scaling function is defined only upto a multiplicative constant. We have made specific choice for this by using the variable as $|\mathbf{x}|/R_s$. The normalization of scaling function $f(r)$ is chosen such that it satisfies

$$\int_{-\infty}^{\infty} d^d \mathbf{x} f(|\mathbf{x}|) = 1 \quad (2.17)$$

$$\int_{-\infty}^{\infty} d^d \mathbf{x} |\mathbf{x}|^2 f(|\mathbf{x}|) = 1 \quad (2.18)$$

In the DA problem, since the number of animals grow as λ^s , the series expansions for $\Psi(\mathbf{x}; y)$ or $A(y)$ in powers of y converge for $y < y_c = 1/\lambda$. For y near y_c , the singular part of the function $A(y)$ varies as $(1 - y\lambda)^{\theta-1}$. For the HCLG problem, this corresponds to a singularity in the series for the density ρ in powers of activity for the activity $z_{LY} = -(1 + \lambda)^{-1}$ [Eq. (2.13)]. This singularity on the negative real line is the Lee-Yang edge singularity for this problem.

For z near the critical value $z = z_{LY}$, this correlation function $G(\mathbf{x}; z)$ is expected to have the scaling form

$$G(\mathbf{x}; z = z_{LY} e^{-\epsilon}) = c \epsilon^{-a} g(b|\mathbf{x}|\epsilon^\nu) + \text{higher order terms in } \epsilon \quad (2.19)$$

where b and c are non-universal, lattice dependent constants. We choose b such that $g(\xi) = \exp(-\xi)$ for large ξ , and c is fixed by requiring $g(0) = 1$.

The scaling function $g(\xi)$ tends to a constant limiting value as ξ tends to zero, and decreases to zero exponentially fast as ξ tends to infinity. Let the power-series expansion of $g(\xi)$ about $\xi = 0$ be given by

$$g(\xi) = \sum_{k=0}^{\infty} g_k \xi^k \quad (2.20)$$

Substituting this in Eq.(2.19), we get

$$G(\mathbf{x}; z) \sim \sum_{k=0}^{\infty} g_k b^k |\mathbf{x}|^k \left(1 - \frac{z}{z_{LY}}\right)^{\nu k - a} \quad (2.21)$$

To get $\phi(\mathbf{x}, s)$, we need to determine the coefficient of z^s in the above expansion. From the binomial expansion of $(1 - \frac{z}{z_{LY}})^{\nu k - a}$ we immediately get

$$G(\mathbf{x}; z) \sim \sum_{s=0}^{\infty} \left(\frac{z}{z_{LY}} \right)^s \sum_{k=0}^{\infty} g_k b^k |\mathbf{x}|^k \frac{\Gamma(a + s - \nu k)}{\Gamma(s + 1) \Gamma(a - \nu k)} \quad (2.22)$$

For fixed k , for large s , we have

$$\frac{\Gamma(s + a - \nu k)}{\Gamma(s + 1)} \rightarrow s^{a-1-\nu k} \quad (2.23)$$

Using this in Eq.(2.22), we get

$$f(|\mathbf{x}| s^{-\nu \perp}) = \sum_{k=0}^{\infty} g_k \left(\frac{|\mathbf{x}|}{s^\nu} \right)^k \frac{1}{\Gamma(a - \nu k)} \quad (2.24)$$

where the correlation length exponent ν for the HCLG problem is the same as the transverse size exponent ν_\perp for directed animals.

For $d = 1$, it is easy to determine $G(x; z)$ explicitly. In this case, using Eq.(2.14) we get the scaling form for $G(x; z)$ as

$$G(x; \epsilon) = \frac{1}{4\epsilon} \exp(-2x\sqrt{\epsilon}) \quad (2.25)$$

so that $a = 1$, $\nu = 1/2$, $b = 2$ and $c = 1/4$. The scaling function $g(\xi)$ is simply given by

$$g(\xi) = \exp[-\xi] \quad (2.26)$$

hence $g_k = 1/\Gamma[k + 1]$. Using this, and the values of a and ν in Eq.(2.24) we get the leading singular behavior of $\phi(x, s)A_s$ on a square lattice to be

$$\phi(x, s)A_s = \frac{1}{4} y_c^{-s} \sum_{k=0}^{\infty} \frac{(-\frac{\sqrt{3}x}{\sqrt{s}})^k}{\Gamma(k + 1)} \frac{1}{\Gamma(1 - \frac{k}{2})} \quad (2.27)$$

Since $\Gamma(1 - \frac{k}{2})$ has poles when k is an even integer, only the odd terms contribute to the sum. The resulting series is easy to sum explicitly, giving

$$\phi(x, s)A_s = \frac{1}{4} 3^s \operatorname{erfc} \left(\frac{\sqrt{3}x}{2\sqrt{s}} \right) + \text{correction to scaling terms} \quad (2.28)$$

where $\operatorname{erfc}(x) = \frac{2}{\sqrt{\pi}} \int_x^\infty e^{-x^2} dx$.

This gives $\phi(x, s)$ for large s to be

$$\phi(x, s) = \frac{\sqrt{3\pi s}}{4} \operatorname{erfc}\left(\frac{\sqrt{3}x}{2\sqrt{s}}\right) + \text{correction to scaling terms} \quad (2.29)$$

From $\phi(x, s)$ we can as well derive the expression for q th transverse moment of the directed animals. The q th transverse moment of a cluster of size s denoted by μ_{qs} is defined as

$$\mu_{qs} = \sum_{i=-s}^s \phi(i, s) |i|^q \quad (2.30)$$

Using the scaling form of $\phi(i, s)$, for large s , we see that (μ_{qs}/sR_s^q) is a universal constant. Denoting it by C_q , we get

$$\frac{\mu_{qs}}{sR_s^q} = C_q = \int_{-\infty}^{\infty} d^d \mathbf{x} |\mathbf{x}|^q f(|\mathbf{x}|) \quad (2.31)$$

For $d = 1$, we get

$$C_q = \frac{1}{q+1} (3)^{\frac{q}{2}} \Gamma\left[1 + \frac{q}{2}\right] \quad (2.32)$$

and $R_s = \frac{2}{3}\sqrt{s}$. Hence we get the scaling function(2.17) in $d = 1$ to be

$$f(r) = \frac{\sqrt{\pi}}{2\sqrt{3}} \operatorname{erfc}\left(\frac{r}{\sqrt{3}}\right) \quad (2.33)$$

In the entire low-density phase of the HCLG, in any dimension d , we expect the correlation function $G(\mathbf{x}; z)$ to have an exponential decay at large $|\mathbf{x}|$. But the behavior of the scaling function $f(r)$ for large r is in general different. Suppose $\ln f(r)$ varies as $-r^\alpha$ for large r . Putting this behavior in Eq.(3), and using $A_s \sim \lambda^s$ and Eq. (2.13), we get

$$G(\mathbf{x}; z_{LY} e^{-\epsilon}) \sim \sum_s \exp(-|\mathbf{x}|^\alpha s^{-\nu\alpha} - \epsilon s) \quad (2.34)$$

For large $|\mathbf{x}|$, the integral can be estimated by steepest descent, and gives $\log g(\xi)$ varying as $\xi^{\frac{\alpha}{1+\nu\alpha}}$. Since this should be linear in ξ , we see that $\alpha = \frac{1}{1-\nu}$. As a check, we see that in $d = 1$, $\nu = 1/2$, and $f(r)$ varies as $\exp(-r^2)$ for large r .

The case $x = 0$ is special, in that the density-density correlation function $G(0, z)$ is always equal to $\rho(1 - \rho)$ for hard-core lattice gas for any d dimensional lattice. Hence, if one knows ρ as a function of the activity z (equivalently, in the DA problem, if one knows the

animal numbers generating function $A(y)$), then one can determine $\Psi(0; y)$ in terms of $A(y)$ alone. For a $d + 1$ dimensional DA on a body-centered hyper-cubical lattice it is given by

$$\Psi(0; y) = \frac{1}{1 + y} A(y) [1 + A(y)] \quad (2.35)$$

For $d = 1$, using $A(y)$ from Eq. (2.7), we get for the square lattice DA problem

$$\Psi(0; y) = \frac{y}{1 - 2y - 3y^2} \quad (2.36)$$

Expanding in powers of y we get

$$\phi(0, s) = \frac{3^s + (-1)^{s-1}}{4A_s} \quad (2.37)$$

where A_s is given in Eq.(2.8). For large s , $\phi(0, s)$ varies as $s^{1/2}$ as expected.

Similar analysis can be extended to higher dimensions. In general the scaling function $f(r)$ tends to a finite value as r tends to 0, and hence $\phi(0, s)$ varies as $s^{1-\theta}$.

2.3 Scaling Function in Large Dimensions

The upper critical dimension of directed animals is 7 [80]. Hence for $d > 7$, mean field theory becomes asymptotically exact and solutions on the Bethe lattice should depict the correct scaling behaviors. We considered a Bethe lattice with coordination number $2d$. We assign a direction to each bond of the Bethe lattice and assume that each animal on d -dimensional hyper-cubical lattice is equivalent to a bond animal on the Bethe lattice with coordination number $2d$. Though this is not a one-to-one mapping; every animal on the Bethe lattice may not correspond to an animal on a corresponding d -dimensional hyper-cubical lattice because of the possibility of loops on the latter. But for dimensions above mean-field dimension these are expected to be irrelevant and scaling behavior is expected to be the same. We can solve the problem exactly on the Bethe lattice for arbitrary co-ordination number to get the transverse scaling behavior for large d [81].

A Bethe lattice is a Cayley tree with boundary sites ignored. We derive the exact self-consistent equations for the animal number generating function and the number of occupied sites at t^{th} shell for arbitrary coordination number γ . $\gamma = 2$ is just the linear chain and is like the 1-dimensional lattice animals problem. The exponents on the Bethe lattice for $\gamma \geq 3$ are the mean-field exponents independent of γ . Consider a Cayley tree with non-boundary sites

having coordination number γ (Fig.2.1 shows a Cayley Tree with $\gamma = 3$). The first shell has a single vertex and the second shell has γ vertices. Clearly the t^{th} shell will have $\gamma(\gamma - 1)^{t-2}$ vertices for $t \geq 2$.

Let $\psi_A(u)$ be the animals number generating function on one of the branches of the second shell (marked A in the Fig.2.1) and $\psi_B(u)$ is the generating function on the whole Bethe lattice, defined as $\psi_B(u) = \sum_{n=0}^{\infty} A_n u^n$, where A_n is the number of lattice animals of size n .

Clearly,

$$\psi_B(u) = 1 + u\psi_A^\gamma(u) \quad (2.38)$$

with $\psi_A(u)$ satisfying the self-consistent algebraic equation of order $\gamma - 1$

$$\psi_A = 1 + u\psi_A^{\gamma-1}(u) \quad (2.39)$$

If $m(t, n)$ is the number of sites in the t^{th} shell in all configurations of animals of size n , we define a generating function $F(u, v)$ as

$$F(u, v) = \sum_{n=1}^{\infty} \sum_{t=0}^{\infty} u^n v^t \quad (2.40)$$

One can solve for $F(u, v)$ and we find,

$$F(u, v) = \psi_B(u) + \gamma uv f(u, v) \psi_A^{\gamma-1}(u) \quad (2.41)$$

here $f_A(u, v)$ is the generating function of the $m(t, n)$ on the A branch (Fig.2.1) of the lattice and satisfies a self-consistent equation

$$f_A(u, v) = \psi_A - 1 + (\gamma - 1)uv f_A(u, v) \psi_A^{\gamma-2} \quad (2.42)$$

In general for any γ coordinated Bethe lattice, Eq.2.39 has solutions which have a u dependence of the form $(1 - \sqrt{1 - u_c u})^{1/(\gamma-2)}$, where u_c is the critical point of the function. Hence in the scaling limit, in general for any γ

$$A_n \sim u_c^{-n} n^{-\frac{3}{2}} \quad (2.43)$$

$$f(u, v) \approx F(u, v) \sim \sum_{t=0}^{\infty} v^t (1 - \sqrt{\epsilon})^t \quad (2.44)$$

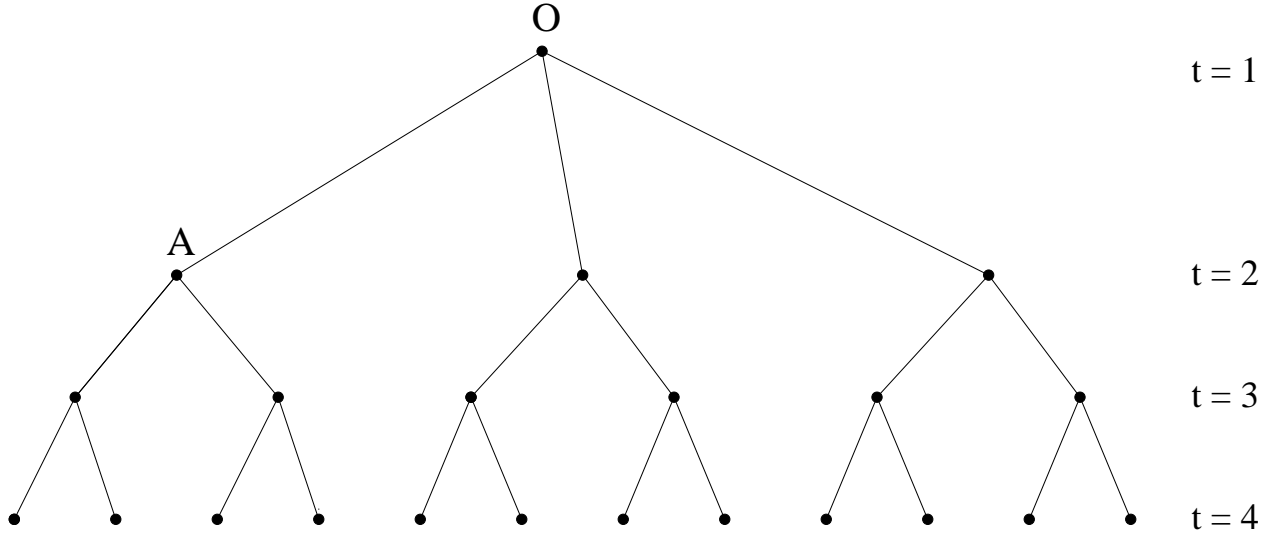


Fig 2.1: A part of a Cayley tree with coordination number 3.

where $\epsilon = 1 - u/u_c$ and only u_c depends on the coordination number. Since the system will have a double root at u_c , solving Eq. 2.39 and its derivative simultaneously gives

$$u_c = \frac{1}{\gamma - 1} \left(\frac{\gamma - 2}{\gamma - 1} \right)^{\gamma - 2} \quad (2.45)$$

and

$$\psi_{Bc} = 1 + \frac{\gamma - 1}{(\gamma - 2)^2} \quad (2.46)$$

For example, for $\gamma = 3$, $u_c = 1/4$.

Hence for large n and fixed value of t , average number of sites in the t^{th} shell, $\phi(t, n)$ scales as

$$\phi(t, n) \sim t \exp\left(-\frac{t^2 u_c}{n}\right) \quad (2.47)$$

On a d -dimensional hyper-cubic lattice, with $d = \gamma/2$, the transverse distance x asymptotically goes as \sqrt{t} (t is the distance defined on the Bethe lattice) and hence

$$\phi(x^2, n) \approx \phi(t, n) \quad (2.48)$$

and we get,

$$\phi(x, n) \sim x^2 \exp\left(-\frac{x^4 u_c}{n}\right) \quad (2.49)$$

As mentioned before, the solutions on the Bethe lattice are reliable for sufficiently large d . In general for a d dimensional lattice, if $g(r, n)$ is the two-point correlation function for the connection between the origin and a site at a distance r , then for large enough d (here $d \geq 8$), total number of site on the surface of radius $r \sim r^{d-1}g(r, n)$. Since this should behave similar to the Bethe lattice solution for coordination number $2d$, we find

$$g(r, n) \sim \frac{1}{r^{d-2}} \exp\left(-\frac{r^2 u_c}{n}\right) \quad (2.50)$$

i.e., $\eta = 0$ for the system. The exponent η for large dimensions ($d > 7$) was shown to be zero rigorously, using lace expansions by Hara and Slade [80]. Here we have given the full scaling function for the correlation function in large dimensions and not just the exponent η .

2.4 Generalized directed animals

In the lattice animal problem only single occupancy per site is allowed. But one can generalise this model and define generalised animals as connected clusters of sites, with each site allowed to be occupied by either different kind of particles or with one or more than one particle. We solved a corresponding model of generalised directed animals exploiting its mapping with lattice gases [81].

Consider a square lattice and let C be the configuration of occupied sites on the line $x + y = T$ and let b be the number of different kinds of particles. We assign a weight y_m to each particle of the m^{th} kind. Let $A_C(\{y_m\})$ be the sum of weights of all distinct configurations of animals, starting with initial configuration C . We define a configuration C by just the number of sites alone. Depending on b each configuration C will have some degeneracy. In particular, if $|C|$ is the number of occupied sites, the degeneracy is $b^{|C|}$. Then $A_C(\{y_m\})$ has a Markovian property just like Eq. 1.5. For example, if $b = 2$, then

$$A_C(y_1, y_2) = \sum_{q=0}^{|C|} y_1^{|C|-q} y_2^q \binom{|C|}{q} \left[1 + \sum_{C'} A_{C'}(y_1, y_2) \right] \quad (2.51)$$

where the sum over C' is over all possible configurations of occupied sites at a line $x + y = T + 1$, consistent with C . Note that though for a given C now there are many more possibilities for C' , they all depend only on the occupancy of C and not on the number of particles at any occupied site in C . This equation can be generalised to any arbitrary integer b .

Now, if we consider a discrete time Markov process on a linear chain with stochastic evolution given by the rule: At time $\tau = 0$ all sites below the line $x + y = 0$ are unoccupied. At time τ , sites on the line $x + y = \tau$ are examined for occupancy. If both $(x + 1, y)$ and $(x, y + 1)$ are unoccupied, the site (x, y) is occupied with probability p_m by the m^{th} kind particle, otherwise it is left unoccupied. Then the Eq.1.5 and 1.6 still turn out to hold true with $p = \sum_{m=1}^b p_m$ and $p_m = -y_m$. These evolution rules satisfy detailed balance corresponding to

$$H = +\infty \sum_{\langle i,j \rangle} n_i n_j - \sum_i \left[\sum_{k=1}^b \ln v_k \delta_{n_{i,k},1} \right] \quad (2.52)$$

where $v_k = p_k/Q$ and $Q = 1 - \sum_{k=1}^b p_k$. n_i is 1 if there is a particle at the i^{th} site and 0 if there is no particle at the i^{th} site, and $n_{i,k}$ = 1 iff there is particle of k^{th} kind at i^{th} site. δ is the Kronecker delta function. For $d = 1$ this Hamiltonian has a $(b + 1) \times (b + 1)$ transfer matrix with all elements of first column being 1. The elements of the first row of the matrix are all non zero and in general the $(m - 1)^{\text{th}}$ element of the first row is v_m . Rest of the entries in the matrix are all zero. Hence this matrix has three eigen values: 0 which is $(b - 1)$ fold degenerate, and

$$\lambda_{1,2} = \frac{1 \pm \sqrt{1 + 4 \sum_{k=1}^b v_k}}{2} \quad (2.53)$$

The generating function of the corresponding animal problem works out to be

$$A_C(\{y_i\}) = \frac{1}{2} \left[\sqrt{\frac{1 + \sum_{k=1}^b y_k}{1 - 3 \sum_{k=1}^b y_k}} - 1 \right] \quad (2.54)$$

We see that this does not change the singularity structure of the generating functions. For example, $\theta = 1/2$ for two dimensional generalised directed animals. Now if we take $b = 2$, i.e. if we assume that the sites can be occupied by two kinds of particles say 1 and 2 and $y_1 = y$ and $y_2 = ay$ be the weight associated with a site occupied by particle of type 1 and 2 respectively, then

$$A_C(y_1, y_2) = \frac{1}{2} \left[\sqrt{\frac{1 + y + ay}{1 - 3y - 3ay}} - 1 \right] \quad (2.55)$$

Hence $a < 1$ would imply that particles of kind 1 dominate whereas if $a = 1$, both kind of particles are equally likely and for $a > 1$ the particles of second kind start dominating.

The critical value y_c depend on a and is equal to $y_c = \frac{1}{3(1+a)}$.

This model can find applications in cluster growth models with more than one kind of cell and in the statistics of clusters in directed percolation with two or more different kinds of species.

One can also consider the case in which each site of the cluster can have one or more particles. In that case all of the above treatment goes through with y_m being the weight associated with a site having m particles. If we take $y_m = y^m$, then clusters with the same number of particles would be equally likely and be given by Eq 2.52.

Hence, we find that this generalised model lies in the same universality class as the DA problem. Actually, we find that the generating function of generalized directed animals on a square lattice with the number of particles allowed per site approaching infinity is same as that of directed animals on a triangular lattice.

Directed Branched Polymers near an attractive line

The plan of the chapter is as follows. In Section 3.1 we will define the model of a directed branched polymer (DBP) near an attractive line. We give the mapping of a $d + 1$ dimensional DBP near a line to a d dimensional HCLG with repulsive interactions in [82] Section 3.2. We consider and solve exactly the $(1 + 1) d$ DBP in the presence of a $1d$ penetrable line in Section 3.3, and in the presence of an impenetrable surface in Section 3.4. In Section 3.5, using Baxter's solution of hard hexagon gas we study $2 + 1$ dimensional DBP in presence of line and calculate the crossover exponent and sticking fraction exactly.

3.1 The Model

We study a model of DBP in presence of $1d$ line parallel to the preferred direction. This is positioned along the line $y = 0$ of the lattice (Fig. 3.1). We have considered the polymer rooted at $(0, 0)$ on the line. The number of sites in \mathcal{A} will be denoted by $s = |\mathcal{A}|$. We define $n(x|\mathcal{A})$ as the number of sites of \mathcal{A} having the transverse coordinate x .

We assign a fugacity y to each of the allowed sites of the cluster. Further, if we associate an additional energy $-E$ with each site on the line, each site on the line will have an additional weight and the fugacity of sites on this line, denoted by y_0 is equal to wy where

$$w = \exp(E/kT) \quad (3.1)$$

Hence $w > 1$ would correspond to an attractive line.

We define $A(w, y)$, the grand partition function of the polymer as

$$A(w, y) = \sum_{\mathcal{A}} y^{|\mathcal{A}|} w^{n_0} = \sum_{s=1}^{\infty} A_s(w) y^s \quad (3.2)$$

where $n_0 = n(0|\mathcal{A})$ and $A_s(w)$ is the partition function of the polymer made of exactly s monomers. For $w = 1$, we get the statistics of equally weighted animals and $A_s(1)$ is the number of distinct directed animals having s sites with given boundary conditions.

The free energy per monomer of the polymer in the thermodynamic limit is given by

$$F(T) = \lim_{s \rightarrow \infty} -\frac{k_B T}{s} \log A_s(w) \equiv k_B T \log(y_\infty(w)) \quad (3.3)$$

where $y_\infty(w)$ is the value of fugacity at which $A(w, y)$ has a singularity for a given value of w .

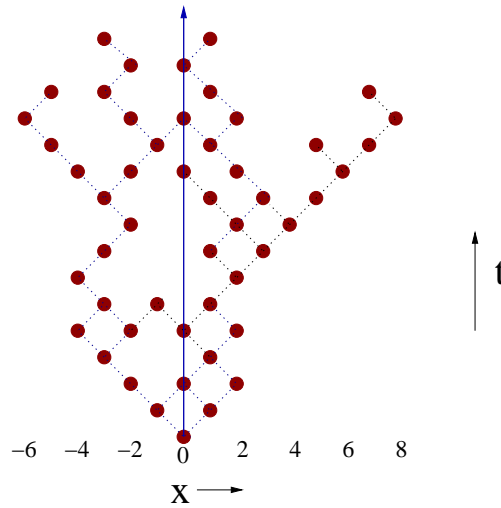


Fig 3.1: A directed branched polymer of size 50, rooted on the surface. The surface is along the t direction

Let $\phi(\mathbf{x}, s)$ be the value of $n(\mathbf{x}, \mathcal{A})$ averaged over all configurations \mathcal{A} of size s . We define a generating function $\Psi(\mathbf{x}; w, y)$ as

$$\Psi(\mathbf{x}; w, y) = \sum_{\mathcal{A}} n(\mathbf{x}|\mathcal{A}) w^{n_0} y^{|\mathcal{A}|} \equiv \sum_s \phi(\mathbf{x}, s) A_s(w) y^s \quad (3.4)$$

For large s , $A_s(w)$ varies as $\lambda(w)^s s^{-\theta}$, where θ is known as entropic critical exponent. Similarly, the transverse size of the polymer for large s scales as s^ν , where ν is the exponent which defines the transverse length scale of the polymer. These exponents take different values in the desorbed, adsorbed and in the critical regions. We will use subscripts de , c and ad to represent critical exponents and other quantities in desorbed, critical and adsorbed phases of the polymer, respectively.

There is a critical value w_c of wall activity such that for $w > w_c$, $\phi(0, s)$ is proportional to s for large s and the transverse size is finite ($\nu_{ad} = 0$). This is the adsorbed phase, in which monomers tend to stick to the surface. $w < w_c$ corresponds to the desorbed phase of the polymer in which only a finite number of monomers stick to the surface. At $w = w_c$ the critical point of the surface transition, the number of adsorbed monomers as a function of polymer size in the large s limit has a behavior given by

$$\phi_c(0, s) \sim s^\alpha; \quad (3.5)$$

where α is known as the crossover exponent of the surface transition.

In the $s \rightarrow \infty$ limit, the fraction of monomers adsorbed is like the order parameter of the surface phase transition. In the constant fugacity ensemble $A(w, y)$ is the partition function with fixed w and y and hence the average polymer size would be given by

$$\langle s(y, w) \rangle = \frac{\sum s y^s w^{n_0}}{\sum y^s w^{n_0}} \equiv \frac{\partial \ln A(w, y)}{\partial \ln y} \quad (3.6)$$

Similarly, the average number of monomers at the surface would be

$$\langle n_0(y, w) \rangle = \frac{\sum n_0 y^s w^{n_0}}{\sum y^s w^{n_0}} \equiv \frac{\partial \ln A(w, y)}{\partial \ln w} \quad (3.7)$$

The sticking fraction, defined as the fraction of polymer segments at the surface, represented by $C_{st}(w, y)$, would be given by

$$C_{st}(w, y) = \frac{\langle n_0(y, w) \rangle}{\langle s(y, w) \rangle} \quad (3.8)$$

In the infinite polymer limit, if we represent the value of fugacity at which $\langle s(y, w) \rangle$ diverges by $y_\infty(w)$ for a given w , then the sticking fraction is only a function of the wall activity w and is given by

$$C_{st}(w) = -\frac{d \ln y_\infty(w)}{d \ln w} \quad (3.9)$$

This is the order parameter of the surface phase transition and is zero for $w \leq w_c$, where w_c is the surface phase transition point.

In general, in the large polymer limit, near the critical value of w , as $w \rightarrow w_c^+$, $C_{st}(w, y)$ is expected to have scaling form

$$C_{st}(w, y) = \epsilon^{1-\alpha} h((w - w_c)\epsilon^{-\alpha}) \quad (3.10)$$

where $\epsilon = 1 - y/y_\infty(w)$. The scaling function $h(u)$ where $u = (w - w_c)\epsilon^{-\alpha}$, is a function of w and y which are both thermodynamic variables. As $u \rightarrow \infty$, $h(u) \sim u^{(1-\alpha)/\alpha}$, and $h(u) = 0$ for negative u .

3.2 General Results

The directed site animal enumeration (DSAE) problem in $d + 1$ -dimensions is related to the time development of thermal relaxation of a hard core lattice gas (HCLG) with nearest neighbor exclusion on d dimensional lattice [24]. In Sec 2.1, we have shown that this correspondence relates the density at a site i in steady state to the sum of weights of all animals rooted at i , i.e.. the grand partition function of the animal. Also, the average number of sites at a given transverse distance \mathbf{x} from the origin for a $d + 1$ dimensional directed animal is related to the density-density correlation function of the lattice gas in d dimensions.

Specifically, if on a $d + 1$ dimensional body-centered hyper-cubic lattice we define the weight of an animal \mathcal{A} to be the product of weights of all occupied sites, with the weight corresponding to a site with \mathbf{x} coordinate i being y_i , then the DSAE problem on this $d + 1$ dimensional lattice gets related to the time development of HCLG with nearest neighbor exclusion on a d dimensional body-centered hyper-cubic lattice with the rates which satisfy detailed balance condition corresponding to the Hamiltonian

$$H = +\infty \sum_{\langle ij \rangle} n_i n_j - \sum_i (\ln z_i) n_i \quad (3.11)$$

where $z_i = -y_i/(1 + y_i)$ and the animal number generating function is just the negative of the density of HCLG with change of variables from z to y . Here we have used the convention that if $\sum_{\langle ij \rangle} n_i n_j = 0$ then the corresponding term in the Hamiltonian is zero. The configurations with any pair of occupied nearest neighbors have infinite energy and do not contribute to the partition function.

The partition function is linear in all z'_i 's. The linearity of the partition function in the z'_i 's implies that in case when the activity about $\mathbf{x} = 0$ is different from that of the rest of the sample, i.e. if we let the activity about $\mathbf{x} = 0$ be z_0 and activity everywhere else be z , then the partition function of the HCLG can be written as

$$Z(z_0, z) = A(z) + z_0 B(z) \quad (3.12)$$

where $A(z)$ and $B(z)$ are polynomials in z . If ρ represents the density of HCLG when the activity about each site is the same, then the density of HCLG about the origin in the present case $\rho_0(z_0, z)$ can be written in terms of ρ as

$$\rho_0(z_0, z) = \frac{z_0 \rho}{\rho z_0 + z(1 - \rho)} \quad (3.13)$$

Same observation has been made by Cardy in [47]. Correspondingly, since $A(w, y)$ is just the negative of $\rho_0(z_0, z)$ with $z_0 = -wy/(1 + wy)$ and $z = -y/(1 + y)$, we can express $A(w, y)$ in terms of $A(1, y)$ and this is given by

$$A(w, y) = \frac{w(1 + y)A(1, y)}{(1 + wy) + A(1, y)(1 - w)} \quad (3.14)$$

Moreover, the density-density correlation function of HCLG, $G(\mathbf{x}; w, z)$ with $w \neq 1$ can be expressed in terms of the $w = 1$ density density correlation function. We find that the density density correlation function is related to $\Psi(\mathbf{x}; w, y)$ on a hyper-cubic lattice as follows

$$\Psi(\mathbf{x}; w, y) = -\frac{1}{1 + y} G\left(\mathbf{x}; w, z = \frac{-y}{1 + y}\right) \quad (3.15)$$

From this we get

$$\frac{\Psi(\mathbf{x}; w, y)}{\Psi(\mathbf{x}; 1, y)} = \frac{w(1 + y)[1 + wy - (1 - A(1, y))(1 - w)]}{[1 + wy + A(1, y)(1 - w)]^2} \quad (3.16)$$

Since ρ is the density of the HCLG, then as discussed in Sec. 2.2, for $\mathbf{x} = 0$, the density density correlation of HCLG is always equal to $\rho(\rho - 1)$ for any dimensiond and hence $\Psi(0; 1, y)$ can be completely expressed in terms of $A(1, y)$:

$$\Psi(0; w, y) = \frac{w(1 + y)A(1, y)(1 + A(1, y))}{[1 + wy + A(1, y)(1 - w)]^2} \quad (3.17)$$

Eq. (3.14-3.17) hold for all dimensions. Hence, in presence of $1d$ surface, a DBP in $d + 1$ dimensions rooted on the surface can be studied using the mapping to HCLG. Moreover the generating functions $A(w, y)$ and $\Psi(0; w, y)$ can be completely expressed in terms of the animal number generating function when the wall is neutral i.e., in terms of $A(1, y)$. We will use these results below to study the effect of an attractive line for DBP in 2 and 3 dimensions.

In the adsorbed regime the number of monomers in direct contact with the wall is proportional to s and $\nu_{ad} = 0$. This implies that the scaling form of $\phi(\mathbf{x}, s)$ in the adsorbed regime would be

$$\phi_{ad}(\mathbf{x}, s) \sim \frac{s}{\xi^d} g(|\mathbf{x}|/\xi) \quad (3.18)$$

where $\xi = (w - w_c)^{-\bar{\nu}}$ is the characteristic length scale in the system. Since we are away from the critical regime, ξ is well behaved and never diverges for finite w . Also ξ is independent of the size s of the polymers. The normalization of scaling function $g(r)$ is chosen such that

$$\int_{-\infty}^{\infty} d^d \mathbf{x} g(|\mathbf{x}|) = 1 \quad (3.19)$$

$A_s(w)\phi(\mathbf{x}, s)$ is the coefficient of y^s in the expansion of $\Psi(\mathbf{x}; w, y)$. In the adsorbed regime, $A_s(w) \sim (y_\infty(w))^{-s}$ for large s and the behavior of $\phi(\mathbf{x}, s)$ is given by Eq. (3.18), hence $\Psi(\mathbf{x}; w, y)$ will have a scaling form

$$\Psi(\mathbf{x}; w, y) \sim \frac{\epsilon^{-2}}{\xi^d} g(|\mathbf{x}|/\xi) \quad (3.20)$$

where $\epsilon = 1 - y/y_\infty(w)$.

Since the scaling function $g(|\mathbf{x}|/\xi)$ has no y dependence, the scaling function of $G(\mathbf{x}; w, z)$ would also be just $g(|\mathbf{x}|/\xi)$ for $w > w_c$.

3.3 Two dimensional Directed Branched Polymer in presence of 1-d penetrable surface

For a penetrable surface, since the configurations spanning through the surface are allowed, there is no loss of entropy per monomer to take into account (Fig 3.1). Hence, $w = 1$ corresponds to a zero gain in free energy per monomer of the surface. This implies that $w_c = 1$ for a DBP in any dimension in presence of a $1d$ line as long as $A(1, y)$ is divergent at a finite value of y . Then the polymer has bulk behavior at the critical point. At $w = 1$, i.e. for directed branched polymer in bulk, we have shown in Section 2.1 by scaling arguments and dimensional analysis that $\phi(\mathbf{x}, s)$ has a scaling form

$$\phi_c(\mathbf{x}, s) \sim s^{1-d\nu_c} f(|\mathbf{x}|\epsilon^{-\nu_c}) \quad (3.21)$$

This implies that $\phi_c(0, s) \sim s^{1-d\nu_c}$, and the crossover exponent α is exactly given by

$$\alpha = 1 - d\nu_c \equiv 1 - \theta \quad (3.22)$$

where ν_c is the transverse correlation exponent of a $d + 1$ dimensional DA in bulk, which is equal to the correlation length exponent for a d dimensional HCLG with nearest neighbor exclusion.

As we go to higher dimensions, even though entropy loss and energy gain balance each other at $w = 1$, the polymer might start binding to a line only at wall activity greater than 1. For directed branched polymers, when $A(1, y_c)$ is finite, $w = 1$ is not the critical point of the surface transition. Instead it is given by

$$w_c = \frac{1 + 1/A(1, y_c)}{1 - y_c/A(1, y_c)} \quad (3.23)$$

where y_c is the large polymer limit fugacity value of the polymer with neutral wall i.e., when $w = 1$.

The $1+1$ d DA gets mapped to a $1d$ HCLG. For $1+1$ dimensional DA's in bulk we derived the exact expressions of $A(1, y)$ and $\Psi(x; 1, y)$ in Sec 2.2. Using them and Eq. 3.14-3.16 we get the expressions for $A(w, y)$ and $\Psi(x; w, y)$ as follows

$$A(w, y) = \frac{2wy(1+y)}{(1-y-wy-3wy^2) + (1+wy)\sqrt{(1-3y)(1+y)}} \quad (3.24)$$

The connected density-density correlation function of the corresponding gas is a simple exponential and hence the generating function $\Psi(x; w, y)$ has the form

$$\Psi(x; w, y) = K(w, y)\exp(-b(y)|x|) \quad (3.25)$$

where it is straightforward to calculate $K(w, y)$ and $b(y)$, and we get

$$K(w, y) = \frac{2wy(1-3y)(1+wy)(1-y+\sqrt{(1-3y)(1+y)})}{[(1-3y)(1+wy)\sqrt{1+y} + (1-y-wy-3wy^2)\sqrt{1-3y}]^2} \quad (3.26)$$

and

$$b(y) = \log(\sqrt{1+y} + \sqrt{1-3y}) - \log(\sqrt{1+y} - \sqrt{1-3y}) \quad (3.27)$$

The generating functions $A(w, y)$ and $\Psi(x; w, y)$ have a branch cut at $y = 1/3$. For $w = 1$, they also have a pole singularity at $y = 1/3$. Hence, clearly the phase transition from desorbed to adsorbed phase occurs at $w = 1$, i.e. $w_c = 1$. For $w \leq 1$, $y_\infty(w) = 1/3$ and for $w > 1$ it is given by the real positive solution of

$$w - y - w(3 + 2w)y^2 - 3w^2y^3 = 0 \quad (3.28)$$

Near the critical point, for $w = 1 + \delta$, to leading order we get $y_\infty(w)$ to be

$$y_\infty(w) = \frac{1}{3} - \frac{\delta^2}{16} + \text{higher order terms} \quad (3.29)$$

The sticking fraction $C_{st}(w, y)$ can also be exactly calculated and we get it to be

$$C_{st}(w, y) = \left[\frac{y(1-w)}{1+y} + \frac{1+wy}{\sqrt{(1+y)(1-3y)}} \right]^{-1} \quad (3.30)$$

From this, near the critical point, we get the scaling form of $C_{st}(w, y)$ to be

$$C_{st}(w, y) = \sqrt{\epsilon} h(u) \quad (3.31)$$

where $\epsilon = 1 - y/y_\infty(w)$ and $u = \epsilon^{-1/2}\delta$ and we get

$$h(u) = \frac{\sqrt{3}}{2} \left[1 + \frac{9u^2}{48} \right]^{\frac{1}{2}} \quad (3.32)$$

This gives the order parameter $C_{st}(w)$ near the critical point to be proportional to $\frac{3\delta}{8}$. For large values of w , expanding $C_{st}(w)$ in powers of $(1/w)$ we get

$$C_{st}(w) \sim \frac{1}{2} - \frac{3\sqrt{2}}{16\sqrt{w}} - \frac{3}{16w} - \dots \quad (3.33)$$

For $w \rightarrow \infty$ it approaches $1/2$, the maximum possible fraction that can stick to wall, as expected.

3.4 Two dimensional Directed Branched Polymer in presence of 1-d impenetrable surface

In the presence of an impenetrable surface, because of loss in entropy per monomer on the wall, the transition from desorbed to adsorbed phase takes place at a non trivial value of

adsorption activity.

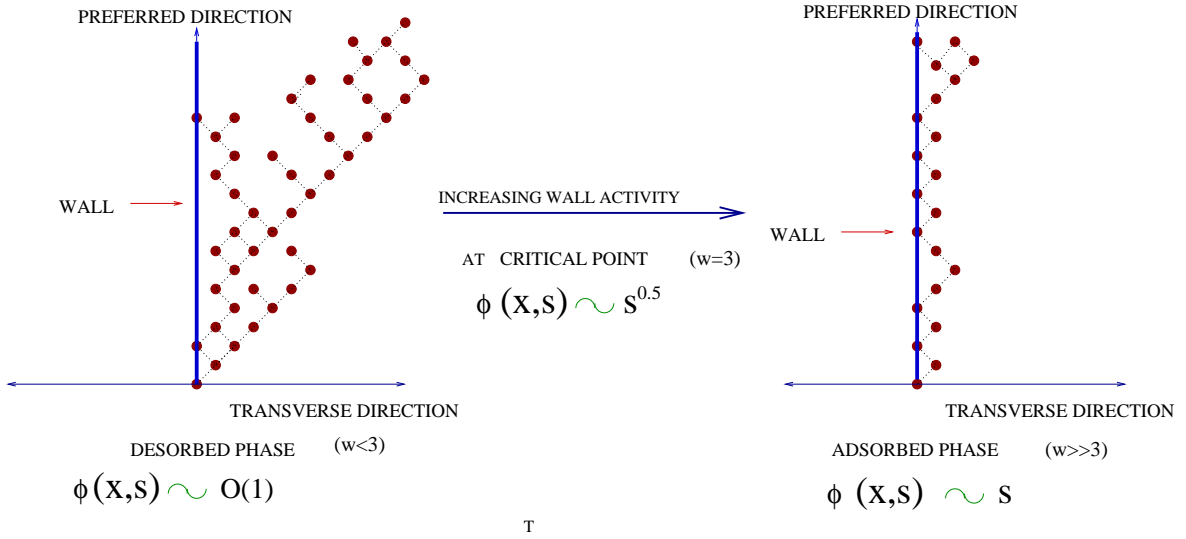


Fig 3.2: Directed branched polymer on a square lattice in presence of a 1-d impenetrable line about the diagonal.

Here we study a DBP in $1 + 1$ dimension on a square lattice, in presence of an impenetrable surface, about the diagonal (Fig 3.2). From the exact generating function $A(1, y)$, $A(w, y)$ and $\Psi(x; w, y)$, it is straightforward to determine the critical value of w and the sticking fraction and the density profile in the desorbed, critical and adsorbed phase of the system. The $1 + 1$ d case in presence of a solid wall along the growth direction can be mapped to the HCLG in 1-d with fugacity 0 for all sites lying along the negative axis. Making use of this mapping we get

$$A(1, y) = \frac{(1 - y - \sqrt{1 - 2y - 3y^2})}{2y} \quad (3.34)$$

and then $A(w, y)$ is easy to get by substituting in Eq. 3.14. This result can also be obtained using the heap method. For an alternate treatment see [83].

The density-density correlation of the corresponding gas is exponential and hence the generating function $\Psi(x; w, y)$ still has a form given by Eq. 3.25, but $K(w, y)$ and $b(y)$ are now given by

$$K(w) = \frac{wy(1 + wy)(\sqrt{1 + y} + \sqrt{1 - 3y})}{(1 + y)(1 - w^2y^2)\sqrt{1 - 3y} + (1 - y - (4 - w)wy^2 - w^2y^3)\sqrt{1 + y}} \quad (3.35)$$

and

$$b(y) = \log(\sqrt{1 + y} + \sqrt{1 - 3y}) - \log(\sqrt{1 + y} - \sqrt{1 - 3y}) \quad (3.36)$$

The generating functions $A(w, y)$ and $\Psi(x; w, y)$ have a branch cut at $y = 1/3$. At $w = 1$, $A(1, y)$ has no divergence and $y_c = 1/3$. Substituting in Eq. (3.23), we get $w_c = 3$. This value is greater than the value for 1 + 1 d DBP with a penetrable surface. This is expected, since the tendency of polymer to grow away from the surface is more when the surface is impenetrable and hence only when the surface gets sufficiently attractive, the polymer starts sticking to it. For $w > 3$, the closest singularity to the origin occurs at

$$y_s = \frac{\sqrt{4w - 3} - 1}{2w} \quad (3.37)$$

For $w \leq 3$ the branch cut singularity $1/3$ dominates and hence $y_\infty(w)$, the infinite polymer limit fugacity value is equal to $1/3$ for $w \leq 3$. Whereas for $w > 3$, $y_\infty(w) = y_s$. Free energy is a constant and the order parameter, $C_{st}(w)$ is zero for $w < 3$.

We get the sticking fraction, $C_{st}(w, y)$ to be

$$C_{st}(w) = \frac{1 - 2y - 3y^2 + (-1 + y + 2y^2)\sqrt{(1+y)(1-3y)}}{y[-2y + (w + 2y - wy)\sqrt{(1+y)(1-3y)} + w(-1 + 2y + 2y^2)]} \quad (3.38)$$

Near the critical point for $w = 3 + \delta$ and $y = y_s(1 - \epsilon)$, we get the same scaling form for $C_{st}(w, y)$ as given by Eq. 3.31, with the scaling function $h(u)$ to be

$$h(u) = \frac{2}{\sqrt{3}} \left[1 + \frac{u^2}{27} \right]^{\frac{1}{2}} \quad (3.39)$$

Hence $C_{st}(w)$ is proportional to $\frac{2\delta}{9}$ near the critical point and approaches $1/2$ as $w \rightarrow \infty$. This is plotted in Fig. 3.3 along with the sticking fraction for the penetrable case. The qualitative behavior in both cases is just the same, the main difference being the shift of the transition point from 1 to 3 and the initial slope. For large value of w it is easy to expand $C_{st}(w)$ in powers of $1/w$. It should be noted that the large w expansion of $C_{st}(w)$ will involve powers of $w^{-1/2}$ in this case as well.

Using the exact equations for generating function for $\Psi(x; w, y)$ we translate these results to the constant number ensemble and we get the function $\phi(x, s)$ in the three regions giving the spread of sites as a function of distance from the wall. Here we give these calculations for the impenetrable case only because the qualitative behavior in both the impenetrable and penetrable cases is exactly the same for 1 + 1 dimensional system.

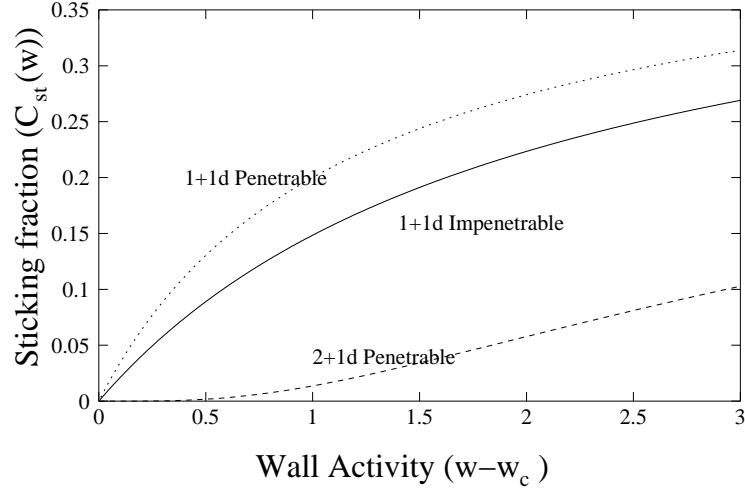


Fig 3.3: Sticking Fraction in presence of line for a directed branched polymer in 1+1 and 2+1 dimensions, when the polymer size tends to infinity.

In the desorbed phase ($w < 3$), expanding near $y_c = 1/3$ as $y = y_c e^{-\epsilon}$, we get the scaling form for $\Psi(x; w, y)$ to be

$$\Psi(x; w, \epsilon) = c(w) \exp(-x\sqrt{3\epsilon}) \quad (3.40)$$

where, $c(w)$ is a w dependent constant and is $\frac{3(3+w)}{2(3-w)^2}$.

To obtain $\phi(x, s)$ for large s , we need to determine the coefficient of y^s in the series expansion of $\Psi(x; w, \epsilon)$ i.e.,

$$\Psi(x; w, \epsilon) \equiv \sum_s \phi(\mathbf{x}, s) A_s(w) y^s = c(w) \sum_{k=0}^{\infty} \frac{(-\sqrt{3}x)^k}{\Gamma[k+1]} (1-3y)^{\frac{k}{2}} \quad (3.41)$$

$$= c(w) \sum_{s=0}^{\infty} (3y)^s \sum_{k=0}^{\infty} \frac{(-\sqrt{3}x)^k}{\Gamma[k+1]} \frac{\Gamma[s-k/2]}{\Gamma[s+1]\Gamma[-k/2]} \quad (3.42)$$

For fixed k and large s ,

$$\frac{\Gamma[s-k/2]}{\Gamma[s+1]} \rightarrow s^{-1-k/2} \quad (3.43)$$

Hence the leading singular behavior of $\phi(x, s) A_s(w)$ in the desorbed phase is given by

$$\phi(x, s) A_s = \frac{3^s c(w)}{s} \sum_{k=0}^{\infty} \frac{(-\sqrt{3}x/\sqrt{s})^k}{\Gamma[k+1]\Gamma[-k/2]} \quad (3.44)$$

Since $\Gamma[-k/2]$ has poles when k is an even integer, only odd terms contribute to the sum. It is easy to sum the resulting series, giving $\phi(x, s)$ for large s in the desorbed phase to be

$$\phi_{de}(x, s) = \frac{3}{2}x \exp\left(-\frac{3x^2}{4s}\right) \quad (3.45)$$

For $w = 3$, $c(w)$ is singular and we have to keep terms till first order in ϵ in the expansion (for $w < 3$ the constant term dominates) and we get

$$\Psi(x; 3, \epsilon) = \frac{1}{\epsilon} \exp(-x\sqrt{3\epsilon}) \quad (3.46)$$

Again, just as in the desorbed phase expanding $\Psi(x; 3, \epsilon)$ in powers of y^s , the average number of sites at a distance x , i.e. $\phi(x, s)$ for the critical region for large s is

$$\phi(x, s) = \frac{\sqrt{3\pi s}}{2} \operatorname{erfc}\left(\frac{\sqrt{3}x}{2\sqrt{s}}\right) \quad (3.47)$$

Hence we see that at $w = 3$ not just the crossover exponent α is equal to $1/2$, but even the scaling form of $\phi(x, s)$ is same as that of a $(1 + 1)$ dimensional DA in bulk [78] and hence same as that of the penetrable wall at the critical point. This unusual result can be understood as coming from exact cancellation of decrease in entropy and increase in internal energy at the critical point. Also note that the value of exponent $\alpha = 1/2$ for DBP is equal to the estimates of α for linear polymers [84].

For $w > 3$, the behavior of the generating function is dominated by the singularity given by Eq. (3.37). For $w \gg 3$, $y_s \approx 1/\sqrt{w}$ and we get the large s behavior of $\phi(x, s)$ to be

$$\phi(x, s) = s \exp(-x) \quad (3.48)$$

i.e., finite fraction of the sites stick to the line passing through the origin as expected.

Similarly, expanding $A(w, y)$ about y_c and then going to constant number (s) ensemble, we get $A_s(w)$ for large s as $A_s(w) \sim \frac{\sqrt{3}}{2\sqrt{\pi}} c(w) 3^s s^{-\frac{3}{2}}$ in the desorbed regime. Hence the number of animals in presence of the $1d$ impenetrable wall i.e. $A_s(1)$ for large s are $A_s(1) \sim \frac{\sqrt{3}}{2\sqrt{\pi}} 3^s s^{-\frac{3}{2}}$. This gives θ_{de} to be $3/2$. This is consistent with the result derived for lattice trees by De'Bell et al [46]. Also we get at the critical point $w = 3$, $A_s(3) \sim \frac{2}{\sqrt{3\pi}} 3^s s^{-\frac{1}{2}}$, implying θ_c to be $1/2$. For $w \gg 3$, $A_s(w) \sim (\sqrt{w})^s$, giving $\theta_{ad} = 0$.

The function $\phi(x, s)$ gives the density profile of the polymer as a function of distance

from the surface. Since the configurations are very different in the two phases, as shown schematically in Fig 3.2, $\phi(x, s)$ is very different in the three regions. In the desorbed phase, it peaks away from the surface at a distance of the order of the average transverse diameter of the polymer in the large s limit. Whereas at the critical point and in the adsorbed phase it peaks at the surface (Fig 3.4).

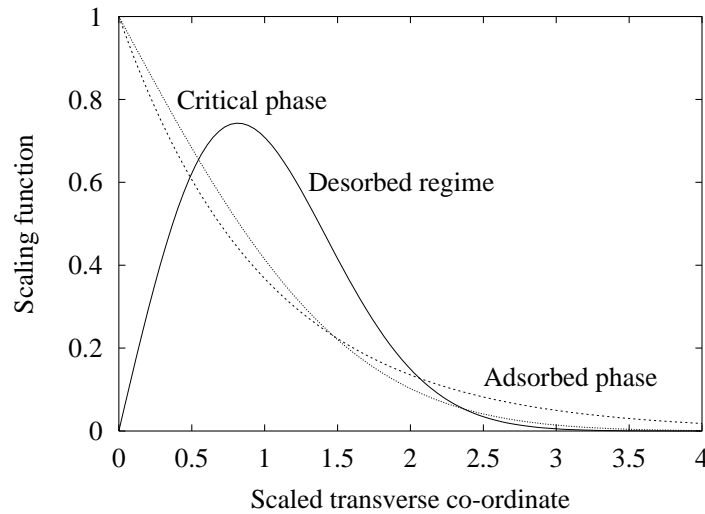


Fig 3.4: Density profile of a 2-dimensional DBP in presence of a 1-dimensional line. The solid line shows the scaling function of $\phi(x, s)$ in the desorbed regime, the dotted line represent the same in the critical region and the dashed curve is for the adsorbed phase.

3.5 Three dimensional Directed Branched Polymer in presence of an attractive line

In $2 + 1$ dimensions, a DBP on a simple cubic lattice with nearest and next nearest neighbor connections gets mapped to the hard hexagon gas model in 2 dimensions at negative activity in the disordered regime, which was solved by Baxter [85]. He obtained the equation for the average density of the gas. It was shown by Joyce that there is an algebraic equation in z (activity of the gas) and ρ (density of the gas) [86].

The equation given by Joyce is quartic in z and 12th order in ρ . For convenience we will reproduce it here [86]

$$\rho(1 - \rho)^{11} - (1 - \rho)^5 P_1(\rho)z + \rho^2(1 - \rho)^2 P_2(\rho)z^2 - \rho^5 P_1(\rho)z^3 + \rho^{11}(1 - \rho)z^4 = 0 \quad (3.49)$$

where

$$P_1(\rho) = (1 - 13\rho + 66\rho^2 - 165\rho^3 + 220\rho^4 - 165\rho^5 + 77\rho^6 - 22\rho^7)$$

$$P_2(\rho) = (1 - 13\rho + 63\rho^2 - 125\rho^3 + 6\rho^4 + 401\rho^5 - 689\rho^6 + 476\rho^7 - 119\rho^8)$$

The density ρ of the HCLG is just the negative of $A(1, y)$ and $z = -y/(1 + y)$. It is straightforward to get an algebraic equation involving $A(1, y)$ and y [87]. As $A(w, y)$ is a simple rational function of $A(1, y)$, y and w (see Eq.3.14), substituting ρ in terms of $A(w, y)$, the grand partition function of the $2 + 1$ dimensional DA in presence of a 1-dimensional line parallel to the main diagonal of the lattice gas passing through the origin, we get a 12 th order polynomial equation in $A(w, y)$, where the coefficients are functions of w and y . The explicit form of the equation is rather tedious and is omitted. Since $A(1, y)$ becomes singular for $y = y_c = 2/(9 + 5\sqrt{5})$, in presence of the 1-dimensional line the polymer will undergo a desorption-adsorption transition at $w = 1$. For $w \leq 1$ the dominant singularity will be y_c and $y_\infty(w) = y_c$. For $w > 1$, at $y_\infty(w)$, $A(w, y)$ tends to infinity and at this point the coefficient of the highest order term must be zero. Since we have a 12th order equation in $A(w, y)$, equating the coefficient of the 12th order term to zero, we get a polynomial equation in y and w ($Q(y, w) = 0$) whose smallest positive real root would be $y_\infty(w)$. This polynomial is 12th order in w . But we can find the root numerically. The free-energy is just $\log(y_\infty(w))$ and hence can be evaluated numerically.

In this case the expressions of $A(w, y)$ and other generating functions are rather complicated and hence it is difficult to go to the constant size ensemble. But at the critical point, the system behaves like a bulk system and since $\theta = 5/6$, by hyper-scaling arguments $\nu_c = 5/12$ which implies that the crossover exponent $\alpha = 1/6$ (Eq. 3.22). And by Eq. 3.10, the sticking fraction $C_{st}(w, y) \sim (1 - y/y_\infty(w))^{5/6}$ as $w \rightarrow 1^+$ asymptotically.

By solving $Q(y, w) = 0$ we get $y_\infty(w)$ as a function of w . Near the critical point for $w = 1 + \delta$, to leading order we get

$$y_\infty(w) = y_c(1 - c\delta^6 + \text{higher order term}) \quad (3.50)$$

where $c = 5(5\gamma)^5$ with $\gamma = (13\sqrt{5} - 25)/50$.

In the large polymer limit, for y very close to y_c , $A(1, y)$ has a scaling form

$$A(1, y) = a_0 \left(1 - \frac{y}{y_c}\right)^{-\frac{1}{6}} \left[1 + a_1 \left(1 - \frac{y}{y_c}\right)^{\frac{5}{6}} + \dots\right] \quad (3.51)$$

where $a_0 = (\sqrt{5}\gamma^{1/6})^{-1}$ [87].

Hence taking $y = y_\infty(w)(1-\epsilon)$ and $w = 1+\delta$ we get the scaling function of $C_{st}(w, y) = \epsilon^{5/6}h(u)$ to be

$$h(u) = \frac{6a_0}{1+y_c}(1+cu^6)^{\frac{5}{6}} - 6cu^5 \quad (3.52)$$

where $u = \delta\epsilon^{-1/6}$. The scaling function $h(u)$ is a function of w and y .

For large w , expanding in power of $1/w$ we get

$$y_\infty(w) \sim \frac{1}{\sqrt{6w}} - \frac{1}{4w} - \frac{11}{16}\sqrt{\frac{3}{2}}\left(\frac{1}{w}\right)^{\frac{3}{2}} - \dots \quad (3.53)$$

and

$$C_{st}(w) \sim \frac{1}{2} - \frac{1}{4}\sqrt{\frac{3}{2w}} - \frac{9}{4w} - \dots \quad (3.54)$$

As $w \rightarrow \infty$, $C_{st}(w)$ approaches $1/2$, the maximum possible fraction of adsorption. It is like the order parameter of the surface transition. It is plotted in Fig 3.3. As is clear from the scaling function, the sticking fraction increases much more slowly than in the $1+1d$ case. This is expected; there, the polymer in 2 dimensions was getting adsorbed at a 1 dimensional surface whereas here a polymer in 3 dimensions is getting adsorbed on a 1 dimensional surface.

Efficiency of Incomplete Enumeration Monte-Carlo method for linear and branched polymers

Monte-Carlo simulations are a very important tool for studying polymers, as exact results are hard to come by, and are available only for the simplest models. We introduced the Incomplete-enumeration (IE) algorithm for Monte-Carlo (MC) simulations in Sec. 1.6.3. IE is an example of a genetic algorithm. In this chapter we make a detailed study of the algorithm for linear and branched polymers [88]. The plan of this chapter is as follows: In Sec. 4.1 we discuss the efficiency criterion for MC algorithms in general, and for IE in particular. In Sec. 4.2 we study the efficiency of IE analytically for some simple cases where the genealogical tree has a simple recursive structure. We also study IE for self avoiding walks (SAW) in this section. In all cases we find that $T_n \sim n^2$. In Sec. 4.3 we propose an improved version of the IE algorithm, which we call improved incomplete enumeration (IIE). For simple random walks $T_n = n$ for the IIE algorithm as compared to $T_n \sim n^2$ for IE. For SAW's, IIE is significantly more efficient and becomes better in higher dimensions, but asymptotic efficiency remains the same and $T_n \sim a_d n^2$ in all dimensions, though the coefficient a_d decreases with increasing dimension. In Sec. 4.4 we study IE for branched polymers or lattice animals on a binary tree. We give a non rigorous argument and numerical evidence to show that $T_n \sim \exp(cn^{1/3})$ for large n for branched polymers on a binary tree. We also study IE and IIE numerically for undirected and directed branched polymers on a square lattice in this section. We find that in both cases $T_n \sim \exp(cn^\alpha)$, $0 < \alpha < 1$.

4.1 Efficiency

In general, in Monte-Carlo methods, the time needed to estimate an ensemble average $\mu = \langle O \rangle$ of some observable O over all clusters of size n averaged over N independent samples would give estimate as $\mu^* = \mu \pm \sigma/\sqrt{N}$, where σ^2 is the variance of O . If correlations are present, the average time required to estimate μ within the fractional error ϵ varies as $(\sigma/\epsilon\mu)^2\tau$, where τ is a measure of correlations in the data. For Metropolis evolution, τ is the auto-correlation time of the observable O . In the case of IE, the efficiency depends on the average time taken by the Monte Carlo algorithm to generate a single run and the degree of correlations present in the different samples produced in the same run. We will take inverse of the average time taken by the Monte Carlo algorithm to obtain one run which generates atleast one configuration of the desired size, as the measure of efficiency.

It is difficult to determine the latter exactly for IE. It depends also on the quantity we want to average. Consider a set of configurations generated by N independent runs of the IE algorithm. Let the probability that a single run produces at least one sample be $P(n)$, and the average number of configurations produced per run be a . Then for large N , we will generate approximately Na configurations, which will be made of approximately $P(n)N$ mutually uncorrelated groups. Thus the average size of a correlated group is $a/P(n)$. It seems reasonable to measure the efficiency of the algorithm in terms of the average CPU time required to produce one independent group of configurations. This overestimates correlations as this treats all samples produced within one run as fully correlated. For example, the value of mean radius of gyration of animals of size 50 on the square lattice is 54.9 and standard deviation σ is 26.9. The average number of samples produced per successful run was 27.5. If we calculate the standard deviation of average radius of gyration of 10^4 consecutive runs, we get $\sigma' = 2.8$. This would have been $\sigma/100 \approx 0.3$ if they were uncorrelated and 4.6 if they were fully correlated. Thus, assuming fully correlated configurations within a run is not an unreasonable estimate.

Other definitions of efficiency are possible, and may be advantageous in specific contexts. For example, one may be interested in some asymptotic properties of the polymer problem, like the branching number λ , or the critical exponent θ . In this case, the value of n is not decided beforehand, and the desired estimate is obtained by suitable extrapolation of data for different n . We can study average number of descendants $\langle X_n \rangle \approx \lambda(1 - \theta/n)$ to estimate λ and θ . Analysis of errors in such quantities is more complicated, and will not be discussed here.

Let T_n be the average CPU time required to obtain one run which generates at least one configuration of size n . If τ_n is the average CPU time for one Monte-Carlo run, then we have

$$T_n = \frac{\tau_n}{P(n)} \quad (4.1)$$

The average CPU time required for one run is estimated easily in terms of the time taken to add or delete a configuration on the genealogical tree. We define this to be one unit of CPU time.

The total CPU time for one MC run is proportional to the number of nodes in the pruned genealogical tree. Let X_j denote the random number of j site configurations generated in a single run. The time to visit the sites of the randomly pruned tree up-to depth n is $\sum_{j=1}^n X_j$. The CPU time in a run is then proportional to the number of nodes in the pruned tree. The average CPU time per run τ_n , would be equal to the sum of average values $\langle X_j \rangle$, averaged over all runs.

$$\tau_n \propto \sum_{j=1}^n \langle X_j \rangle \quad (4.2)$$

For linear and branched polymers, the total number of configurations A_n of a given size n is known to vary as

$$A_n \sim A\lambda^n n^{-\theta} \quad (4.3)$$

for large n . Here A is a constant, λ is called the growth constant and θ is a critical exponent. Since each configuration with n sites has a probability Ξ_n (Eq. (1.15)) of being generated, and there are A_n total number of configurations, $\langle X_n \rangle = \Xi_n A_n$, giving

$$\tau_n = \sum_{j=1}^n A_j \Xi_j \quad (4.4)$$

Since $\langle X_n \rangle$ can be directly estimated in IE, we get a way to estimate the number of configurations $\langle X_n \rangle$ by simulations. This can be used to estimate λ and θ .

A study of the efficiency of the algorithm is complicated as $P(n)$ depends on the structure of the genealogical tree, and is difficult to determine theoretically.

An upper bound on working of this algorithm is the time for exact enumeration of all the samples, which is exponential in n . Consider the case in which $p_i = p$ for all i . So long as

$p\lambda > 1$, $\langle X_n \rangle$ will grow exponentially with n . As $P(n) \leq 1$, this implies that T_n increases exponentially with n if $p\lambda > 1$. Also, if $p\lambda < 1$, then $P(n)$ varies as $(p\lambda)^n$ to leading order, but τ_n remains finite ($\tau_n \geq \tau_1$). Thus again T_n increases exponentially with n . These two considerations together imply that a good choice of p is that it should be chosen to be approximately $1/\lambda$. However, finding the optimal choice of $\{p_i\}$ for a given problem is non trivial. We investigate this in the next section for some illustrative cases.

4.2 Optimising the Incomplete enumeration algorithm

4.2.1 Systems with Uniform genealogical tree

The simplest of enumeration problems is the enumeration on a uniform genealogical tree. For example, random walks which are models for linear polymers without self exclusion correspond to a uniform genealogical tree of branching number λ . The number of nodes at level n is λ^{n-1} .

Consider a uniform genealogical tree with two descendants per node. In this case, the number of nodes at level n would be 2^{n-1} . For a given choice of $\{p_i\}$, the probability of connection of root with level r , denoted by $P(r)$ follows a simple recursion relation

$$P(r+1) = 2p_r P(r) - p_r^2 P^2(r) \quad (4.5)$$

with $P(1) = 1$. The average CPU time per run τ_n is given by

$$\tau_n = 1 + \sum_{i=2}^n 2^{i-1} \Xi_i \quad (4.6)$$

First we try to determine the p_i 's that minimises T_n for small n .

For small sizes one can try systematic optimisation. Let us choose $n = 2$. Then on the binary tree, $P(2) = 2p_1 - p_1^2$ and $\tau_2 = 1 + 2p_1$. This gives,

$$T_2 = \frac{2p_1 + 1}{2p_1 - p_1^2} \quad (4.7)$$

Minimising with respect to p_1 , we get the minimum value of T_2 to be $(3 + \sqrt{5})/2 \approx 2.618$ for $p_1 = (\sqrt{5} - 1)/2 \approx 0.618$.

Similarly, the time (T_3) of IE for reaching level 3 from level 1, is given by

$$T_3 = \frac{1 + 2p_1 + 4p_1p_2}{2p_1(2p_2 - p_2^2) - p_1^2(2p_2 - p_2^2)^2} \quad (4.8)$$

It is easy to check that T_3 in this case takes its minimum value for $p_1 = 0.534$ and $p_2 = 0.618$. Similarly for $n = 4$, the minimum occurs at $p_1 = 0.516$, $p_2 = 0.534$ and $p_3 = 0.618$. For large n , the best choice for the p_i approach $1/2$. By optimising for all $n \leq 30$, we find that the best choice for p_i is well described by the approximate formula $p_i \approx \frac{1}{2}(1 + 0.5/(n - i)^2)$.

For large r , if $p_r \rightarrow p^*$, Eq. (4.5) can be approximated by $P(r+1) = 2p^*P(r) - p^{*2}P(r)^2$. For $2p^* < 1$, we get $P(r) \rightarrow (2p^*)^r$ decreases exponentially with r . For $(2p^*) > 1$, it leads to $P^*(\infty) \sim (2p^* - 1)$.

We have already argued that p_i should be close to $1/\lambda$, else the algorithm is inefficient since T_n varies as $\exp(n)$. Consider now the case where $p_i = \frac{1}{\lambda}(1 + \alpha/i^m)$, where α and m are parameters that we can vary to find the optimal values. In this case, $\langle X_n \rangle = \prod_i (1 + \alpha/i^m)$, and $P(n)$ is approximately given by

$$\frac{\partial P(n)}{\partial n} = \frac{\alpha}{n^m} P(n) - \frac{1}{\lambda^2} P^2(n) \quad (4.9)$$

Then, if $m > 1$, we see that $\langle X_n \rangle$ tends to a constant for large n , and τ_n is proportional to n . Also, $P(n)$ varies as $1/n$, and we have $T_n \sim n^2$.

If $m = 1$, and $-1 < \alpha < 1$, then $\langle X_n \rangle$ varies as n^α , and hence $\tau_n \sim n^{\alpha+1}$. Also, Eq. (4.9) gives $P(n) \sim A(1 - \alpha)n^{\alpha-1}$. Interestingly, in the T_n , these powers cancel and we get $T_n = \tau_n/P(n) \sim C_\alpha n^2$. We find that $C_\alpha \sim 1/(1 - \alpha)$, hence the best choice for α is $\alpha = 0$.

If $m < 1$, then $\langle X_n \rangle$ varies as $\exp(n^{1-m})$, and $P(n)$ varies as n^{-m} , and hence T_n varies as $\exp(n^{1-m})$ to leading order. Thus in this case $m < 1$ leads to a suboptimal performance of the algorithm.

On a binary tree for $p_i = \frac{1}{2}$, we get $T_n = n^2/4$. From systematic optimisation we saw that there exists a nontrivial optimal value for each p_i which depends on the depth of the genealogical tree to be reached. This value for the uniform binary tree was $p_i \approx \frac{1}{2}(1 + 0.5/(n - i)^2)$. But even with this choice for large n we get $T_n \approx n^2/4$. This result is generalised straight forwardly to the k -node uniform tree. For the choice, $p_i = 1/k \forall i$, we get $T_n = \frac{(k-1)n^2}{2k}$.

4.2.2 Systems with recursively defined genealogical tree

It is necessary to check how non-uniformity of trees can change the above conclusions. The simplest of non-uniform trees are the recursively defined trees. The number of branches from a given node still follow a definite pattern which repeats and depends on the coordination number of the parent node. We consider some examples

A node with k descendants will be called a k -node. Consider a tree specified by the rule that the descendants of a 2-node are a 2-node and a 3-node, and the descendants of a 3-node are a 2-node and two 3-nodes. We specify such a tree by the notation (23, 233) tree. If $B_2(n)$ and $B_3(n)$ are the number of distinct trees of n levels with 2 and 3 descendants at level $n - 1$ respectively, then

$$B_2(n) = B_2(n - 1) + B_3(n - 1) \quad (4.10)$$

$$B_3(n) = B_2(n - 1) + 2B_3(n - 1) \quad (4.11)$$

From these linear recursion equations it is easy to see that $B_2(n)$, $B_3(n)$ and also the total number of nodes at depth n , A_n , all grow as $(\lambda)^n$ for large n , where $\lambda = (3 + \sqrt{5})/2$.

We now look at the efficiency of IE on this tree. Take all $p_i = p$. We define $P_2(r)$ and $P_3(r)$ as the probabilities that a 2-node and a 3-node respectively are connected to at least one node r levels below. Clearly they have the following recursions

$$1 - P_2(r + 1) = (1 - pP_2(r))(1 - pP_3(r)) \quad (4.12)$$

$$1 - P_3(r + 1) = (1 - pP_2(r))(1 - pP_3(r))^2 \quad (4.13)$$

with $P_2(1) = P_3(1) = 1$.

For large r , near the fixed point we get $P_2(r) \approx \frac{p}{1-p} P_3(r)$. Substituting in the second equation, we find that the linear term vanishes for $p = 1/\lambda$ and the difference equation can be approximated by $\partial P_2 / \partial r \sim -P_2^2$, which implies that $P_2(n)$ and $P_3(n)$ decay as $1/n$ for large n . We get $P_2(n) \approx \frac{\lambda^2}{(1+\lambda)n}$. The total CPU time at $p = 1/\lambda$ is $\frac{(5+\sqrt{5})n}{10}$. It gives the upper bound on the time per independent run to be $\frac{(\lambda-2)(1+\lambda)}{(3\lambda-2)} n^2 \approx 0.382n^2$.

We can similarly analyse the other recursively defined trees. Consider for example, the tree given by the rule (23, 223). We find that the growth constant λ is 2.4142 and for $p_i = 1/\lambda$ for IE this gives $T_n \approx 0.396n^2$. On a (33, 233) with growth constant 2.732 for $p_i = 1/\lambda$ for IE this gives $T_n = \frac{(\lambda+4)}{4(\lambda+2)} n^2 \approx 0.35n^2$. It is easy to convince oneself that for all recursively defined trees we get $T_n \sim n^2$.

It is instructive to see the results of systematic optimisation over $\{p_i\}$ in case of non uniform trees. Similar analysis for (23,233) tree (Fig. 1.6) between level 1 and 2 gives $p_1 = 0.618$. Similarly optimising T_3 between level 1 and 3 gives $p_1 = 0.562$ and $p_2 = 0.484$. An optimisation between level 1 and 4 gives the best values of p_i 's to be $p_1 = 0.562$, $p_2 = 0.42$ and $p_3 = 0.467$. We see that the optimal value of p_i in this case depends on n . By optimising till $n = 30$, where n is the depth of the genealogical tree, we find that for tree levels away from root and bottom, the optimal value of p_i approaches $1/\lambda$ with increasing i and the asymptotic behaviour of the algorithm remains the same as long as we choose $p_i \approx 1/\lambda$. The optimal p_i values as a function of i are plotted in Fig.4.1. The optimising value of p_i are a bit higher than $1/\lambda$ near the two ends $i = 1$ and $i = n$. This extra optimisation does not change the $T_n \sim Kn^2$ dependence, and in fact does not change the asymptotic value of K either.

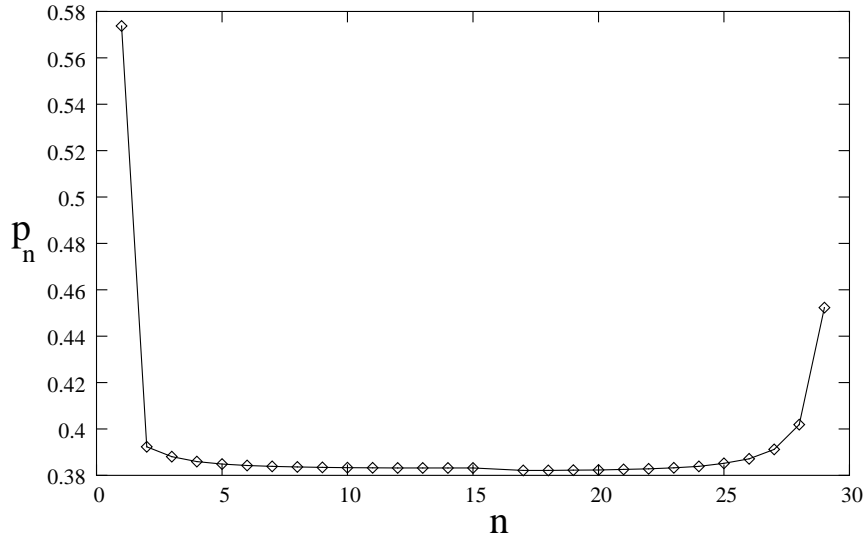


Fig 4.1: Plot of optimum values of p_i on a (23, 233) tree of depth 30

The incomplete enumeration algorithm generates a bond percolation process on the genealogical tree, where each link is present independently with a probability p . We define the percolation threshold p_c on the tree to be such that for all $p > p_c$, there is a non zero probability that the starting node belongs to an infinite cluster. For $p < p_c$ the probability of connection between root and level n usually goes down exponentially in n . At p_c it is expected to decrease as a power law in n and for $p > p_c$ it takes a finite value in the limit of $n \rightarrow \infty$. The p_c on a tree is bounded from below by $1/\lambda$ [20]. For the genealogical trees which we discussed, the p_c was equal to $1/\lambda$ and the optimal behaviour of the algorithm was achieved for $p_i \approx 1/\lambda = p_c$.

4.2.3 Self avoiding Walks

We now consider IE for SAW. For a SAW on a d dimensional lattice, the number of configurations $A_n \sim \lambda^n n^{\gamma-1}$, where λ is a lattice dependent constant and γ depends only on the dimension. The exponent γ is known to be 1 for $d > 4$, and $\gamma = 43/32$ for $d = 2$ [6]. The exact value of λ is known for the hexagonal lattice [16], and a fairly precise numerical estimate, which matches well with root of a quartic equation with integer coefficients is known on the square lattice [17].

The genealogical tree for SAW is not uniform. For example, for rooted SAW (one end fixed at origin) on a square lattice, the number of different allowed choices of the n^{th} step for $n > 1$ varies from 0 to 3, depending on the walk. In this case it is difficult to determine the probabilities of connection up-to level n analytically but we have estimated $P(n)$ numerically by simulations. We choose $p_i = \lambda^{-1}(1 + 1/i)^{1-\gamma}$, so that on the average we get order one configurations of size n per run for large n . With this choice of p_i our numerical simulations show that the probability of reaching level n goes down as $1/n$ and hence whenever level n is reached, on an average $\sim n$ SAW's of size n are generated. This also implies that p_c is indeed $1/\lambda$ on the SAW genealogical tree. We did 10^6 Monte-Carlo simulations and generated walks up-to size 10,000 on a square lattice. We have plotted T_n in Fig 4.2. Our numerical fit suggests T_n for IE to be $(0.42 \pm 0.01)n^2$.

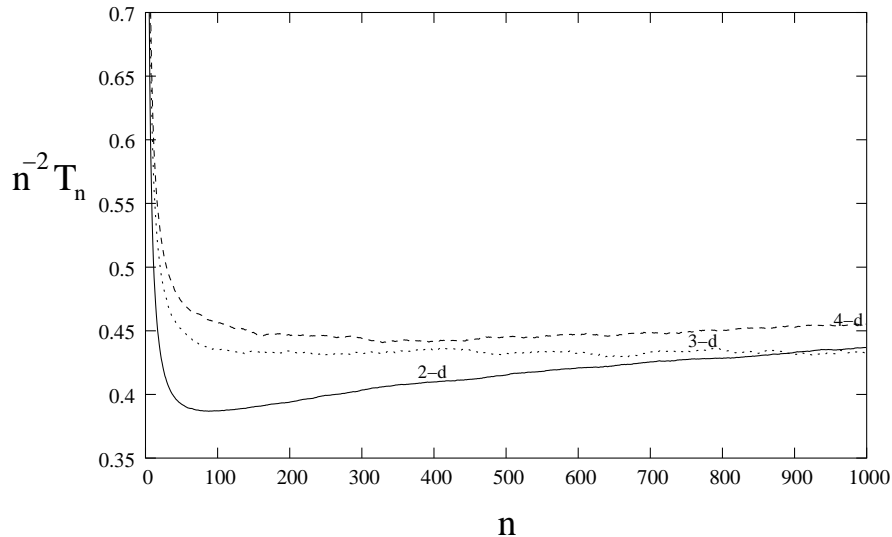


Fig 4.2: T_n/n^2 of IE as a function of size n for SAW on a 2, 3 and 4 dimensional hyper cubic lattice.

In 3 dimensions, $\lambda = 4.6839$ and $\gamma = 1.16$ [6] and nearly 90% nodes have coordination number 5. Hence the tree is more uniform than the $2d$ case and we get $T_n \approx 0.43n^2$ (Fig.

4.2).

The genealogical tree becomes more and more uniform as we go to higher dimensions. In general on a d dimensional hyper-cubic lattice the maximum branching possible is $2d - 1$ and in the limit $d \rightarrow \infty$ the growth constant has an expansion [6]

$$\lambda = 2d - 1 - \frac{1}{2d} - \frac{3}{(2d)^2} - \dots \quad (4.14)$$

Hence the dominant branching is $2d - 1$ and the probability of a node branching into $2d - 1$ branches increases with dimension, and the lower branching numbers occur with much smaller frequencies. The probability of connection to level n is hard to obtain analytically for any d .

In Fig. 4.2 we have also shown a plot of efficiency of IE in 3 and 4 dimensions for SAW. In few hours one can simulate 10^5 Monte-Carlo runs for walks of size 1000 on a Pentium-4 machine. We get $T_n \sim n^2$ for 2,3 and 4 dimensions. This leads us to conclude that the small non uniformity of the genealogical tree is unimportant and T_n varies as n^2 in all dimensions for SAW.

We note that for SAW's, other algorithms like pivot are known to be more efficient. For the pivot algorithm the correlation time for end to end length varies as n^x with $x < 1$ in two dimensions [65]. However, if we want to study some variable like correlation in the direction of consecutive steps of the walk, the correlation time will have to satisfy the inequality, $T_n \geq n$, as one would need to update each step about $O(1)$ times to affect the nearest neighbour correlations.

4.3 Improved Incomplete Enumeration (IIE)

The main limitation of IE is attrition: the probability of generating n -site configurations in a given Monte-Carlo run goes down with n . One way to increase the probability of survival is to redistribute weight amongst the descendants in such a way that while the probability that a particular node is selected remains the same as before, the probability that at-least one of the descendants is chosen is increased. We call this 'Improved Incomplete Enumeration(IIE)'.

Suppose in the implementation of IE as outlined in Sec. 1.6.3, we come to a node with degree j . Then in IE, each link is independently deleted with a probability $(1 - p)$, and the probability that all links are deleted is $(1 - p)^j$, which is non zero, even if the expected

number of descendants of this node is $pj > 1$. In IIE, the links are not deleted independently. The probability that any given node is selected remains p , but the probability that at least one node is selected increases. This is implemented as follows: If there are j descendants of a node and each link downward is present with probability p , then we choose $\text{Int}(pj)$ edges at random and give them weight one, and select one of the edges out of the remaining j at random and give it a weight one with probability $\text{Frac}(pj)$ and delete all the other edges.

Hence we see that in IIE, though the average probability of selection of an edge remains p , it enhances the probability of connection between level 1 and level n of the genealogical tree and hence the probability of success in a given Monte Carlo run. For example, as will be discussed in the next section, on a regular tree with $p = 1/\lambda$, the probability of connection up-to n levels below in IIE is exactly one whereas it goes as $1/n$ in IE.

4.3.1 Systems with recursively defined genealogical tree

In IIE one redistributes the sum of probabilities of connection from a node to the next level. On a uniform binary tree $y_i = 2 \forall i$ and with $p_i = 1/2$, $y_i p_i = 1$ and hence for $p_i = 1/2$ with IIE probability of reaching any level n of the tree after n steps is exactly 1 and exactly one configuration of any given size is generated in the process and hence $T_n = n$. With $p_i = 1/k$ this result holds for any k node uniform tree. Clearly $p_i = 1/k$ is the best choice in this case, since an absolute lower bound on time T_n of the algorithm is n .

If we use the improved algorithm for a (23,233) tree, $\langle X_n \rangle$ and hence the average CPU time per run will remain the same. We can also determine the connection probabilities $P_2(n)$ and $P_3(n)$. The coupled difference equations for $P_2(r)$ and $P_3(r)$ have no cubic term. The recursions are

$$P_2(r+1) = p(P_2(r) + P_3(r)) \quad (4.15)$$

$$P_3(r+1) = p(P_2(r) + 2P_3(r)) - \frac{3p-1}{3}(2P_2(r)P_3(r) + P_3^2(r)) \quad (4.16)$$

which at $p = 1/\lambda = p_c$ gives $P_2(n)$ varying as $1/n$ for large n . The time per independent run comes out to be $\frac{\lambda(3-\lambda)}{3} \approx \frac{1}{3}$ times that in incomplete enumeration. That is, IIE is nearly three times more efficient than IE in this case.

IIE certainly works better than IE. But, except for the uniform tree, the difference between IE and IIE is only in the coefficient of n^2 . While performance of IIE improves as the

genealogical tree becomes more and more uniform, there is no qualitative difference in the efficiency of IE and IIE on a recursively defined non uniform tree.

4.3.2 IIE for Self avoiding walks

We studied IIE on a d dimensional hyper-cubic lattice for $d = 2$ to 10.

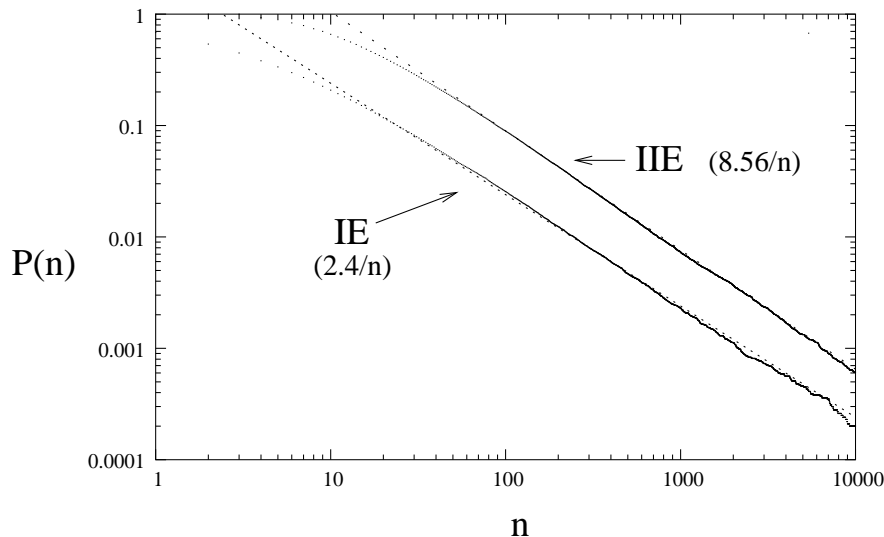


Fig 4.3: Probability of getting a walk of size n on a square lattice for IE and IIE.

IIE enhances the performance of the algorithm by increasing the probability of connection between root and level n . For SAW on a square lattice, Fig. 4.3 shows the probability of connection $P(n)$ for IE and IIE both. $P(n)$ is roughly 3.5 times bigger for IIE. In two dimensions, T_n is of order $0.12n^2$ for IIE. In three dimensions the performance is even better and $T_n \approx 0.056n^2$, which is roughly a factor of 7.5 less than the time taken by IE.

In general we find on a d -dimensional hyper-cubic lattice IIE has a efficiency $T_n = a_d n^2$ where a_d is a decreasing function of dimension for generating SAW's. Fig.4.4 shows the plot of IIE for dimensions 2 to 10. The memory requirement of the algorithm just increases linearly with system size in all dimensions and we could perform 10^5 MC runs for walks up to sizes 1000 in a few hours of computer time on a Pentium-4 (speed is 2.4 GHz) machine. We find that a_d decreases as d^{-2} approximately, i.e. the algorithm performs better with increasing dimension.

We conclude that for IE and IIE for SAW, $T_n = a_d n^2$. The probability of connection between root and level n does not depend on γ . It depends only on the non-uniformity of

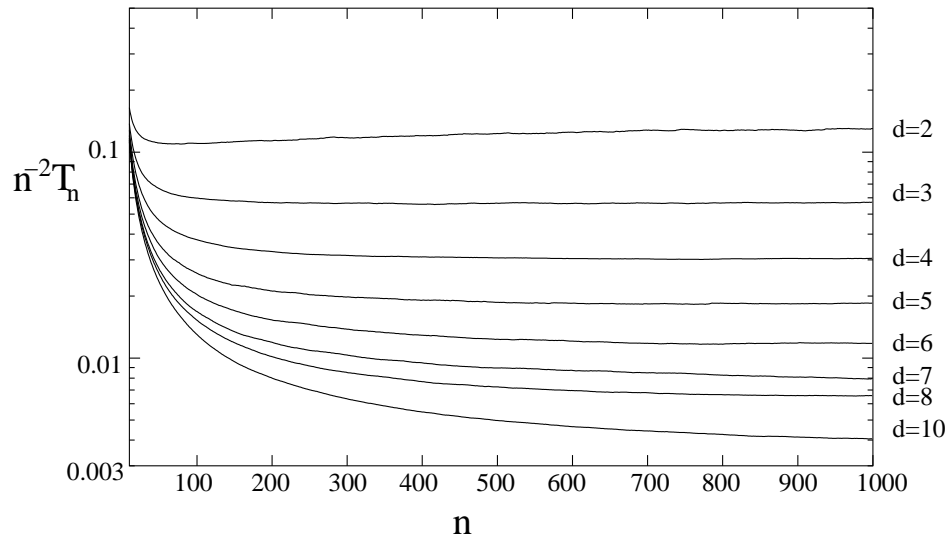


Fig 4.4: T_n/n^2 of IIE vs size n for SAW on a 2, 3, 4, 5, 6, 7, 8 and 10 dimensional hyper cubic lattice.

the tree. The genealogical tree is more uniform in higher dimensions and the constant a_d depends on dimension. For IE, the change in a_d with dimension is quite insignificant. But a_d can be decreased significantly by redistributing weights. This is a strong numerical evidence that the performance of this algorithm is always $O(n^2)$ independent of the dimension and the value of γ for linear polymers.

A further enhancement in the probability of connection can be achieved by choosing the pruning only after looking deeper, but we found that because of the increase both in the memory requirement and in the CPU time to generate one configuration, there is no net gain over IIE.

4.4 Lattice Animals and Branched Polymers

In this section we will study the IE algorithm for branched polymers. Since the efficiency of IE is polynomial in n for linear polymers, it seems plausible that it will be so also for branched polymers. There are two important ways in which the genealogical tree for branched polymers differ from that for linear polymers. There are several equally reasonable, computationally easy to implement choices of rules to define parentage, and in all of them the degree of a node is not bounded. The number of possible descendants of a node is of the order of its perimeter sites and hence the maximum of the degree of nodes at level n increases linearly with n . The average number of descendants λ is of $O(1)$, and the number

of nodes with large branching number is exponentially small. But this makes an important difference in the fluctuations of the number of animals of a given size generated in a given run.

The structure of the genealogical tree for lattice animals is more complex than for self-avoiding walks. We studied the algorithm on the genealogical tree obtained by using Martin's labelling scheme [77]. We have tried two or three variations of the priority rules, and our results are insensitive to these changes.

4.4.1 Lattice animals on a Binary tree

We first discuss our results for the animals on a binary tree. This simple case is more analytically tractable. The generating function of total number of lattice animals on a binary tree is well known [20] and it is $A(y) = \sum_0^\infty A_r y^r = (1 - \sqrt{1 - 4y})/2y$, where A_r is the total number of animals with r sites. A_r are the Catalan numbers, which come up in many other contexts in combinatorics [89]. For large r this gives $A_r \sim 4^r r^{-\frac{3}{2}}$. The growth constant λ in this case is 4.

The number of descendants of a node at level r in the genealogical tree for this problem lies between 2 to $(r + 1)$. In this case the genealogical tree is easily characterised: The root site is a 2-node. A k -node has k descendants, and the degree of these descendants are $k + 1, k, \dots, 3, 2$ respectively. This is seen as follows: the node corresponds to a branched polymer with k unblocked perimeter sites, which are ordered by some priority rule. The m^{th} descendant of this node is a node of degree $(k + 2 - m)$ and corresponds to first $(m - 1)$ perimeter sites blocked, m^{th} site occupied and $(k - m)$ allowed for further occupation. Since on a binary tree every site has two downward neighbours, hence we see that a k -node will give rise to nodes with $k + 1, k, \dots, 2$ descendants (Fig. 4.5). For example, in Fig. 4.6, the top node corresponds to an animal of one site, and has two growth sites. If the first of these two sites is occupied, then the corresponding animal has three growth sites. If it is blocked it has two growth sites and so on.

The total number of nodes at a level r is equal to A_r . Let $B_r(k)$ is the number of k -nodes at level $(r - 1)$. We can determine the distribution of the branching number. We find that $B_r(k)$ satisfies the following relation

$$B_r(k) = A_{r-2} - \sum_{s=2}^{k-2} B_{r-1}(s) \quad (4.17)$$

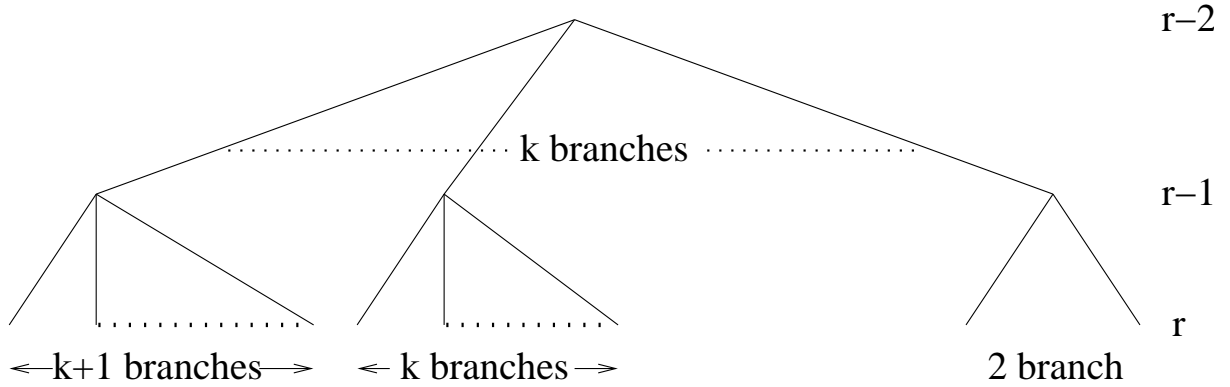


Fig 4.5: A node at level $r - 2$ on the genealogical tree of lattice animal enumeration on a binary tree with k descendants. Here $k \leq (r - 1)$

As $r \rightarrow \infty$, $1/4$ of the nodes at a level have 2 offsprings and $1/4$ of the total nodes have 3 offsprings. And level r has exactly one node with degree $(r + 1)$. For $k \geq 4$, it can be shown that in the asymptotic limit ($r \rightarrow \infty$), the fraction of nodes having k offsprings is $(k - 1)/2^k$ for $r \gg k$.

To find the efficiency factor T_n , we have to determine the probability of connection of root to a level. If $P(k, r)$ is the probability of a node with k offsprings to be connected to at-least one node r levels below it, then $P(k, r)$ has a recursion

$$P(k, r + 1) = 1 - \prod_{s=2}^{k+1} (1 - pP(s, r)), \quad k = 2 \text{ to } \infty \quad (4.18)$$

with initial conditions

$$P(k, 1) = 1 \forall k \geq 2 \quad (4.19)$$

and p is the probability with which we choose any edge of the tree. $P(2, r)$ will give the probability of connection of root to level r on the genealogical tree. Eq. (4.18) is a nonlinear equation. This equation can also be written as

$$1 - P(k, r) = (1 - P(k - 1, r))(1 - pP(k + 1, r - 1)) \quad k > 2 \quad (4.20)$$

This equation is also valid for $k = 2$ if we choose the convention that $P(1, r) = pP(2, r - 1)$.

These equations have the following properties:

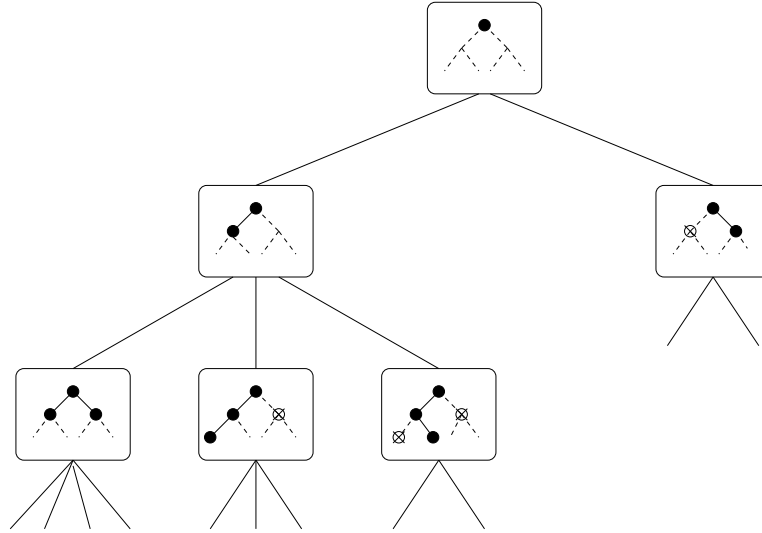


Fig 4.6: First few levels of the genealogical tree for lattice animals on a binary tree. Solid circles represent the occupied sites and crossed circles denote blocked sites on the Bethe lattice. Dotted lines sketch the underlying Bethe lattice, whereas solid lines represent the bonds present.

1. For $p < 1/4$, $P(k, r)$ tends to zero as r tends to infinity exponentially fast for any fixed k . In fact, if we consider r as a time like variable and k as space like variable, then $P(k, r)$ has a travelling front solution in this regime ($P(k, r) \cong F(k - vr)$).
2. For $p = 1/4$, the velocity of travelling front goes to zero. The distance moved by the front increases as $r^{1/3}$ and $P(k, r) \sim F(k - r^{1/3})$. As $F(x) \sim \exp(x)$ for $x \rightarrow -\infty$, this implies that $P(2, r) \sim \exp(-cr^{1/3})$ for large x .
3. For $p > 1/4$, as r goes to infinity, $P(k)$ tends to a non trivial fixed point function $P^*(k)$ greater than zero.

This may be seen as follows. The fixed point equation in terms of fixed point variables $P^*(k)$ is

$$1 - P^*(k) = (1 - P^*(k - 1))(1 - pP^*(k + 1)) \quad (4.21)$$

Clearly, $P^*(k) = 0 \forall k$ is a trivial fixed point of this equation. For $p > 1/4$, there is a non trivial fixed point with $P^*(k)$ non zero monotonic increasing, with $P^*(k) \approx 1 - (1 - p)^k$ for large k . However, a closed form solution for any $p > 1/4$ is difficult.

On numerically iterating Eq. (4.18) in r , we find that the equation has a travelling front solution for $p \leq 1/4$ and has nontrivial fixed point for $p > 1/4$.

Eq (4.21) has two stationary solutions, i.e. $P^*(k) = 1 \forall k$ and $P^*(k) = 0 \forall k$. For $p \leq 1/4$, $P^*(k) = 0$ is the stable solution while $P^*(k) = 1$ is an unstable solution. Our initial conditions given by Eq (4.19) are steep. Starting with these initial conditions, on numerical iteration we find that as r increases, a front separating the stable solution $P = 0$ and the unstable solution $P = 1$ moves in the forward direction. From the translational invariance of Eq. (4.18) one expects a running wave solution. We find that the front moves with a constant velocity and hence, $P(k, r)$ for large k and v must tend to the asymptotic form

$$P(k, r) \sim F(k - vr) \tag{4.22}$$

We define $k^*(r)$, the width of the front by the equation,

$$P(k^*(r), r) = \frac{1}{2} \tag{4.23}$$

Fig. 4.4.1 shows a plot of numerically determined $P(k, r)$ with respect to $k - k^*(r)$ for p near $1/4$. Curves for p below, above and at $p = 1/4$ all collapse on the same line. Actually, a travelling front for $P(k, r)$ as defined by Eq. (4.20) exists for all k , $-\infty < k < \infty$, if we take boundary conditions such that $P(-\infty, r) = 0$ and $P(\infty, r) = 1$.

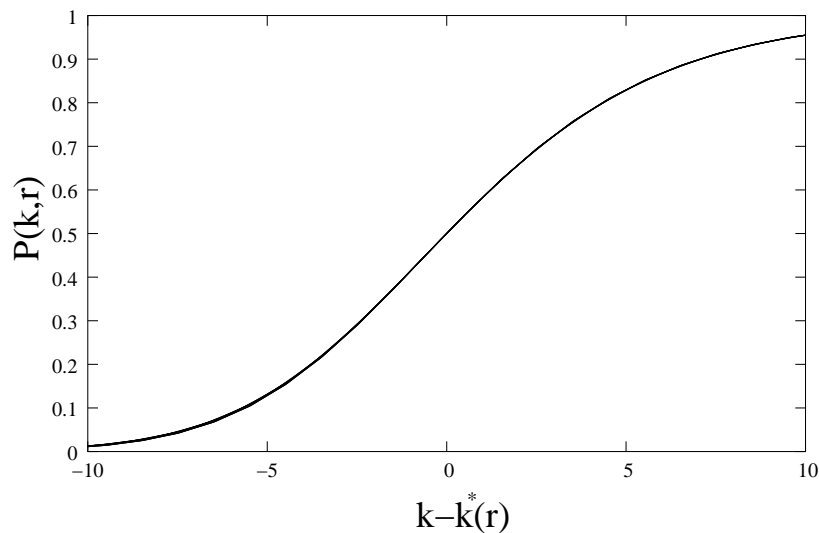


Fig 4.7: Plot of $P(k, r)$ versus scaled $k - k^*(r)$, for $p = 0.25$ and $p = 0.25 \pm 0.0001$ and $r = 100, 300$ and 600 . All the nine curves collapse to the same front profile.

At $p = 1/4$, the velocity of the travelling front is zero. If we plot $P(k+1, r)$ as a function of $P(k, r)$, we find that as r increases the graph approaches a limiting form. Thus for the

asymptotic wavefront, $P(k+1, r)$ is a single valued nonlinear function of $P(k, r)$. We have plotted these values for different r in Fig. 4.8 and they all are very close and seem to lie on the same curve. Hence if we start from a point on this curve and iterate the fixed point equation Eq. (4.21) with $p = 1/4$, we generate a travelling front. We have not been able to deduce the functional form of this function, which corresponds to a first order difference equation for $P^*(k)$ from the second order equation Eq. (4.21). Eq. (4.21) turns out to be a stiff equation and one has to be careful while iterating it in the increasing k direction. We iterated Eq. (4.21) starting with different sets of values of $P^*(k+1)$ and $P^*(k)$ given by Fig. 4.8 and found the equation yields a travelling front same as the one shown in Fig. 4.4.1.

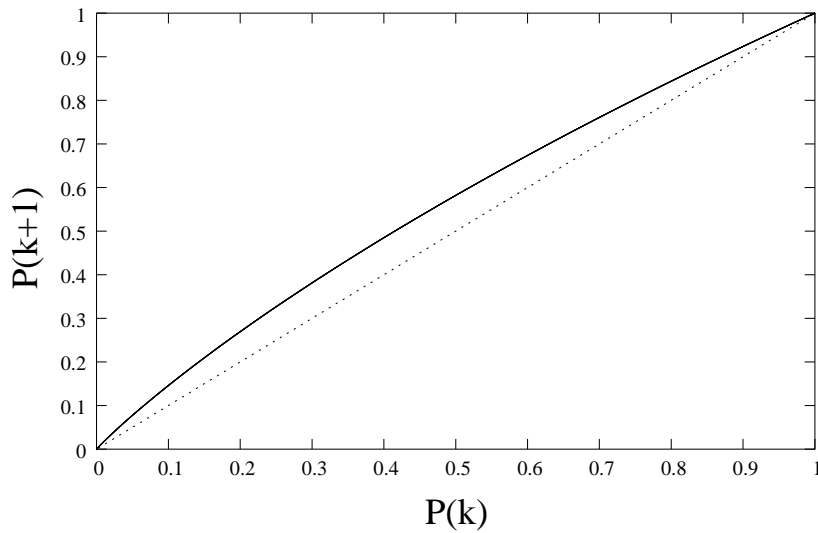


Fig 4.8: Plot of $P(k+1)$ as a function of $P(k)$ at $p = 1/4$ for $r = 25000, 26000, 28000$ and 30000 . All the curves are very close and approach a limiting form with increasing r . The dotted line is just the line $x = y$.

We could not solve the full non-linear difference equation Eq. (4.18). Keeping only the terms linear in P will give an upper-bound on $P(k, r+1)$, i.e.

$$P(k, r+1) \leq p \sum_{s=2}^{k+1} P(s, r) \quad (4.24)$$

We can represent this set of equations in matrix form also. Hence if \mathcal{P}_r represents the infinite column array with k^{th} entry being $P(k, r)$ then

$$\mathcal{P}_r \leq p^r M^r \mathcal{P}_0 \quad (4.25)$$

where M is the transition matrix. If λ_m is the largest eigenvalue of M then for $p < 1/\lambda_m$, in the limit of $r \rightarrow \infty$, \mathcal{P}^* will be 0, i.e. $P^*(k) = 0$ for all k , and for $p < 1/\lambda_m$.

The elements $M_{i,j}$ of the transition matrix M are such that, $M_{i,j} = 1$ for $j \leq (i + 1)$ and 0 otherwise. If we truncate M beyond $n \times n$ (M_n), then the determinant D_n of M_n comes out to be

$$D_n = A(\lambda) \left[\frac{1}{x_1^{n+1}} - \frac{1}{x_2^{n+1}} \right] \quad (4.26)$$

with $x_1, x_2 = \frac{-1}{2} \pm \sqrt{1 - \frac{4}{\lambda}}$, and $A(\lambda) = 1/\sqrt{1 - \frac{4}{\lambda}}$ is a coefficient which does not depend on n . Then equating $D_n = 0$ in the $n \rightarrow \infty$ limit gives $\lambda_m = 4$. This implies that for $p < 1/4$, $P(k, r)$ will decay exponentially with increasing r and Eq (4.24) will work well. Hence, by definition percolation threshold p_c of this tree is $1/4$.

The linearised recursion can be solved explicitly, and we get,

$$P(k, r) = p^r \frac{\Gamma[k + 2r - 1]}{\Gamma[k + r - 1]\Gamma[r + 1]} \quad (4.27)$$

which for large r gives

$$P(k, r) \sim \frac{1}{4\sqrt{\pi r}} \exp \left[\ln 2 \left(k + r \frac{\ln(4p)}{\ln(2)} \right) \right] \quad (4.28)$$

If we assume a travelling front solution of kind $P(k, r) \propto \exp(\lambda(k - vr))$ to be valid in the tail of the distribution, then substituting in linearised recursion (Eq.(4.24)), for a given p we get a spectrum of travelling wave like solutions parametrised by λ with the velocity v of the front given by

$$v = \frac{1}{\lambda} \ln \frac{1 - \exp(-\lambda)}{p} - 1 \quad (4.29)$$

In this case, it is known that the front actually chooses a unique velocity given by the minimum of right hand side of Eq. (4.29) with respect to λ [90]. The front velocity is given by

$$v^* = \frac{2\exp(-\lambda^*) - 1}{1 - \exp(-\lambda^*)} \quad (4.30)$$

where λ^* is the solution of the transcendental equation

$$\frac{-1}{\lambda^*} \ln \frac{1 - \exp(-\lambda^*)}{p} + \frac{\exp(-\lambda^*)}{1 - \exp(-\lambda^*)} = 0 \quad (4.31)$$

Near $p = 1/4$, we can take $v \approx \ln(4p)/\ln(2)$ and $\lambda \approx \ln 2$. Travelling front solutions have been found in a large variety of problems in physics [91].

The linearisation of Eq (4.18) would be valid only for $p \leq 1/4$ and $k < k_o(r)$. Beyond that the linear solution will grow beyond one whereas the solution of the full nonlinear equation will saturate to 1. Here $k_o(r)$ is the value of k at which $P(k, r)$ given by Eq. (4.28) becomes of $O(1)$ and is equal to

$$k_o(r) = \frac{-r \ln(4p)}{\ln 2}, \text{ for } p < \frac{1}{4} \quad (4.32)$$

At $p = 1/4$, the asymptotic velocity of the front is zero and the front advances as a sub linear power of r . This is the critical point of the percolation on this tree, and Eq. (4.28) gives a algebraic decaying solution for sufficiently small k . This is only an upper bound to the actual value. On numerically iterating Eq. (4.18) for r up to order 10^4 , we found unexpectedly that it decays as a stretched exponential in r .

The fixed point equation as given by Eq. (4.21) is again a nonlinear equation. To find the dependence of the probability of connection of root, $P(2, r)$, on the width of the front we solved the linearised fixed point equation. On solving, we find that it goes as $2^{-k^*(r)}$ for large r , where $k^*(r)$ is the width of the distribution. Hence in general, $P(2, r) \sim \exp(-ak^*(r))$.

We further studied the width $k^*(r)$ of the front as a function of r for different values of p . At $p = 1/4$ we found $k^*(r) \sim r^{1/3}$. Fig. 4.9 shows a plot of $k^*(r)$ as a function of $r^{1/3}$. For $p = 1/4$, the plot is a straight line. This implies that $P(2, r) \sim \exp(-cr^{1/3})$ at $p = 1/4$. For $p < 1/4$, $k^*(r)$ varies linearly with r and tends to a constant for $p > 1/4$. We can directly iterate Eq. (4.18). In Fig 4.10 we have plotted $-\log(P(2, r))$ as a function of $r^{1/3}$ which comes out to be a straight line. Fig 4.9 and Fig. 4.10 are strong numerical evidence that the probability of connection goes as $\exp(-cr^\alpha)$ for branched polymers on binary tree. Our numerical studies give $\alpha = 0.333 \pm 0.005$ and $c = 2.47 \pm 0.01$.

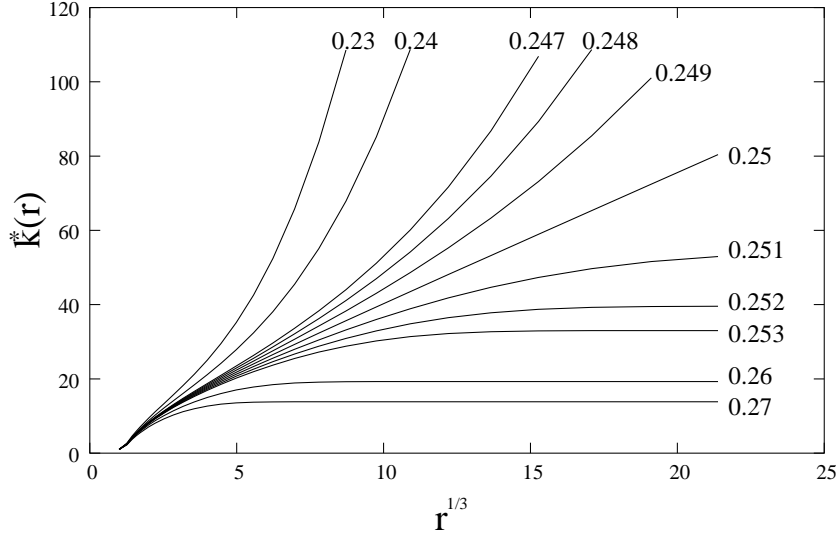


Fig 4.9: The width $k^*(r)$ of the travelling front as a function of $r^{1/3}$ for different values of p . The value of p increases from left to right. Curves of left of $p = 1/4$ are for $p < 1/4$ and the ones on right are for $p > 1/4$. For $p = 1/4$ the graph approaches a straight line as $r \rightarrow \infty$.

4.4.2 Heuristic argument for the stretched exponential behaviour of $P(n)$ at $p = 1/4$

We now present a heuristic argument to understand why k^* varies as $r^{1/3}$ at p_c . Let us consider a genealogical tree of lattice animals on a binary tree, in which nodes with more than k descendants are deleted. We denote the probability that the maximum degree of a node connected to root down to level r is k_m , by $H_2(k_m)$ and the probability that a k_m node is connected to at least one node r levels down on the truncated genealogical tree by $J_{k_m}(r)$.

Now on a truncated tree, transition matrix M is no longer infinite. It is now a $k_m \times k_m$ matrix with $M_{i,j} = 1$ for $j \leq (i + 1)$ and 0 otherwise. Here $M_{i,j}$ represents the i^{th} row and j^{th} column entry of M , and we find the critical value of p which is just inverse of the largest eigenvalue of M to be a function of k_m and is equal to

$$p_c(k_m) = \frac{1}{4} \left(1 + \tan^2 \left(\frac{\pi}{k_m + 1} \right) \right) \quad (4.33)$$

For $p < p_c(k_m)$, $J_{k_m}(r)$ decays exponentially with r . In the large r limit it is given by

$$J_{k_m}(r) \sim \exp(r \log(p/p_c(k_m))) \quad (4.34)$$

At $p = 1/4$, we get $J_{k_m}(r) \sim \exp(-br/k_m^2)$, where b is a constant.

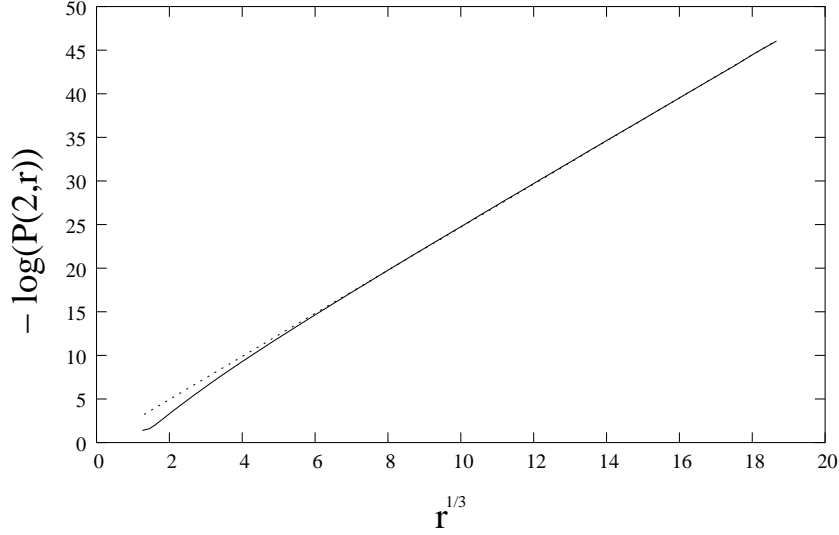


Fig 4.10: Thick line is the plot of $-\log(P(2,r))$ as a function of $r^{1/3}$, when p is taken to be $1/4$. The dotted line is a straight line of slope 2.47.

It is easy to get a lower bound on $H_2(k_m)$, as an order k_m node occurs for the first time at level k_m and the probability of connection of root to this node is p^{k_m} . Hence

$$H_2(k_m) \geq p^{k_m} = 4^{-k_m} \quad (4.35)$$

Hence, since $p = 1/4$ is less than $p_c(k_m)$ for any finite k_m , $J_{k_m}(r) \sim \exp(-br/k_m^2)$, where $b = \pi^2$. Since $H_2(k_m) \geq \exp(-a_p k_m)$, for large r we get

$$P(2,r) \geq \max_{k_m} \left[\exp \left(-a_p k_m - \frac{br}{k_m^2} \right) \right] \quad (4.36)$$

which gives

$$P[2,r] \geq \exp(-cr^{1/3}) \quad (4.37)$$

where $c = \frac{3}{2}(2ba_p^2)^{\frac{1}{3}}$. If we take $H_2(k_m)$ to be as given by Eq. (4.35), we get a lower bound on $P(2,r)$. Taking $b = \pi^2$ and $a_p = \log 4$ we get $c = \frac{3}{2}(2\pi^2 \log^2 4)^{1/3} = 5.04$. This should be compared with the numerical estimate $c \cong 2.47$.

Thus our numerical simulations and qualitative arguments show that probability of connection goes down as a stretched exponential at $p = 1/4$, the p_c of the genealogical tree of lattice animals on binary tree as opposed to r^{-1} decay for linear polymers. So if we

chose $p_i = 1/4 \forall i$, then $\langle X_r \rangle \sim r^{-3/2}$ and hence the average computer time to generate one statistically independent sample of size r , T_r would go as $\exp(cr^{1/3})$ to leading order.

Clearly the algorithm is not working well and one would like to enhance its efficiency if possible. We tried to study the algorithm by choosing p_i such that its asymptotic value is $1/4$. We chose $p_i = \frac{1}{4}(1 + \frac{x}{i^m})$ and studied T_r as a function of x and m .

As argued earlier, taking $m = 1$, we can change τ_r and $P(r)$ by multiplicative factors which are powers of r . This will not make much of a difference, as the leading dependence remains $\exp(cr^{1/3})$. Using $m < 1$, seems to be more interesting.

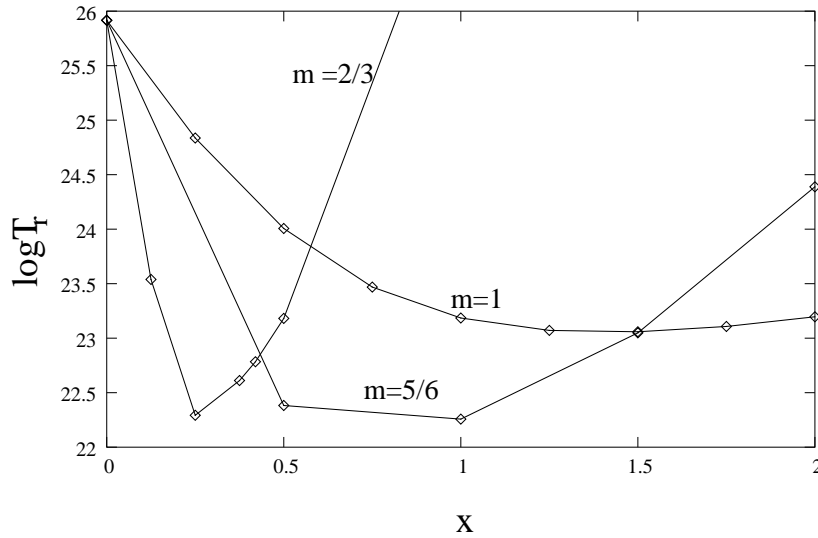


Fig 4.11: Plot of $\log T_n$ for $m = 2/3, 5/6$ and 1 as a function of x for $n = 1000$.

For $m < 1$, the average CPU time per Monte-Carlo run would vary as $\exp(xr^{1-m})$. In case of linear polymers, we saw that time complexity of the algorithm for $m = 1$ for any x is polynomial in r . Hence, $m < 1$ was clearly a bad choice. But in the case of lattice animals, this increase in numerator is exactly cancelled by a corresponding increase in $P(r)$. For $2/3 \leq m < 1$, τ_r increases as $\exp(xr^{1-m})$ and $P(r)$ varies as $\exp(-cr^{1/3} + xr^{1-m})$ to leading order for large r . These cancel to give $T_r \sim \exp(cr^{1/3})$ independent of m . To monitor the behaviour of various prefactors, we study this numerically. Fig. 4.11 shows plot of T_r for $r = 1000$, for $m = 2/3, 5/6$ and 1 as a function of x . For $1 \geq a \geq 2/3$, to leading order T_r goes as $\exp(cr^{1/3})$, but there exist a non trivial value of x at which T_r is minimum for a given m . If we look at T_r at best value of x for $m = 2/3, 5/6$ and 1 , we find that as r increases the difference is not significant.

Hence we conclude that to leading order, $T_r \sim \exp(cr^{1/3})$, for the best choice of p . For

all $2/3 \leq m \leq 1$, there exists a range of x for which the time complexity of the algorithm will remain qualitatively the same.

4.4.3 Lattice Animals on a 2 dimensional square lattice

We also studied the efficiency for lattice animals on a square lattice. From exact series enumeration the A_r is known to vary as λ^r with $\lambda \approx 4.06257$ [55]. In this case also the number of offsprings a node at level r can have is $O(r)$ and the genealogical tree in this case though more complicated, is qualitatively similar. Numerically, we find that the probability distribution of the number of descendants k (of a randomly chosen node) has a maximum at $k = 4$, with $Prob(k = 4) \approx 1/4$. We enumerated lattice animals up-to sizes 1000 using IE with 10^6 Monte-Carlo runs. It took time of order one day on a Pentium-4 (2.4MHz) machine. With IIE we generated samples of size 2000 with 2×10^6 Monte-Carlo runs in 2-3 days time. These sizes are of same order as those produced using the cut and paste type algorithms.

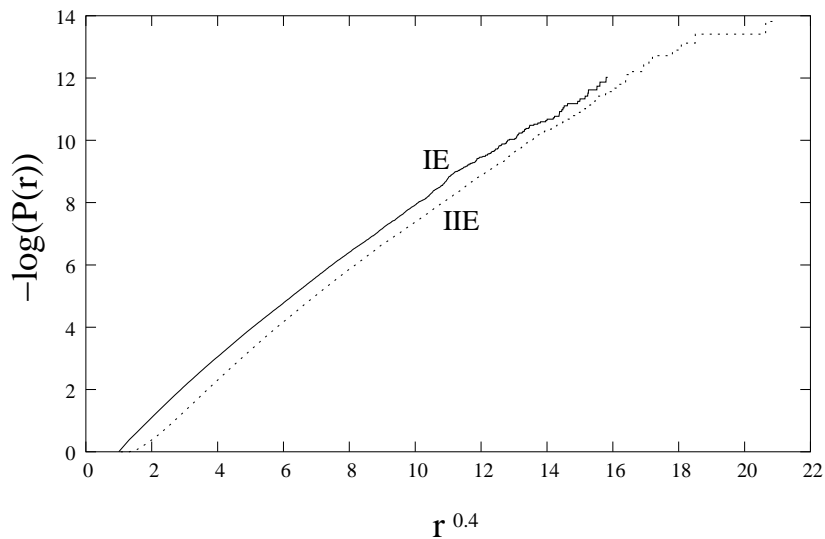


Fig 4.12: Plot of $-\log(P(2, r))$ versus $r^{0.4}$ for lattice animals on a square lattice with IE and IIE

In this case, we find that $P(r)$ has the stretched exponential form $P(n) \sim \exp(-cn^\alpha)$, with $\alpha \approx 0.4$ for both IE and IIE. Fig. 4.12 shows $[-\log P(r)]$ varies approximately linearly with $r^{0.4}$. We also studied the directed lattice animals (DA) on a square lattice. In this case we find that, $\alpha = 0.32 \pm 0.02$ (Fig. 4.13).

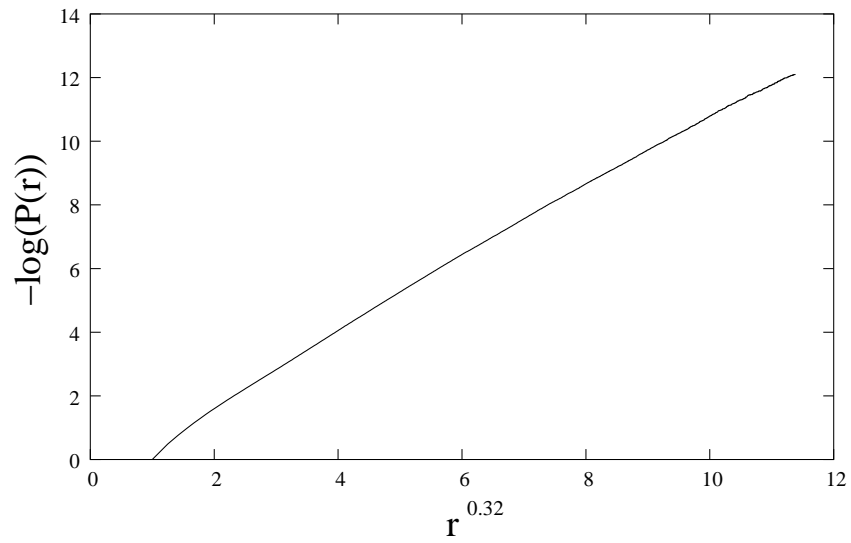


Fig 4.13: Plot of $-\log(P(r))$ versus $r^{0.32}$ for directed animals with IIE.

Rooted Spiral-trees in two, three and four dimensions

The model of rooted spiral trees was defined in Section 1.5. In this chapter, in Section. 5.1 we will derive the generating function for enumeration of a subset of all possible spiral trees and thus obtain a lower bound on the growth constant λ_{spiral} of the spiral trees on a square lattice. In Section. 5.2, we study spiral trees on a square lattice using both exact enumeration and Monte-Carlo methods. In Section. 5.3 and Section. 5.4 we give our numerical estimates for spiral trees on three and four dimensional hyper-cubic lattice. We find that the spiral constraint can be implemented in two ways for $d > 2$. We studied both of them and surprisingly found the two implementation of spiral rules belonging to two different universality classes [92].

5.1 Lower Bound on Growth Constant on a Square lattice

Some pictures of randomly generated large spiral trees are shown in Fig. 5.1. One notes very long one dimensional structures with infrequent turns. Hence, a simple counting of structures of the kind shown in Fig.5.2 should give a good estimate of the growth constant λ . The generating function of trees of this type is easy to determine. If $A_1(x)$ is the generating function, we get

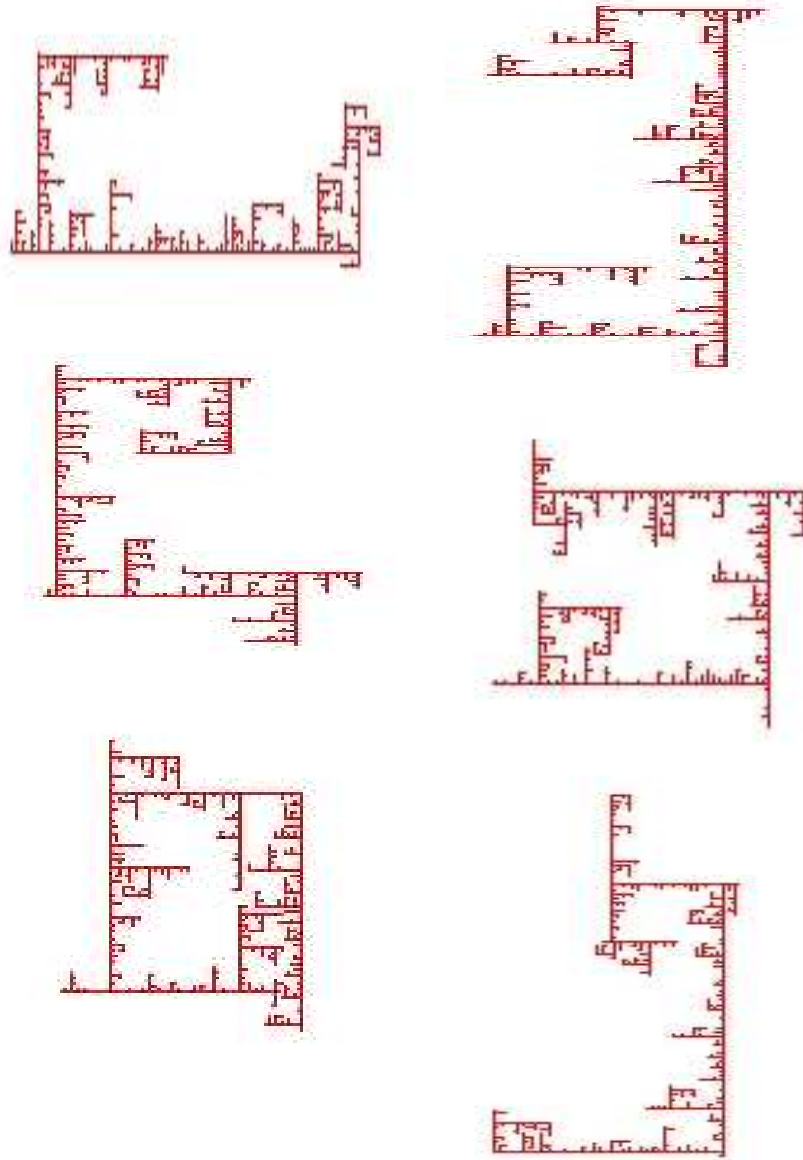


Fig 5.1: Randomly generated spiral trees of 1000 sites in 2-dimensions using the incomplete-enumeration algorithm

$$A_1(x) = \frac{x}{1-x} + \frac{x^3}{(1-x)^2} A_1(x) \tag{5.1}$$

here first term comes from trees which are just the one-dimensional line of variable size along the y -axis and the second term counts trees with atleast one horizontal bend. From Eq. 5.1 we get, $A_1(x) = \frac{x(1-x)}{1+x^2-2x-x^3}$. The number of trees of this type grows as λ_1^n , with $\lambda_1 = 1.754878$. It is straightforward to include more complicated branches in such a counting to get a better lower bound. This we proceed to do below.

Consider a subset of all the spiral trees on a square lattice rooted at the origin, which lie strictly in the first quadrant $x \geq 0, y \geq 0$; starting at the origin, and not touching $y = 0$ and $y = 1$ except at points $(0, 0)$ and $(0, 1)$ respectively. If $Q(x)$ is the generating function for spiral trees in a quadrant and if $q_{4,n}$ is the coefficient of x^n in the expansion of $([Q(x)]^4)/x^3$, then

$$A_n \geq q_{4,n} \tag{5.2}$$

where A_n is the n^{th} term of $A(x)$, the generating function of all spiral trees on the square lattice.

The enumeration of graphs contributing to $Q(x)$ can be made easier by noticing that these graphs can be formed by combination of smaller graphs. We define an articulation point [93] as a point on y -axis such that the tree above is an allowed spiral tree in the quadrant above that part (note that these trees are defined in the upper quadrant and they never touch $y = 0$ axis, except at $(0,0)$). For example, the solid squares represent the articulation points of the graph in Fig. 5.2, and Fig. 5.3 shows a spiral tree with no articulation point. Hence, these spiral trees can be seen as trees having y axis as a backbone on which spiral graphs are connected at different articulation points maintaining the spiral constraint.

Let $B(x)$ be the generating function of the quadrant spiral trees with no articulation points. $B(x)$ can be seen as the sum of generating functions of irreducible graphs with i sites along y -axis. We represent them by $B_i(x)$ (see Fig. 5.4), then $B(x) = \sum_{i=1}^{\infty} B_i(x)$. The full generating function in terms of $B(x)$ would be

$$Q(x) = x(1 + B(x) + B^2(x).....) = \frac{x}{1 - B(x)} \tag{5.3}$$

where $B_i(x)$ are spiral graphs starting with i -sites along the y -axis. It is easy to see that $B_1(x) = x, B_2(x) = \frac{x^3}{1-x}$ and $B_3(x) = \frac{x^6}{(1-x-x^3)(1-x)}$. One can write $B_4(x)$ with some effort

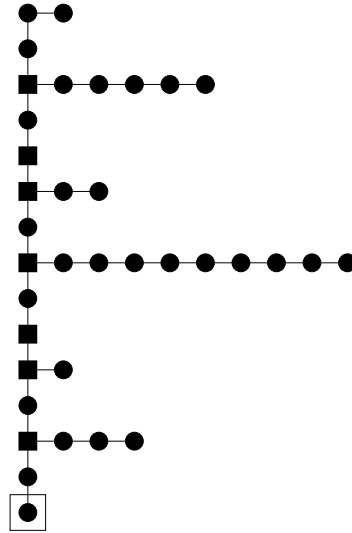


Fig 5.2: A simple counting problem of backbone with arbitrary long straight offshoots. Minimum distance between two offshoots is 2 so that the tree constraint is not violated. Solid squares represent the articulation points of the graph.

but we do not have a general form for $B_i(x)$ for all i .

We restrict the graphs contributing to $B_i(x)$ to be graphs such that they have i sites along the y axis and have at least one downward branch with $i - 1$ sites. This would not include structures like Fig. 5.3. We will represent the generating function of these graphs by $Q_1(x)$. Then we can represent $B_i(x)$ in terms of two other generating functions, $V_i(x)$ and $W_i(x)$. We define $V_i(x)$ as the generating function of spiral subgraphs starting with having i sites along y -axis. $W_i(x)$ is the generating function of spiral subgraphs starting with i -sites along y -axis and ending with a downward branch with $i - 1$ sites (Fig.5.5). Then,

$$B_i(x) = W_i(x) + \frac{W_i(x)V_{i-1}(x)}{x^{i-1}} \quad (5.4)$$

Also, $V_i(x)$ can be rewritten in terms of $W_i(x)$ as

$$V_i(x) = xV_{i-1}(x) + W_i(x) + \frac{W_i(x)V_{i-1}(x)}{x^{i-1}} \quad (5.5)$$

By expressing $Q_1(x)$ in terms of $B_i(x)$ and $B_i(x)$ in turn in terms of $W_i(x)$, we can reduce the computational time. If W_n is the number of graphs of size n contributing to $W(x)$ ($W(x) = \sum_{i=1}^{\infty} W_i(x)$), and Q_n is the number of graphs of size n contributing to $Q_1(x)$, then W_n grows more slowly than Q_n . We enumerated W_n and using them we could generate a

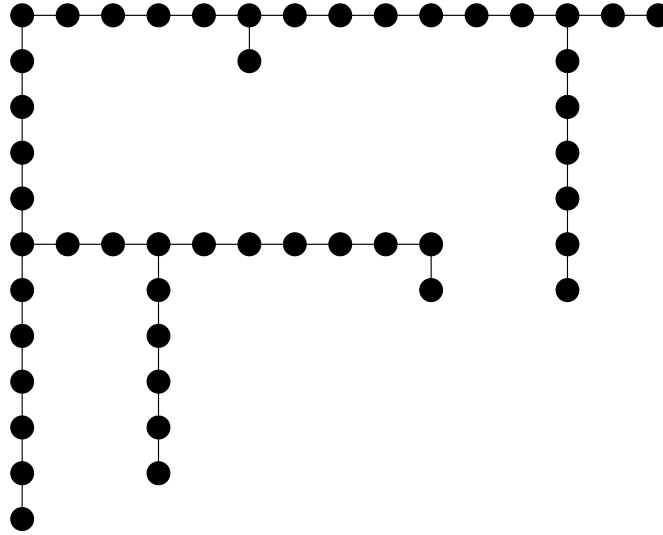


Fig 5.3: An example of an irreducible spiral graph with no articulation point. This is also an example of a graph not included in $Q_1(x)$

56 term series for $Q_1(x)$. The computation time for W_n grows more slowly, and roughly as $(1.8)^n$, in contrast to $(2.04)^n$ for the Q_n series.

If we restrict the graphs contributing to $B_i(x)$, $W_i(x)$ and $V_i(x)$ to the graphs having comb-like structure (by comb-like structure we mean graphs with one dimensional backbone having vertical straight lines of arbitrary lengths), then it turns out that one can get the exact expression for these generating functions. We represent them by $\tilde{V}_i(x)$, $\tilde{W}_i(x)$ and $\tilde{B}_i(x)$. It is easy to see that for comb like structures,

$$W_i(x) \geq \tilde{W}_i(x) = \frac{x^{2i}}{1-x} + \frac{x^{2i}}{1-x} \frac{K(x)}{1-x} + \frac{x^{2i}}{1-x} \left(\frac{K(x)}{1-x} \right)^2 + \dots \quad (5.6)$$

where $K(x) = x^2 \sum_{j=1}^{i-2} x^j$. Hence,

$$\tilde{W}_i(x) = \frac{x^{2i}(1-x)}{1-2x+x^2-x^3+x^{i+1}} \quad (5.7)$$

Similarly, we get

$$\tilde{V}_i(x) = \frac{x^{i+1}(1-x+x^2-x^i)}{1-2x+x^2-x^3+x^{i+1}} \quad (5.8)$$

and hence

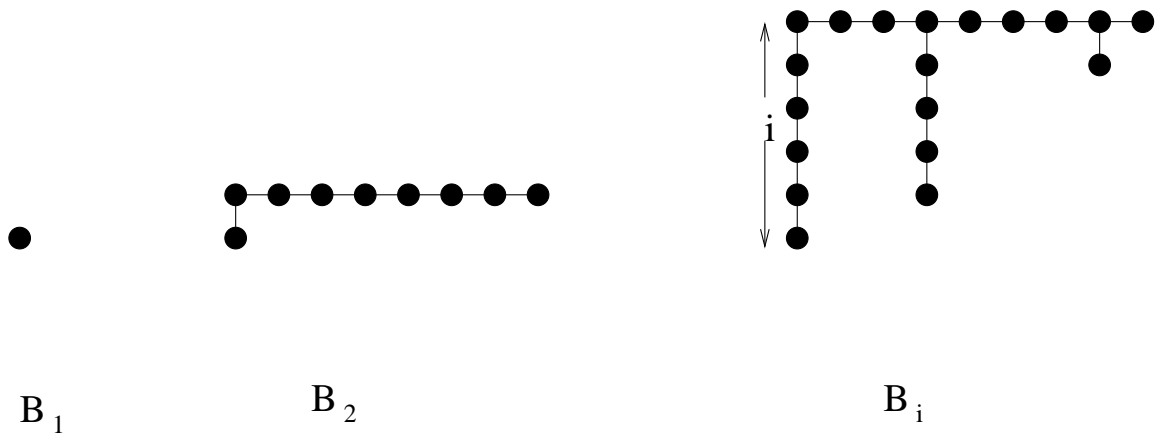


Fig 5.4: Schematic figure of spiral trees contributing to $B_i(x)$. $B_1(x)$ is just a single vertex.

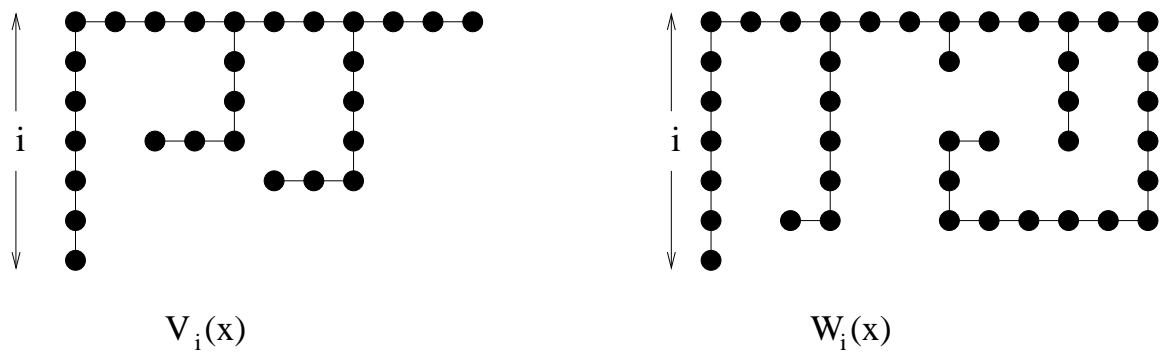


Fig 5.5: Example of graphs contributing to $V_i(x)$ and $W_i(x)$ respectively.

$$B_i(x) \geq \tilde{B}_i(x) = \frac{x^{2i}(1-x)^2}{(1-2x+x^2-x^3+x^i)(1-2x+x^2-x^3+x^{i+1})} \quad (5.9)$$

Substituting in Eq. 5.3 we get the generating function, $\tilde{Q}_1(x)$ for this subset of spiral trees in a quadrant. This generating function has a singularity at $x_c = 0.51662$ which gives the growth constant λ' of these trees to be 1.93565. Since this counts only a subset of all the spiral trees on a square lattice, this is a rigorous lower bound on λ_{spiral} for spiral trees on a square lattice.

For the full $Q_1(x)$, we derived a 55 term series. This series is given in Table 5.1. If we assume,

$$Q_n \sim \lambda_1^n n^{-\theta_1} \quad (5.10)$$

then we got estimates of λ_1 and θ_1 to be

Cluster size(n)	A_n	Cluster size(n)	A_n
4	2	30	67231660
5	4	31	133149845
6	7	32	263802053
7	13	33	522850068
8	25	34	1036643261
9	48	35	2056018929
10	92	36	4079092115
11	178	37	8095287385
12	345	38	16070435197
13	672	39	31911288108
14	1310	40	63383684512
15	2560	41	125928086949
16	5011	42	250250858092
17	9824	43	497430669322
18	19282	44	988985669035
19	37890	45	1966729333270
20	74531	46	3911949831518
21	146744	47	7782751762274
22	289155	48	15486797698499
23	570204	49	30823085860957
24	1125202	50	61358440154867
25	2221827	51	122167029706091
26	4389751	52	243283788357669
27	8677757	53	484562545163938
28	17163089	54	965299790910033
29	33961624	55	1923306810488493

Table 5.1: Series for the number of quadrant spiral trees on a square lattice

$$\lambda_1 = 2.0449 \pm 0.0001 \quad (5.11)$$

$$\theta_1 = 0.830 \pm 0.01 \quad (5.12)$$

5.2 Spiral trees on a square lattice

5.2.1 Exact enumeration

Since the number of configurations of a given cluster size is exponential in cluster size, the computational complexity of the algorithm for enumeration of all lattice animals or trees grows exponentially with the cluster size. For direct enumeration algorithms like Martin's algorithm [77], the time required to generate all the configurations of a given size grows as λ^n , where λ is the growth constant and n is the cluster size and the memory requirement grows like a polynomial in cluster size. For lattice trees and animals, a finite lattice method [56] with an associated transfer matrix algorithm was used by Conway [94]. Conway generated a 25 term series for lattice animals using this algorithm. This series has recently been extended to 46 terms by Jensen [55] with a slight improvement in the algorithm. Both space and time requirements of this algorithm are found numerically to approximately grow as 1.4^n . The growth constant of lattice animals in contrast is approximately 4.06. Hence a considerable improvement in time is obtained by the transfer matrix algorithm at the cost of memory.

The spiral constraint, cannot be easily implemented using the transfer matrix. Hence we have used Martin's algorithm for spiral trees, making use of the four-fold rotational symmetry of the lattice. Our series for the number of trees and their average moment of inertia is given in Table 5.2.

Using this we generated a series of spiral trees on square lattice up to 37 terms (Table 5.2). Earlier known series had only 25 terms.

For analysing the series data we tried a four parameter sequential fit to the data of the form

$$A_n = B\lambda^n(n + \delta)^{-\theta} \quad (5.13)$$

where δ is an adjustable fixed parameter and B is a constant. We did a linear fit on the logarithm of Eq. 5.13 using A_n, A_{n+1}, A_{n+2} and A_{n+3} to estimate values of B, δ, λ_n and θ_n . For spiral trees on square lattice we found a good convergence in successive values of λ_n and θ_n for δ lying between 2.03 and 2.04. Fixing $\delta = 2.0367$ and $B = 0.18124$ we get a very good convergence of λ_n and θ_n for different values of n . These are given in Table 5.3. From this we estimate

Cluster size(n)	A_n	$\langle I_{pl,n} \rangle$
1	1	0
2	4	1
3	14	3.142857
4	40	6.800000
5	105	12.266667
6	268	19.656716
7	674	28.919881
8	1660	40.159036
9	4021	53.513056
10	9612	69.074906
11	22734	86.926014
12	53276	107.140851
13	123916	129.787372
14	286376	154.926432
15	658100	182.624835
16	1504900	212.938547
17	3426464	245.919131
18	7771444	281.619675
19	17565064	320.089299
20	39576360	361.374917
21	88916877	405.522760
22	199252252	452.577078
23	445438310	502.580546
24	993616344	555.575100
25	2211923712	611.601183
26	4914811468	670.697934
27	10901498938	732.903853
28	24141259980	798.256392
29	53379537257	866.791847
30	117861710196	938.545859
31	259891311248	1013.553288
32	572356464452	1091.848086
33	1259008971656	1173.463504
34	2766351037428	1258.432171
35	6071954146120	1346.786006
36	13314252070412	
37	29167189621351	

Table 5.2: The number of spiral trees on a square lattice and their average moment of inertia.

$$\lambda = 2.11433 \pm 0.00010 \tag{5.14}$$

$$\theta = -1.3667 \pm 0.0010 \tag{5.15}$$

We have tried fits with non analytic corrections to scaling of the form $B\lambda^n(n+\delta)^{-\theta}[1+a/n^\Delta]$, but we didn't get good convergence for Δ . Instead, $B\lambda^n(n+\delta)^{-\theta}[1-\alpha e^{-\beta n}]$ seems to fit much better with $\alpha \approx 0.32$ and $\beta \approx 0.35$.

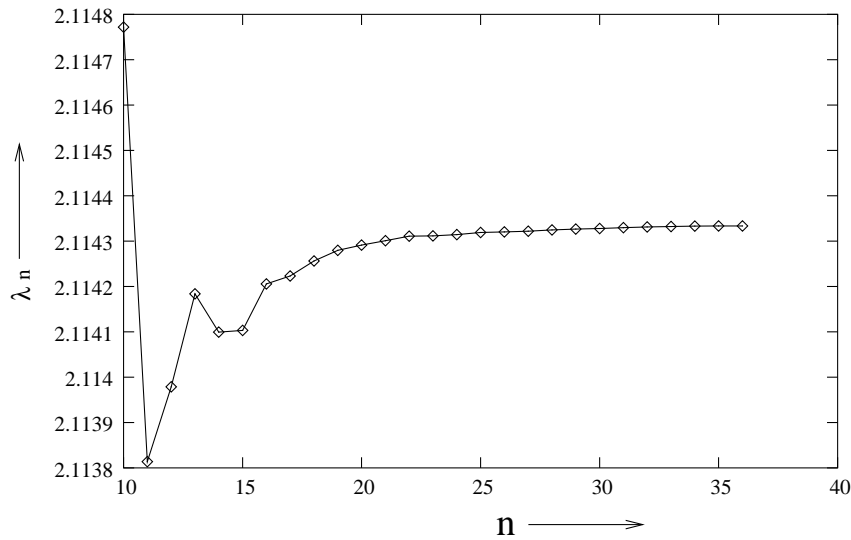


Fig 5.6: Figure shows the convergence of λ_n for spiral trees on a square lattice.

For the radius of gyration data we used a sequential fit of the form

$$\log I_{i,n} = (2\nu_i + 1)\ln(n + \delta) + u + \frac{v}{(n + \delta)^2} \tag{5.16}$$

where i stands for pl or \perp as the case maybe and u and v are constants.

For spiral trees in a plane $I_{\perp,n}$ would be zero and by symmetry the sum of squares of x coordinate of all sites for all configurations of clusters of size n equal to the sum of squares of y -coordinate. Using Eq. 5.14 for sequential fit to our 35 term series we get a good convergence for δ lying between -0.33 and -0.35 . Fixing $\delta = -0.338$ we get the estimates of ν_{pl} to be (see Table 5.3)

$$2\nu_{pl} = 1.3148 \pm 0.0010 \tag{5.17}$$

n	λ_n	θ_n	$2\nu_{pl,n}$
5	2.078982187	-1.4143616	1.2918751
6	2.118727624	-1.3598402	1.3047319
7	2.117039314	-1.3623751	1.3092198
8	2.115352878	-1.3651395	1.3108492
9	2.114617151	-1.3664433	1.3117861
10	2.114771869	-1.3661493	1.312420
11	2.113813740	-1.3680905	1.3128895
12	2.113978775	-1.3677359	1.3132536
13	2.114183882	-1.3672706	1.3135423
14	2.114099443	-1.3674721	1.3137672
15	2.114103267	-1.3674625	1.3139586
16	2.114205656	-1.3671946	1.3141194
17	2.114223238	-1.3671466	1.3142505
18	2.114256310	-1.3670527	1.3143596
19	2.114279786	-1.3669834	1.3144497
20	2.114291286	-1.3669483	1.3145234
21	2.114301033	-1.3669174	1.3145839
22	2.114310834	-1.3668854	1.3146334
23	2.114311487	-1.3668832	1.3146734
24	2.114314464	-1.3668728	1.3147059
25	2.114318963	-1.3668566	1.3147321
26	2.114320428	-1.3668513	1.3147529
27	2.114321722	-1.3668464	1.3147694
28	2.114324605	-1.3668351	1.3147823
29	2.114326551	-1.3668274	1.3147921
30	2.114327932	-1.3668217	1.3147994
31	2.114329734	-1.3668142	1.3148047
32	2.114331349	-1.3668072	1.3148083
33	2.114332328	-1.3668029	1.3148104
34	2.114333055	-1.3667997	1.3148113
35	2.114333550	-1.3667974	1.3148113
36	2.114333553	-1.3667974	
Es. Val.	2.11433 ± 0.0001	-1.3667 ± 0.001	1.3148 ± 0.001

Table 5.3: Values of λ_n , θ_n and ν_n from sequential fit to data for spiral trees of size n to $n + 3$ on a square lattice. See Fig. 5.6 and Fig. 5.7

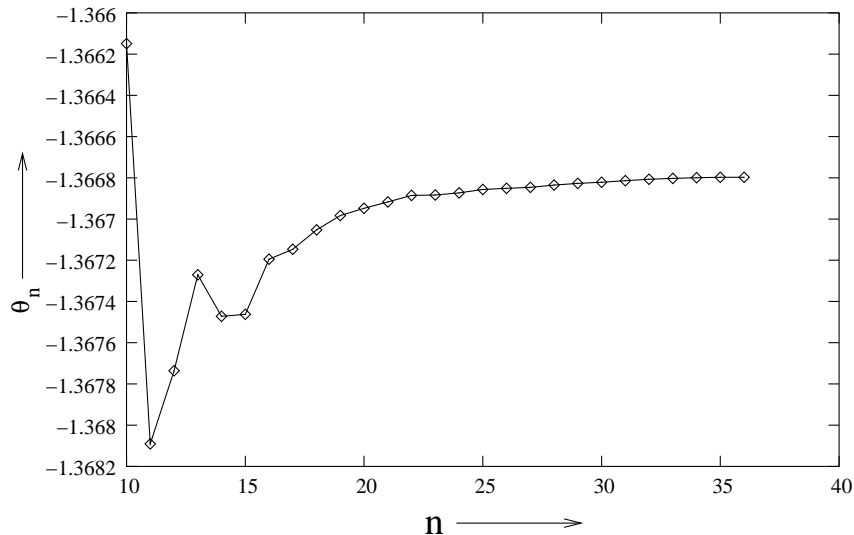


Fig 5.7: Figure shows the convergence of θ_n for spiral trees on a square lattice.

These estimates are much more precise than the earlier estimates $\lambda = 2.1166 \pm 0.001$, $\theta = -1.307 \pm 0.006$ and $2\nu_{pl} = 1.306 \pm 0.010$ using a 25 term series. We can rule out the dimensional reduction conjecture with fair confidence.

Above we presented our estimates using four parameter fits. Method of differential approximants has almost become a standard technique for such analysis [95]. In this case, the generating function has a divergent singularity at x_c . We tried zeroth order differential approximants, they are listed in Table 5.4. We find a very poor convergence in values of x_c and θ . Out of 70 approximants, 15 show spurious singularities (singularities with $|x_c| < 0.45$). We have listed 20 values which showed best convergence. From these we get, $\lambda = 2.1142 \pm 0.002$ and $\theta = -1.39 \pm 0.02$. Clearly the series is not very well behaved. This is reflected in the slow convergence of our series. Also Monte-Carlo generated random spiral trees of sizes 1000 (Fig. 5.1) suggest that the asymptotic behaviour of the series might set in rather late. Because of poor convergence of differential approximants, we relied on parameter fits for series analysis.

5.2.2 Monte-Carlo analysis

With exact enumeration, we are restricted to clusters of size thirty seven in two dimensions. The main problem is with the extrapolation since the crossover sizes are likely to be large, as the total angle turned by the largest spiral arm about the origin for a spiral tree of size 1000 is about 2π only (Fig. 5.1). This indicates that the crossover value above which asymptotic be-

$[l, m]$	$x_c = 1/\lambda$	θ	$[l, m]$	$x_c = 1/\lambda$	θ
[14, 13]	0.47288256	-1.36083	[15, 18]	0.47307144	-1.39078
[14, 14]	0.47290325	-1.36384	[14, 17]	0.47307308	-1.39106
[15, 13]	0.47290516	-1.36413	[16, 17]	0.47307863	-1.39209
[16, 15]	0.47294898	-1.37035	[17, 15]	0.47308675	-1.39369
[13, 15]	0.47297513	-1.37499	[16, 19]	0.47309052	-1.39421
[16, 13]	0.47303007	-1.38409	[18, 15]	0.47310355	-1.39686
[13, 16]	0.47303305	-1.38436	[17, 18]	0.47310906	-1.39788
[16, 16]	0.47305593	-1.38800	[15, 16]	0.47311001	-1.39775
[14, 15]	0.47305793	-1.38863	[18, 18]	0.47311071	-1.39822
[15, 17]	0.47306712	-1.39002	[17, 19]	0.47311091	-1.39826

Table 5.4: Estimates of critical exponents and growth constant from differential approximants. We looked at approximants for $l \geq 9$ and $l - 3 \leq m \leq l + 3$. We have tabulated here 20 values which showed the best convergence.

haviour sets in would be of order 10^3 . We tried to study larger spiral trees using MC methods. MC simulation of branched polymers is a challenging problem. Because of branching, most MC algorithms which are good for linear polymers show critical slowing down for branched polymers. For lattice trees there have been some studies using the cut and paste dynamic MC technique [96]. But with spiral constraint, algorithms involving large scale non local moves are not useful. We used an improved version of incomplete enumeration algorithm proposed recently by us (Section 4.4 and also [88]). Using it we could study spiral trees of sizes up to one thousand on a square lattice.

We have already shown pictures of some typical spiral trees thus generated in Fig.5.1. Clearly, their structure is very different from lattice trees without spiral constraint. Because of the constraint they tend to branch much less. For spiral constraint, earlier numerical evidence suggest that unlike lattice trees and animals, spiral tree and animal do not lie in same universality class. The reason is that by allowing loops, the polymer can bend much more often and hence spiral animals would be more compact than the spiral trees.

We studied spiral trees up to sizes 1000 using incomplete enumeration MC method. We made 10^7 MC runs. The moment of inertia tensor $I_{pl,n}$ as a function of n is plotted in Fig 5.8 and Fig 5.9. Assuming the asymptotic form to be such that

$$\log(I_{pl,n}) = \log C + (2\nu_{pl} + 1)\log n + \frac{D}{n} \quad (5.18)$$

Using above written form, we get the estimate of ν_{pl} to be (Fig 5.8 and Fig 5.9)

$$2\nu_{pl} = 1.312 \pm 0.010 \quad (5.19)$$

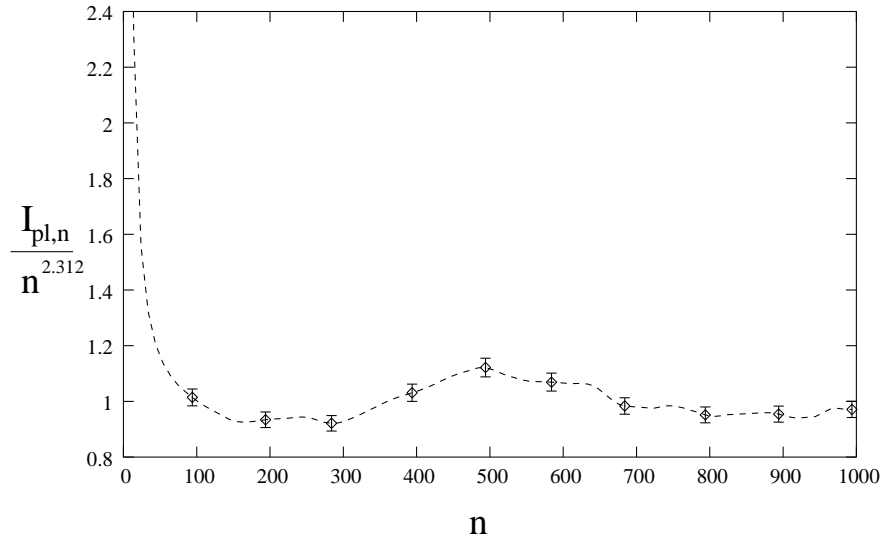


Fig 5.8: Plot of $\frac{I_{pl,n}}{n^{2.312}}$ as a function of n for Monte-Carlo generated spiral trees on a square lattice.

In incomplete enumeration MC algorithm [88], each configuration of n sites is generated with equal probability P_n which is just $\prod_{i=1}^n p_i$, where p_i is the probability with which an edge between level i and $i+1$ on the genealogical tree of the problem is chosen. By keeping track of the average number of clusters of a given size generated in a given run, one can estimate the growth constant λ and the critical exponent θ . But, the variance of the number of clusters increases as $\exp(n^\alpha)$, $0 < \alpha < 1$ for large n . Hence, instead we counted the number of descendants of each spiral tree generated. This approach has been used previously in [54, 96]. The mean number of descendants of a tree of size n gives a direct estimate of A_{n+1}/A_n . We represent the mean number of descendants by M_n . This is plotted in Fig. 5.10. A linear fit of the form $\lambda(1 - \theta/n)$ to this data gives $\lambda = 2.116 \pm 0.01$ and $\theta = -1.29 \pm 0.02$. For better estimates we assume

$$\log M_n = \log \lambda - \theta \log \left(\frac{n + \delta}{n - 1 + \delta} \right) \quad (5.20)$$

With this we get the following estimates for $n \leq 200$ which are in agreement with the value obtained by extrapolating the exact series expansions.

$$\lambda = 2.1145 \pm 0.0010 \quad (5.21)$$

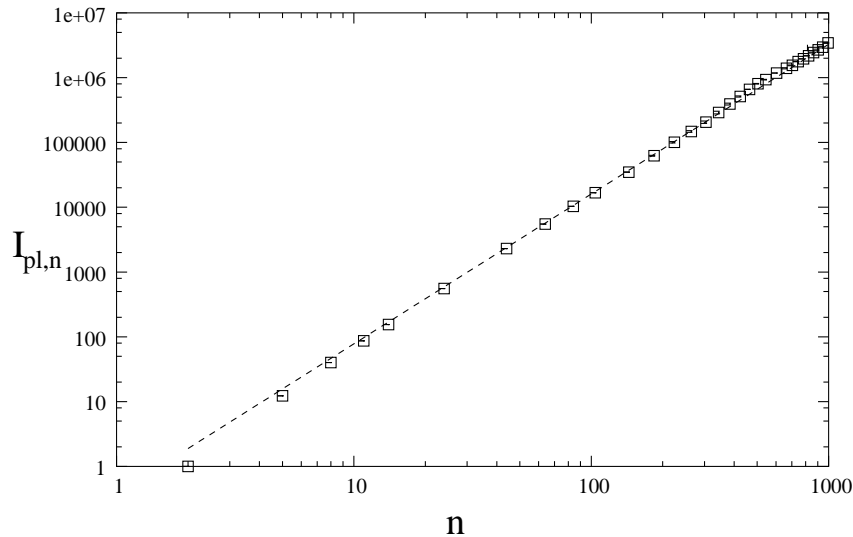


Fig 5.9: Plot of $I_{pl,n}$ versus n for Monte-Carlo generated spiral trees on a square lattice. The dotted line is a straight line with slope 2.312.

$$\theta = -1.364 \pm 0.010 \quad (5.22)$$

with $\delta = 1.8$.

5.3 Spiral trees on a cubic lattice

In dimensions higher than two, the spiral constraint defined as the projection of the path joining any site of the tree to the root in $x - y$ plane containing no left turn, can be employed in two ways. Bose et. al. [54] defined it such that for the projected path from origin to site on $x - y$ plane only forward and right turns are allowed. But in dimensions higher than two, we can define another variation where trees as long as they do not violate the tree constraint and the projection on $x - y$ plane is spiral, are allowed. We will call the spiral trees with only forward and right turns allowed ST_1 .

If we allow for back-turns also, we would get different series because for example, Fig 5.1 shows one spiral tree of six sites which would not be a valid configuration if we consider only forward and right turns. We call the spiral trees with back-turns allowed as ST_2 . Naively, one would expect these two to belong to the same universality class. We generated the series till $n = 17$ on a cubic lattice using both definitions, however we find the two series behaving differently. Series for ST_1 and ST_2 are given in Table 5.5 and 5.6 respectively.

For ST_1 , for A_n the number of configurations, using Eq. 5.13 we find that the sequential

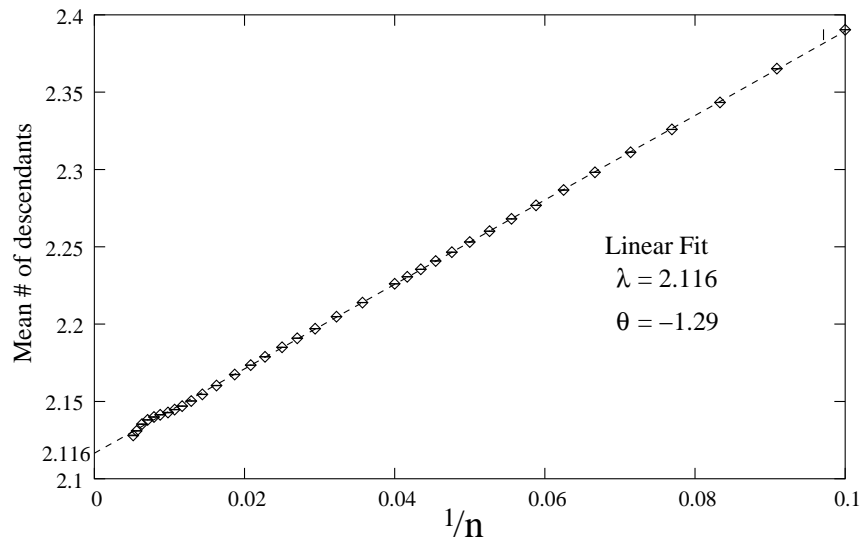


Fig 5.10: Monte-Carlo estimates of ratios of the number of configurations on a square lattice. The straight line gives a linear fit of the form $\lambda(1 - \theta/n)$ to the data.

fit shows a good convergence around $\delta = 2.43$. With $\delta = 2.43$ and $B = 0.094$, the values of λ and θ obtained are listed in Table 1. For ν_{pl} and ν_{\perp} , we used fitting form as given in Eq. 5.16, with $\delta = -1.46$ and $\delta = -0.43$ respectively. The sequential fits are given in Table 5.7 and the estimates are listed in Table 5.9.

Similarly, we obtained 17 term series for ST_2 . The sequential fits are given in Table 5.8 and the values of λ , θ , ν_{pl} and ν_{\perp} are listed in Table 5.9.

The difference in value of λ for ST_1 and ST_2 is understandable as ST_2 has a greater number of configurations. More surprisingly, the critical exponents θ , ν_{pl} and ν_{\perp} within our error estimates are different in two models. In neither case, the conjectured dimensional reduction (Eq.1.13 and 1.14) seems to be satisfied.

5.4 Spiral trees in four dimensions

On a hyper cubic lattice in four dimensions we generated a series till $n = 13$. We also correct the mistakes in the earlier series reported for ST_1 in [54]. The corrected series is given in the Table 5.10. We also obtained a 13 term series for ST_2 (see Table 5.11). The estimates of λ and critical exponents are listed in Table 5.9.

We also performed Monte-Carlo simulations using incomplete enumeration algorithm for spiral trees up to size 50. Our estimates from MC simulations for ST_1 are given in Table

n	A_n	$\langle I_{pl,n} \rangle$	$\langle I_{\perp,n} \rangle$
1	1	0.	0.
2	6	0.66666	0.333333
3	41	1.85366	1.07317
4	260	3.63076	2.27692
5	1568	6.02296	3.98214
6	9190	9.06464	6.19913
7	53090	12.75954	8.91987
8	303900	17.09588	12.1405
9	1727691	22.0606	15.8606
10	9767426	27.6424	20.0821
11	54966550	33.8322	24.8071
12	308138528	40.6214	30.0376
13	1721739000	48.0022	35.7754
14	9592901762	55.9676	42.0229
15	53314247488	64.5112	48.7822
16	295644339728	73.6274	56.0556
17	1636179620652	83.3112	63.8454

Table 5.5: Exact enumeration values of the number of spiral trees ST_1 on a cubical lattice and their average moments of inertia.

n	A_n	$\langle I_{pl,n} \rangle$	$\langle I_{\perp,n} \rangle$
1	1	0	0.
2	6	0.666666	0.333333
3	41	1.85366	1.07317
4	260	3.63076	2.27692
5	1576	6.00762	4.00761
6	9342	9.00192	6.30208
7	54890	12.60084	9.17041
8	320952	16.7848	12.6182
9	1869907	21.5398	16.651
10	10861750	26.8572	21.2772
11	62939998	32.7312	26.5047
12	364004296	39.156	32.3409
13	2101795408	46.1276	38.7927
14	12119643750	53.6422	45.8667
15	69805866848	61.6968	53.5693
16	401668709200	70.2898	61.9068
17	2309283650656	79.4192	70.8851

Table 5.6: Exact enumeration values for number of spiral trees ST_2 on a cubical lattice and their average moments of inertia.

n	λ_n	θ_n	$2\nu_{pl,n}$	$2\nu_{\perp,n}$
5	5.153269	-1.019107	0.847865	1.128949
6	5.275382	-0.810187	0.865641	1.098419
7	5.310873	-0.743662	0.871330	1.083814
8	5.319667	-0.725590	0.874191	1.077873
9	5.327658	-0.707695	0.875922	1.073809
10	5.334141	-0.691977	0.876525	1.070550
11	5.337903	-0.682161	0.876502	1.068326
12	5.339533	-0.677605	0.876303	1.067085
13	5.340111	-0.675880	0.876176	1.066526
14	5.340282	-0.675339	0.876139	1.066334
15	5.340255	-0.675428	0.876197	1.066365
Es. Val.	5.340 ± 0.02	-0.675 ± 0.05	0.876 ± 0.05	1.066 ± 0.05

Table 5.7: Values of λ_n , θ_n and ν_n from sequential fit to data for spiral trees ST_1 on a cubical lattice.

n	λ_n	θ_n	$2\nu_{pl,n}$	$2\nu_{\perp,n}$
5	5.694072	-0.143802	1.054721	1.200021
6	5.719085	-0.123718	1.013833	1.171160
7	5.710159	-0.132441	0.989310	1.153823
8	5.695471	-0.149408	0.977105	1.147515
9	5.689143	-0.157845	0.969817	1.144294
10	5.687350	-0.160552	0.963977	1.141637
11	5.686110	-0.162645	0.959561	1.139686
12	5.684763	-0.165153	0.956738	1.138646
13	5.683809	-0.167099	0.955250	1.138243
14	5.683473	-0.167843	0.954653	1.138124
15	5.683632	-0.167463	0.954662	1.138134
Es. Val.	5.683 ± 0.02	-0.167 ± 0.05	0.954 ± 0.05	1.138 ± 0.05

Table 5.8: Values of λ_n , θ_n and ν_n from sequential fit to data for spiral trees ST_2 on a cubical lattice.

	$ST_1(d=3)$	$ST_2(d=3)$	$ST_1(d=4)$	$ST_2(d=4)$
λ	5.340 ± 0.020	5.683 ± 0.020	9.62 ± 0.10	10.20 ± 0.10
θ	-0.675 ± 0.050	-0.167 ± 0.050	-0.11 ± 0.10	0.29 ± 0.10
ν_{pl}	0.44 ± 0.05	0.477 ± 0.05	0.34 ± 0.05	0.37 ± 0.05
ν_{\perp}	0.54 ± 0.05	0.69 ± 0.05	0.44 ± 0.05	0.45 ± 0.05

Table 5.9: Estimates of critical exponents and growth constant from series analysis in three and four dimensions.

n	A_n	$\langle I_{pl,n} \rangle$	$\langle I_{\perp,n} \rangle$
1	1	0.	0
2	8	0.5	0.5
3	80	1.35	1.5
4	800	2.54	3.030
5	7912	4.05864	5.10010
6	77656	5.89816	7.70862
7	759172	8.04822	10.84584
8	7403292	10.49742	14.50268
9	72073417	13.23410	18.67008
10	700774524	16.24692	23.34
11	6806914432	19.52526	28.5052
12	66064406668	23.0592	34.1596
13	640741734643	26.8396	40.2974

Table 5.10: Exact enumeration data for the number of spiral trees ST_1 on four dimensional hyper-cubic lattice and their average moments of inertia.

n	A_n	$\langle I_{pl,n} \rangle$	$\langle I_{\perp,n} \rangle$
1	1	0.	0.
2	8	0.5	0.5
3	80	1.35	1.5
4	800	2.54	3.030
5	7960	4.05226	5.10754
6	79048	5.87628	7.74208
7	785748	7.99822	10.93174
8	7822676	10.40506	14.6724
9	78011513	13.08484	18.95778
10	779189988	16.0274	23.7816
11	7793590224	19.22410	29.1376
12	78049539204	22.6676	35.0206
13	782488672931	26.3518	41.4252

Table 5.11: Exact enumeration data for the number of spiral trees ST_2 on four dimensional hyper-cubic lattice and their moments of inertia.

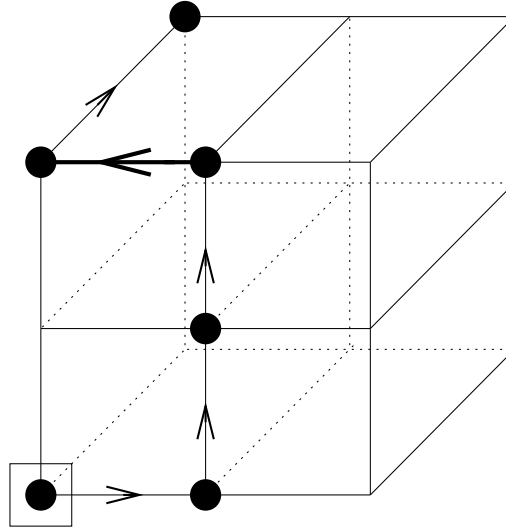


Fig 5.11: This configuration will contribute to spiral trees ST_2 of six sites but not to ST_1 .

	$ST_1(d = 4)$	$ST_2(d = 4)$
λ	9.60 ± 0.1	10.2 ± 0.1
θ	-0.13 ± 0.1	0.17 ± 0.1
ν_{pl}	0.33 ± 0.02	0.38 ± 0.05
ν_{\perp}	0.451 ± 0.020	0.455 ± 0.050

Table 5.12: Estimates of critical exponents and growth constants from Monte-Carlo simulations in four dimensions.

5.11.

Though we cannot rule out the possibility of θ being zero in both series analysis and Monte-Carlo simulations, it seems unlikely.

Summary of Results and Discussion

In this chapter we will summarise the results of Chapters 2-5.

6.1 Directed animals (Directed branched polymers)

In Chapter 2 of this thesis we studied the model of directed animals and found a mapping between distribution of sites in transverse direction and density-density correlation function of a lattice gas model. Specifically, we obtained the exact scaling function of the distribution for DA's in $1 + 1$ -dimensions. DA's are anisotropic and their average size in transverse and longitudinal direction scales with different exponents. The properties of DA in longitudinal direction can be obtained by studying the time evolution of the HCLG with the stochastic evolution rules described in Sec 2.1. Unfortunately, this cannot be solved exactly and hence the exact value of the size exponent $\nu_{||}$ in longitudinal direction is not known in any dimension. Though using Markovian property of the generating functions, one can get very good numerical estimates [97], finding it exactly remains an open important problem. In Sec. 2.3 we solved the DA problem on Bethe lattice obtaining the exponent and scaling functions in both longitudinal and transverse directions. In Sec. 2.3 we defined a model of generalized DA and found that model lies in the same universality class as the DA problem.

We gave the mapping of a $d + 1$ dimensional directed branched polymer in presence of a line to a d dimensional HCLG with repulsive interactions in Chapter 3. For DBP in $1 + 1$ dimensions we show that the behavior at the transition point for penetrable and impenetrable wall is the same, and not just the crossover exponent but even the density profile is the same. This implies that for $1 + 1$ dimensions, for impenetrable surface, at the phase transition point the decrease in entropy is exactly compensated by the change in internal energy. This seems to be a special property of polymers in 2 dimensions. Even for linear polymers the exponent for both cases is the same and hence it has been argued that for a linear polymer

in 2 dimensions in presence of a impenetrable surface the phase transition point corresponds to the point where surface effects vanish completely and the system behaves like bulk [43]. Here we are able to show it explicitly for directed branched polymers. Also, note that the value of the exponent $\alpha = 1/2$ for DBP is equal to the estimates of α for branched polymers [99] and linear polymers in [84] in two dimensions. In fact, for adsorption of an undirected d -dimensional branched polymer on a $(d - 1)$ -dimensional surface, the crossover exponent α is conjectured to be $1/2$ in all spatial dimensions [98].

Using Baxter's solution of hard hexagon gas we calculated the crossover exponent and sticking fraction exactly for $2 + 1$ dimensional DBP in presence of line in Sec 3.5. The scaling function of sticking fraction is a function of two thermodynamic variables. We have derived its exact form in $1 + 1$ and $2 + 1$ dimensions. This thus provides a simple soluble model where a nontrivial scaling function of more than one thermodynamic variable can be explicitly calculated. There are very few such exact nontrivial scaling functions of more than one thermodynamic variable known [100].

6.2 Incomplete enumeration algorithm

In Chapter 4 we studied the efficiency of a MC method known as IE. We also give an improvement on IE, which we call improved incomplete enumeration (IIE). Its a stochastic growth algorithm, similar to other stochastic growth algorithms like PERM. We find the efficiency of IE to be different for linear and branched polymers. This is due to the fact that genealogical tree for the latter is much more non uniform.

For self avoiding walks, in any dimension, the time to generate an independent sample of n steps $T_n \sim a_d n^2$, independent of dimension for both IE and IIE. For IE there is no significant change in a_d with dimension. But for IIE $a_d \sim d^{-2}$. In the limiting case of SAW on binary tree $T_n = n$ for IIE.

For branched polymers T_n increases as $\exp(cn^\alpha)$ with $0 < \alpha < 1$ in all dimensions for both IE and IIE. Redistributing weights does not change the value of α . IIE works better than IE, but the difference is only in the coefficient c . The exponent α depends weakly on the dimension, its relation to the usually studied exponents of the branched polymer problem eg. θ, ν is not clear at present.

As discussed in Section 4.4, the genealogical tree for cluster enumeration is not unique and one might argue that Martin's scheme is not the optimal choice. We tried to generate

the genealogical tree using some variations of this rule, but we did not find any significant change in the efficiency of the algorithm.

For branched polymers, the degree of a node in the genealogical tree is not bounded, and the maximum degree increases with depth of the genealogical tree. However, the fractional number of nodes with high degree is very small. For genealogical tree corresponding to animals on a binary tree we find the fractional number of k -nodes goes down exponentially with k for large k (Eq. (4.17)). Similar behaviour was observed for branched polymers and directed branched polymers on a square lattice numerically. It is interesting that even an exponentially rare distribution of nodes with large degree seems to be enough to change the behaviour of efficiency of the algorithm on the tree.

In the case of branched polymers, we found that the T_n for IE varies as $\exp(cn^\alpha)$ with $0 < \alpha < 1$. While this is not very good, one can find problems for which IE's performance is even worse with $\alpha = 1$. As an example, consider self avoiding walks on a disordered lattice, obtained by removing a fraction $(1 - u)$ of bonds at random from a square lattice. It is known that the average number of self avoiding walks of length n varies as $(u\lambda)^n$ [101], where λ is the growth constant of the self avoiding walks on the same lattice with $u = 1$. Hence the growth constant of the corresponding genealogical tree would also be $u\lambda$. Now if we consider a square lattice, the $\lambda \approx 2.638$ and the bond percolation threshold is $1/2$. For $1/\lambda < u < 1/2$, all clusters would be finite with probability 1, and the probability that cluster contains n sites would decrease exponentially with n . In this case, IE will be inefficient and even for best choice, T_n will vary as $\exp(cn)$.

One could argue that IE is a rather inefficient algorithm, which gives reasonable performance only for a small selected set of problems. We do not think so. In fact, the causes that make IE inefficient are also operative in the much larger class of genetic type algorithms. The high degree of correlations between different samples generated is a common feature of many of these algorithms which employ pruning and enrichment. For example, one could expect a similar behaviour to occur in the Berreti-Sokal algorithm [66] for branched polymers. The correlations arise because in all such 'evolutionary' type algorithms different samples generated often share a common ancestor in the past. Whether our results can be generalised to a larger class of PERM type algorithms is an interesting question for further study.

6.3 The Spiral trees problem

We studied rooted spiral trees in two three and four dimensions on hyper cubic lattices using numerical techniques. This is an interesting model. Our results show the presence of many universality class as among lattice trees with different implementation of the spiral constraint. Also dimensional reduction which has played an important role in lattice tree/animals problem and was conjectured for this model doesn't seem to hold. Our numerical evidence as presented in this thesis does not support the conjecture; clearly our estimates of critical exponents do not satisfy Eq. 1.13 and 1.14. Spiral tree is computationally a very challenging problem. Lattice tree/animal itself are not easy to generate and because of a further spiral constraint the situation becomes worse and most nonlocal algorithms will not work well here. So this problem shows the need for and the importance of stochastic growth algorithms. It seems IE is ideally suited for such problems. I could generate spiral trees up to size 1000 on a square lattice using IIE. This problem also shows a need to work and think of some new MC techniques to tackle these problems.

In Chapter 5, we also obtained a non-trivial lower bound on the value of growth constant λ_{spiral} on a square lattice. Our bound is $\lambda_{spiral} \geq 1.93565$, whereas numerical estimates for it is $\lambda_{spiral} \approx 2.114$. For quadrant spiral trees on a square lattice, we obtained exact series up to sizes 55. There are very few such long series known for lattice models. The series gives a estimate of $\lambda = 2.044$ for these quadrant spiral trees. This value is significantly smaller than for the full spiral trees. This indicates that that trees where spiral turns a lot are important. Actually, for large clusters of size 10^3 generated by Monte Carlo, the total angle turned by the largest spiral arm about the origin is about 2π . It is possible that the structure of spiral trees is such that this angle tends to infinity as n tends to infinity. In this case the crossover value above which asymptotic behaviour sets in would be expected to be of order 10^3 , and series analysis for smaller n may not give correct limiting behaviour.

The spiral constraint for trees seems to be very special. For example, the structure of spiral trees is very different from spiral animals with loops allowed [102]. Different implementation of the constraint in $d > 2$, seems to give different critical behaviour, suggesting different universality classes. A variety of self avoiding walks with different step restrictions rules on simple cubic lattice were studied in [103] using exact enumeration. Their analysis suggested the same universality class for SAW's with various restrictions (including the spiral constraint) as for the unrestricted SAW's. In contrast, our studies show different critical behaviour of spiral trees with different geometrical restrictions in three and four dimensions.

Bibliography

- [1] P. G. de Gennes 1979, *Scaling Concepts in Polymer Physics*, Cornell University Press Ithaca and London
- [2] C. Vanderzande 1998, *Lattice Models of Polymers*, Cambridge Lecture Notes in Physics, Cambridge University Press
- [3] E. J. Janse van Rensburg 2000, *The Statistical Mechanics of Interacting Walks, Polygons, Animals and Vesicles*, Oxford Lecture Series in Mathematics and its Applications **18**, OXFORD University Press.
- [4] N. Goldenfeld 1992, *Lectures on Phase Transitions and the Renormalisation Group*, Frontiers in Physics Vol. **85**, PERSEUS BOOKS, *Reading Massachusetts*
- [5] J. Cardy 1996, *Scaling and Renormalisation in Statistical Physics*, Cambridge Lecture Notes in Physics, Cambridge University Press.
- [6] N. Madras and G. Slade 1993, *The Self-Avoiding Walk*, Birkhauser Boston.
- [7] T. C. Lubensky and J. Issacson 1979, *Phys. Rev. A* **20** 2130
- [8] P. G. de Gennes 1972, *Phys. Lett. A*, **38**, 339
- [9] Stauffer and Aharony 1992, *Introduction to Percolation Theory* 2nd ed., Taylor and Francis, London
- [10] G. Parisi and N. Sourlas 1981, *Phys. Rev. Lett.*, **46**, 871
- [11] D. C. Brydges and J. Z. Imbrie 2003, *Annals of Mathematics*, **158** 1019
- [12] F. Y. Wu 1982, *Rev. of Mod. Phys.*, **54**, 235
- [13] B. Duplantier and H. Saleur 1986, *Physical Review Letters* **57** 3179

- [14] K. Binder 1997, Applications of Monte-Carlo Methods to statistical physics, Rep. Prog. Phys. **60** 487-559.
- [15] A. D. Sokal, Monte-Carlo Methods for the Self Avoiding Walk 1995, in Monte Carlo and Molecular Dynamics Simulations in Polymer Science, ed. K. Binder, Oxford University Press New York 47-124, hep-lat/9405016
- [16] B. Nienhuis 1982, Phys. Rev. Letts. **49**, 1062
- [17] I. Jensen and A. J. Guttmann 1999, J. Phys. A. **32**, 4867-4876.
- [18] D. J. Klein 1981, J. Chem. Phys. **75** 5186
- [19] N. Madras 1995, J. Stat. Phys. **78** 681
- [20] G. Grimmett 1989, Percolation, Springer-Verlag New-York
- [21] F. Family 1982, J. Phys. A:Math. Gen. **15** L 583
- [22] J. D. Miller and K. De'Bell 1993, J. Phys. I France **3** 1717-1728.
- [23] S. Lai and M. E. Fisher 1995, J. Chem. Phys. **103** 8144; Y. Park and M. E. Fisher 1999, Phys. Rev. E **60** 6323
- [24] D. Dhar 1983, Physical Review Letters **51**, 853
- [25] J. Cardy 1982, J. Phys. A:Math. Gen. **15** L593
- [26] D. Dhar, M. K. Phani and M. Barma 1982, J. Phys. A:Math Gen. **15** L 279; D. Dhar 1982, Physical Review Letters **49** 959.; D. Dhar 1986, Physica A **140**, 210
- [27] J. P. Nadal, B. Derrida and J. Vannimenus 1982, J. Physique **43** 1561
- [28] H. E. Stanley, S. Redner, Z. R. Yang 1982, J. Phys. A:Math. Gen. **15** L-569
- [29] D. G. Beauchamps and G. Viennot 1988, Adv. in App. Mathematica **9** 334
- [30] A. Conway 1996, J. Phys. A:Math. Gen. **29** 5273
- [31] Bousquet-Mélou M 1998, Disc. Math **180** 73
- [32] H. Hinrichsen 2000, Adv. Phys., **49**, 815
- [33] P. Di Francesco and E. Guitter 2002, J. Phys. A: Math and Gen., **35** 897.

- [34] S. C. Chang and R. Shrock 2001, *Physica* **A296** 13
- [35] D. Dhar 1986, The directed animals and related problems, in *Field Theory, Quantum Gravity and Strings* Eds. H. J. deVega and N. Sanchez, *Lecture Notes in Physics* Vol. **246** (Springer, Berlin)
- [36] F.Y. Wu et. al 1996, *Phys. Rev. Lett.*, **76**, 173
- [37] E. Eisenriegler 1993, *Polymer Near Surfaces*, World Scientific
- [38] I. Norde 1995, *Surface and Interfacial Aspects of Biomedical Applications*, Plenum, New York
- [39] K. De'Bell and T. Lookman 1993, *Rev. of Modern Phys.* **65** 87
- [40] A. L. Stella and C. Vanderzande 1990, *Int. J. of Modern Phys. B* **4** 1437
- [41] V. Privman, G. Forgacs and H. L. Frisch 1988, *Physical Review B* **37** 9897
- [42] P. K. Mishra, S. Kumar and Y. Singh 2003, *Physica A* **323** 453
- [43] E. Bouchaud, J. Vannimenus 1989, *J. Phys. France* **50** 2931
- [44] R. J. Rubin 1965, *J. Chem. Phys.* **43** 2392
- [45] S. N. Majumdar 1990, *Physica A* **169** 207
- [46] K. De'Bell, T. Lookman and D. Zhao 1991, *Physical Review A* **44** 1390
- [47] J. Cardy 2001, *J. Phys. A:Math. Gen.* **34** L665
- [48] I. Hargittai and C. A. Pickover eds. 1992, *Spiral Symmetry*, World Scientific, Singapore.
- [49] V. Privman 1983, *J. Phys. A:Math. Gen* **16** L571
- [50] A. J. Guttmann and N. C. Wormald 1984, *J. Phys. A:Math. Gen.* **17** 271
- [51] G. H. Hardy and S. Ramanujan 1918, *Proc. London Math. Soc.* **2**, 17-75.
- [52] R. Roy 2000, *Percolation Theory and Particle Systems*, Universities Press (India) Limited Hyderabad.
- [53] T. C. Li and Z. C. Zhou 1985, *J. Phys. A:Math. Gen.* **18** 67

- [54] I. Bose, P. Ray and D. Dhar 1988, J. Phys. A:Math. Gen **21** L219
- [55] I. Jensen 2001, J. Stat. Phys. Vol. **102** 865-881.
- [56] I. G. Enting 1980, J. Phys. A:Math. Gen. **13** 3713.
- [57] I. Jensen 2004, J. Phys. A **37** 5503-5524.
- [58] M. Doi and S. F. Edwards 1986, The Theory of Polymer Dynamics, Clarendon Press-Oxford.
- [59] F. T. Wall and F. Mandel 1975, J. Chem. Phys. **63** 4592-4595.
- [60] N. Madras and A. D. Sokal 1988, J. Stat. Phys. **50** 109
- [61] S. Caracciolo, A. Pelissetto and A. D. Sokal 1990, J. Stat. Phys. **60** 1
- [62] F. T. Wall and J. J. Erpenbeck 1959, J. Chem. Phys. **30** 634-637.
- [63] P. Grassberger and W. Nadler 2000, Go with the winners - Simulations, cond-mat/0010265, Proceedings der Heraeus-Ferienschule "Vom Billardtisch bis Monte Carlo: Spielfelder der statistischen Physik", Chemnitz, October 2000;
- [64] E. J. Janse van Rensburg, S.G. Whittington, and N. Madras 1990, J. Phys. A **23** 1589.
- [65] T. Kennedy 2002, J. Stat. Phys. **106** 407-429
- [66] A Berreti and A.D.Sokal 1985, J. Stat. Phys. **40** 483
- [67] E. J. Janse van Rensburg and N. Madras J. Phys. A:Math. Gen. **25** 303-333(1992); J Phys. A:Math. Gen. **30** 8035-8066 (1997); E. J. Janse van Rensburg and A. Rechenitzer 2003, Phys. Rev E **67** 0361161-0361169
- [68] S. You and E. J. Janse van Rensburg 2001, Phys. Rev. E vol. **64** 0461011-0461019.
- [69] H. P. Hsu, W. Nadler and P. Grassberger 2005, J. Phys. A Vol. **38** 775.
- [70] J. S. Liu 2001, Monte-Carlo Strategies in Scientific Computing, Springer Series in Statistics, Springer.
- [71] M. N. Rosenbluth and A W Rosenbluth 1955, Journal of Chemical Physics **23** 356-359.
- [72] P. Grassberger, Phys. Rev. E **56**, 3682 (1997).

- [73] H. P. Hsu and P. Grassberger 2005, *J. Stat. Mech.* p01007 (2005)
- [74] S. Redner and P.J. Reynolds 1981, *J. Phys. A* **14** 2679.
- [75] D. Dhar and P. M. Lam 1986, *J. Phys. A: Math. Gen.* **19** L1057-1061
- [76] P. M. Lam 1986, *Phys. Rev. A*, Vol. **34** 2339-2345.
- [77] J. L. Martin 1974, *Computer Techniques for Evaluating Lattice Constants, Phase Transitions and Critical Phenomena*, Eds. Domb and Green, vol. **3**.
- [78] Sumedha and D. Dhar 2003, *J. Phys. A:Math. Gen.* **36** 3701
- [79] D. A. Kurtz and M. E. Fisher 1979, *Phys. Rev. B* **20** 2785
- [80] T. Hara and G. Slade 1990, *J. Stat. Phys.*, **59** 1469-1510
- [81] Sumedha, unpublished.
- [82] Sumedha, *J. Phys. A:Math. Gen.*, Vol.**37**, 3673(2004)
- [83] E. J. Rensburg and Rechnitzer 2001, *Journal of Statistical Physics* **105** 49
- [84] I. Guim and T. W. Burkhardt 1988, *J. Phys. A:Math. Gen.* **22** 1131
- [85] R. J. Baxter 1979, *J. Phys. A:Math. Gen.* **13** L61
- [86] G. S. Joyce 1988, *J. Phys. A:Math. Gen.* **21** L983
- [87] G. S. Joyce 1989, *J. Phys. A:Math. Gen.* **22** L919
- [88] Sumedha and D Dhar 2004, cond-mat/0408640 (to be published *J. Stat. Phys.*)
- [89] R. P. Stanley 1999, *Enumerative Combinatorics*, Vol.2 Chapter 6, Cambridge University Press, Cambridge-New York.
- [90] Wim van Saarloos 2003, Front propagation into unstable states, *Phys. Rep.* **386** 29
- [91] E. Brunet and B. Derrida 1997, *Phys. Rev. E* **56** 2597; S. N. Majumdar and P. L. Kaprivsky 2003, *Physica A* **318** 161
- [92] Sumedha, cond-mat/0410395(to be published in *J. Stat. Phys.*).
- [93] J. W. Essam 1971, *J. Math. Phys.* **12** 874.

-
- [94] A. Conway 1995, J. Phys. A:Math. Gen. **28** 335.
- [95] D. S. Gaunt and A. J. Guttmann 1974, Eds. Domb and Green, vol. **3**.
- [96] E. J. Janse van Rensburg and A. Rechnitzer 2003, Phys. Rev. E **67** 036116.
- [97] D. Dhar 1988, J. Phys. A **21**, L893.
- [98] H. K. Janssen and A. Lyssy 1994, Phys. Rev. E **50** 3784.
- [99] S. L. A. de Queiroz 1995, J. Phys. A:Math. Gen: **28** 6315; S. You and E. J. Rensburg 2001 Phys. Rev. E **64** 046101
- [100] J. Cardy 2003, cond-mat/0302495
- [101] K. Barat and B. K. Chakrabarti 1995, Statistics of self-avoiding walks on random lattices, Phys. Rep. **258** 377.
- [102] I. Bose 2000, Lattice Animals and the Percolation Model under Rotational Constraint, Percolation Theory and Particle Systems, Eds. Rahul Roy, University Press, India.
- [103] A. Rechnitzer and A. L. Owczarek 2000, J. Phys. A:Math. Gen. **33** 2685.

List of Publications

1. **Distribution of Transverse Distances in Directed Animals,**
Sumedha and Deepak Dhar, J. Phys. A:Math. Gen., Vol.**36**, 3701(2003) (cond-mat/0303450)
2. **Directed Branched Polymer near an Attractive Line,**
Sumedha, J. Phys. A:Math. Gen., Vol.**37**, 3673(2004) (cond-mat/0402061)
3. **Efficiency of the Incomplete Enumeration algorithm for Monte-Carlo simulation of linear and branched polymers**
Sumedha and Deepak Dhar, cond-mat/0408640 (to be published in J. Stat. Phys.)
4. **Rooted Spiral Lattice Trees on Hyper-cubic lattices.**
Sumedha, cond-mat/0410395(to be published in J. Stat. Phys.).